CHAPTER 1

INTRODUCTION

1.1 Introduction

Underwater Optical Wireless Communication (UOWC) is a high-speed data transmission technique that uses light to transfer information through water. It offers higher bandwidth and lower latency compared to traditional acoustic communication system. UOWC is suitable for short-range applications such as underwater sensor networks and remotely operated vehicles. However, its performance is affected by absorption, scattering, and turbulence in the water. These environmental factors limit the range and reliability of the optical link. As a result, designing efficient and robust UOWC system remains a key research focus. This chapter presents a concise overview of the thesis, along with the motivation, key challenges, defined objectives, and the adopted research methodology.

1.2 Motivation

The demand for reliable and high-speed underwater communication system has grown significantly with the increasing interest in applications such as oceanographic data collection, underwater surveillance, Autonomous Underwater Vehicle (AUV) coordination, and environmental monitoring. Among the available technologies, UOWC has emerged as a promising solution due to its potential for high bandwidth and low latency. However, the practical realization of UOWC system remains a considerable challenge due to the complex and dynamic nature of the underwater environment. Issues such as signal fading, beam scattering, and misalignment exacerbated by turbulence, pointing errors, and mobility severely limit transmission reliability and range. Fig. 1.1 shows the architecture of a UOWC system showing optical transmission in underwater environments.

1

Thesis

by DUSHYANT CHAUHAN

CHAPTER 1

INTRODUCTION

1.1 Introduction

Underwater Optical Wireless Communication (UOWC) is a high-speed data transmission technique that uses light to transfer information through water. It offers higher bandwidth and lower latency compared to traditional acoustic communication system. UOWC is suitable for short-range applications such as underwater sensor networks and remotely operated vehicles. However, its performance is affected by absorption, scattering, and turbulence in the water. These environmental factors limit the range and reliability of the optical link. As a result, designing efficient and robust UOWC system remains a key research focus. This chapter presents a concise overview of the thesis, along with the motivation, key challenges, defined objectives, and the adopted research methodology.

1.2 Motivation

The demand for reliable and high-speed underwater communication system has grown significantly with the increasing interest in applications such as oceanographic data collection, underwater surveillance, Autonomous Underwater Vehicle (AUV) coordination, and environmental monitoring. Among the available technologies, UOWC has emerged as a promising solution due to its potential for high bandwidth and low latency. However, the practical realization of UOWC system remains a considerable challenge due to the complex and dynamic nature of the underwater environment. Issues such as signal fading, beam scattering, and misalignment exacerbated by turbulence, pointing errors, and mobility severely limit transmission reliability and range. Fig. 1.1 shows the architecture of a UOWC system showing optical transmission in underwater environments.
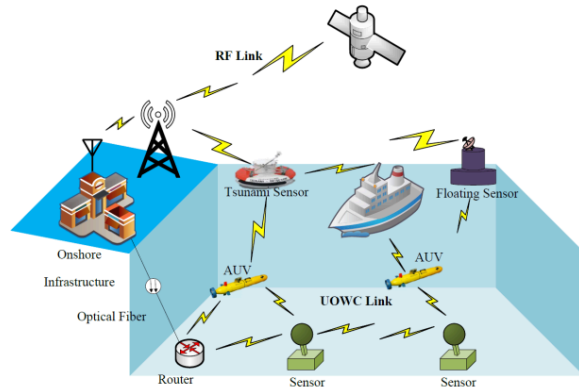
Figure 1.1 Architecture of a UOWC system showing optical transmission in underwater environment

These limitations highlight the need for a robust, adaptive, and intelligent communication framework that can address both physical-layer impairments and environmental unpredictability. This thesis is motivated by the objective of overcoming these barriers through a multi-faceted approach that integrates Multiple Input Multiple Output (MIMO) based spatial diversity, dual-hop cooperative relaying to enhance range and mitigate line of sight (LoS) dependency, and Reed-Solomon (RS) channel coding for robust error correction. Furthermore, the incorporation of deep learning, particularly Convolutional Neural Networks (CNNs), offers the ability to dynamically learn and adapt to nonlinear distortions and complex underwater variations. By combining these strategies, this work aims to develop a robust UOWC system capable of maintaining reliable performance across a range of challenging underwater scenarios.

1.3   Challenges

The underwater environment is highly dynamic and unpredictable, characterized by physical disturbances, environmental variability, and mobility-induced misalignments. These factors collectively contribute to signal degradation, reduced

2

transmission range, and increased error rates. Moreover, conventional physical-layer solutions often fall short under severe underwater conditions, necessitating the integration of advanced signal processing, error correction, and adaptive control techniques. The key challenges encountered in UOWC system are summarized below:

1. Severe signal fading due to absorption and scattering in the underwater medium, which limits communication reliability.

2. Non-linear distortion and temporal signal fluctuations caused by dynamic changes in water properties.

3. Limited transmission range, especially in turbid water, due to high attenuation of optical signals.

4. Beam wandering and misalignment caused by underwater currents, vibrations and movement of transceivers.

5. Turbulence-induced channel fading, leading to fluctuations in signal strength and quality.

6. Pointing errors due to transmitter-receiver misalignment, particularly in mobile underwater platforms.

7. High Bit Error Rates (BER) resulting from burst errors that cannot be corrected by simple error detection techniques.

8. Interruption of communication links under unpredictable environmental conditions such as salinity changes or temperature gradients.

9. Dependency on LOS propagation, which limits flexibility in network topology and link availability.

10. Inadequacy of physical-layer solutions, especially in strong turbulence or high-noise environments.

11. Need for intelligent and adaptive mechanisms to dynamically compensate for distortions and fading in real time.

12. Security vulnerabilities, as optical signals may be intercepted or distorted without appropriate protection.

13. Limited energy and computational resources in underwater nodes, restricting complex signal processing algorithms.

14. Lack of standardized UOWC models and protocols for real-world deployment across varying underwater conditions.

1.4 Objectives

UOWC system face several critical challenges that hinder their reliable and efficient deployment in practical environments. One major problem is the severe signal fading and line-of-sight dependency, which reduce communication reliability in turbulent underwater conditions. Additionally, limited transmission range and high path loss impaired by misalignment and mobility pose serious constraints on system performance. Moreover, the absence of robust error correction and data protection mechanisms makes this system vulnerable to transmission errors and security threats. Lastly, non-linear distortion and dynamic channel fluctuations further degrade link stability and data fidelity, especially under real-time operating conditions.

To solve these problems, the following objectives have been formulated:

Objective 1: To develop a MIMO-based UOWC system that mitigates fading and line-of-sight limitations by leveraging spatial diversity, enhancing communication reliability under underwater turbulence conditions.

Objective 2: To design a dual-hop relaying-based UOWC system that enhances transmission range and reliability by mitigating path loss and accurately modelling the impact of pointing errors caused by underwater misalignment and mobility.

Objective 3: To enhance the reliability and security of UOWC system by integrating robust channel coding schemes such as RS codes for effective error correction and protection against data interception in turbulent underwater environments.

Objective 4: To develop an adaptive UOWC system employing machine learning, specifically CNNs, to dynamically mitigate non-linear distortion and turbulence-induced fluctuations, thereby enhancing real-time link stability and data fidelity.

1.5 Research methodology

This research adopts a comprehensive and structured methodology that integrates physical-layer modelling, cooperative communication techniques, channel coding schemes, and deep learning-based signal processing to enhance the performance and reliability of UOWC system under challenging underwater conditions.

The following steps outline the core methodology employed throughout this thesis:

- The study begins with the detailed modelling of the UOWC channel under moderate to strong turbulence conditions. Relevant parameters such as absorption, scattering, and turbulence-induced fading are incorporated to simulate realistic underwater environments. The model accounts for statistical channel behaviour to accurately reflect performance under varying conditions.

- A MIMO UOWC architecture is developed to mitigate the limitations of LoS communication. The system design includes the integration of spatial diversity techniques to enhance communication robustness. Analytical derivations are performed to obtain closed-form expressions for key performance metrics such as BER, outage probability, and ergodic capacity for the proposed MIMO-based configuration.

- To address the range limitation and signal attenuation in long-distance communication, a dual-hop cooperative relaying-based UOWC framework is proposed. The system is designed to split a long optical link into two hops using an intermediate relay. The methodology includes modelling the end-to-end performance under Málaga fading and considering the effect of pointing errors due to misalignment. Closed-form performance expressions are derived to evaluate system behaviour under various configurations.

- To overcome the limitations of physical-layer-only approaches, robust channel coding techniques are incorporated. The study focuses on the design and analysis of RS codes for burst error correction and data integrity. Analytical modelling includes the derivation of expressions for decoding error probability and error correction capability under varying turbulence levels. The RS coding scheme is integrated with the system model to examine its effectiveness under strong channel impairments.

- A deep learning framework based on CNNs is proposed for modulation classification in UOWC system. The model is trained to classify different modulation formats such as Phase Shift Keing (PSK) and Quadrature Amplitude Modulation (QAM) under Gamma–Gamma turbulence conditions. The methodology includes dataset generation, model training, validation, and

5

testing, aiming to establish an intelligent signal processing approach that can adapt to dynamic underwater environments.

Each of these components is developed in a modular fashion and evaluated within a simulated UOWC environment to ensure the reliability, adaptability, and scalability of the proposed solutions. The combined methodology serves to address key challenges in underwater communication, including fading, attenuation, alignment errors, and non-linear distortions.

1.6   Thesis outline

The thesis is outlined as follows

Chapter 2 (Literature Review): This chapter presents a detailed review of existing research and ongoing developments in the field of UOWC. It examines various communication techniques, modulation schemes, and system architectures proposed in the literature. Furthermore, the chapter highlights the limitations of current approaches and identifies research gaps that form the foundation for the discussions and contributions in the subsequent chapters.

Chapter 3 (Design and performance evaluation of a novel MIMO Underwater Optical Wireless Communication link over Gamma–Gamma fading channel): In this chapter, a novel MIMO-based UOWC system employing the Gamma-Gamma distribution is designed to mitigate signal fading and line-of-sight limitations by leveraging spatial diversity. The system is developed for both detection schemes, i.e. Intensity Modulation/Direct Detection and heterodyne detection to enhance communication reliability under varying levels of underwater turbulence. Additionally, closed-form expressions for key performance metrics, including average bit error rate, outage probability, and ergodic capacity, are derived to provide a comprehensive analytical evaluation of the proposed system.

Chapter 4 (Performance analysis of dual-hop relaying in Malaga-distributed Underwater Optical Wireless Communication system with pointing error): In this chapter, a dual-hop relaying-based UOWC system employing the Málaga distribution is designed to enhance transmission range and improve link reliability. The system

6

effectively mitigates path loss and accurately models the impact of pointing errors arising from underwater misalignment and mobility. Furthermore, closed-form expressions for average bit error rate, outage probability, and ergodic capacity are derived to analytically evaluate the performance of the proposed system under various underwater turbulence conditions.

Chapter 5 (Performance evaluation of Reed–Solomon coded Underwater Optical Wireless Communication system over Gamma-Gamma fading channel): In this chapter, the reliability and security of underwater optical wireless communication system are enhanced by integrating robust channel coding schemes, specifically Reed-Solomon codes, to enable effective error correction and provide protection against data interception in turbulent underwater environments. The performance of the RS-coded UOWC system is analysed under Gamma-Gamma fading channels, with a focus on evaluating the decoding error probability as a key performance metric.

Chapter 6 (Deep learning-based constellation signal classification in Underwater Optical Wireless Communication system): In this chapter, deep learning techniques are leveraged to perform modulation classification in UOWC system. The approach involves converting raw modulated signals into constellation images and utilizing a pre-trained Convolutional Neural Network, specifically SqueezeNet, to classify the modulation schemes. This method enhances the system's ability to intelligently recognize signal types under varying underwater conditions, contributing to more adaptive and efficient communication.

Chapter 7 (Conclusions, Future Scope and Social Impact): This chapter provides a comprehensive summary, further implementation and social impact of the research findings.

Each chapter builds upon the previous one to progressively enhance the system's reliability and performance under real-world underwater conditions. The outlined structure ensures a logical flow of ideas, from problem formulation and theoretical development to system design and proposed solutions, thereby providing a comprehensive foundation for the research conducted in this work.

1.7 Conclusion

This chapter provided an overview of the research work, beginning with a general introduction to UOWC system, followed by the motivation behind selecting this research domain. The key challenges associated with UOWC were identified, forming the basis for the well-defined research objectives. A systematic research methodology was outlined to address these challenges using a combination of physical-layer techniques, cooperative communication strategies, error correction coding, and signal classification methods. Finally, the thesis structure was presented to guide the reader through the subsequent chapters. Together, these elements lay the foundation for the detailed investigation and proposed solutions that follow in the thesis.

CHAPTER 2

LITERATURE REVIEW

2.1 Introduction

UOWC has emerged as a promising technology for high-speed, low-latency underwater data transmission, suitable for applications such as sensor networks, real-time video monitoring and AUV control. Unlike traditional acoustic communication, UOWC offers significantly higher bandwidth but is also more susceptible to environmental impairments. The underwater optical channel is highly dynamic and affected by absorption, scattering, and turbulence, which severely limit the communication range and reliability. In addition to these physical limitations, UOWC system face challenges such as the requirement for LOS alignment, vulnerability to beam misalignment due to underwater mobility, and sensitivity to variations in temperature and salinity. These factors often lead to burst errors, signal fading, and frequent link interruptions, making it difficult to maintain stable and efficient communication. To address these challenges, extensive research has been conducted across various domains of UOWC system design. The following sections present a detailed review of the relevant literature in this field.

2.2 Channel modelling in UOWC system

Channel modelling in UOWC system is essential for accurately characterizing the impact of the underwater environment on signal propagation. Key factors such as absorption, scattering, turbulence and temperature gradients influence the optical signal's attenuation and distortion. Various statistical models, including exponential, log-normal, and Gamma-Gamma (GG) distributions, are used to represent different turbulence regimes. The performance of UOWC links under the influence of air bubbles has been experimentally evaluated, demonstrating that varying bubble populations can significantly affect signal attenuation and transmission reliability. These findings offer important insights for the design of robust UOWC system in

practical underwater environments [1]. The impact of turbulence-induced fading on spatial diversity schemes such as Single Input Multiple Output (SIMO) and MIMO has been analytically studied using accurate statistical distributions. The results showed substantial improvements in BER, laying a foundation for exploiting diversity in underwater environments to enhance communication quality [2]. A subsequent detailed analysis of MIMO-based UOWC system incorporated channel modelling, symbol detection, and error mitigation strategies. This study revealed that combining spatial multiplexing with robust detection algorithms and diversity channels can significantly increase throughput, positioning MIMO as a strong candidate for deep-sea communication [3]. The challenges of vertical Non-Line-of-Sight (NLoS) optical propagation in underwater scenarios have been addressed through proposed channel estimation and error correction techniques. The use of RS coding in particular was shown to enhance system robustness against multipath-induced signal distortions [4].

The spectral characteristics of oceanic turbulence and their role in generating optical scintillation have been analysed, highlighting the relationship between turbulence scales and signal degradation. This emphasizes the need for advanced models like the Gamma–Gamma and Málaga distributions for designing high-fidelity UOWC system [5]. Spatial diversity strategies have also been simulated in UOWC channels employing multiple photodetectors. Results demonstrated that MIMO architectures, when paired with optimized detection strategies, can form a scalable and dependable solution for deep-water data transmission [6]. To enhance signal strength and link stability, the combination of optical amplification with spatial diversity has been proposed. Multi-aperture system were found to significantly improve SNR, particularly under conditions of high absorption and scattering [7]. Performance characterization of UOWC channels has been supported by both analytical and experimental validations. The introduction of novel modulation schemes and innovative photodetector arrangements proved effective in maximizing spectral efficiency under turbulent conditions [8]. The effect of turbulent-flow-induced scintillation on underwater optical beams has been studied in detail. The findings emphasized how environmental dynamics impact intensity fluctuations and proposed methods such as beam shaping and enhanced channel coding to mitigate scintillation

10

noise [9]. A unified statistical model has been developed to capture various underwater fading conditions under a single framework. The Exponential Gamma–Gamma (EGG) based model showed high accuracy in predicting intensity fluctuations and facilitated the derivation for BER and capacity [10].

A broad review of practical UOWC system deployments identified key limitations, including beam divergence, hardware alignment issues, and challenges in real-time adaptation. These insights provide a benchmark for aligning theoretical modelling with real-world constraints [11]. A general stochastic modelling approach for UOWC links has yielded closed-form expressions for capacity and BER across different turbulence intensities. This approach effectively bridges theoretical analysis and practical performance evaluation [12]. Validation of the GG distribution under strong turbulence conditions has shown it to be a reliable model across various environmental scenarios. This supports its continued use in future analytical and simulation studies involving underwater optical communication [13]. Table 2.1 shows a comparison of various distribution functions used to model underwater channel.

Table 2.1 Comparison of various distribution functions used to model underwater channel

Distribution	Mathematical Type	Applicable Turbulence Regime	Strengths	Limitations
Lognormal [14]	Single-lobe, log-amplitude Gaussian	Weak turbulence	Simple and classical model	Fails under moderate/strong fading
K-Distribution [15]	Bessel function-based heavy tail	Strong turbulence	Handles strong turbulence with large variance	Not valid for weak turbulence

11

Weibull [16]	Two-parameter distribution	Moderate (empirical fits)	Useful in empirical studies	Physically less interpretable
Exponentiated Weibull [17], [18]	Three-parameter skewed extension	Moderate to strong	Excellent empirical fit for irradiance fluctuations	Increased computational complexity
Gamma-Gamma [14]	Product of two independent Gamma RVs	Moderate to strong	Composite modelling of small and large-scale fading	Not accurate under weak turbulence
Generalized Gamma [19]	Unified form (Weibull/Gamma special case)	Weak to strong	Best overall GoF across multiple regimes	Parameter estimation can be intensive
Proposed model using Gamma-Gamma and Spatial Diversity [20]	Composite fading + aperture diversity gain	Moderate to strong	Enhances performance with spatial diversity (e.g., MIMO)	Requires multi-aperture deployment

2.3 Relaying techniques for enhancing link performance

Recent studies have significantly advanced the understanding of multi-hop and dual-hop strategies in UOWC system, particularly under conditions of severe turbulence and alignment uncertainties. A unified analytical framework has been developed for

evaluating dual-hop UOWC system affected by composite turbulence-induced fading and pointing errors. This framework models end-to-end BER and Outage Probability (OP) using the Málaga distribution, offering a flexible representation of underwater turbulence varying from weak to strong regimes. It also accounts for beam misalignment caused by mobility or water currents and provides closed-form expressions that capture both fading and geometrical losses [21].

The average channel capacity of plane wave propagation under oceanic turbulence modelled by the GG distribution has been analysed with a focus on Refractive Index (RI) fluctuations caused by environmental variability. The analysis demonstrates how scintillation impacts system capacity and highlights the importance of statistical averaging over the fading process to gain an accurate understanding of long-term link reliability [22]. Further contributions to turbulence modelling have resulted in closed-form expressions for OP and Ergodic Capacity (EC) under anisotropic turbulence modelled by the Málaga distribution. These findings reveal that spherical wavefronts exhibit greater resilience to deep fades than plane waves and confirm that pointing errors exacerbate performance degradation in turbulent conditions [23].

The capacity of point-to-point UOWC links operating in turbulence-dominated regimes has also been evaluated by incorporating beam wander and spatial misalignment effects. The results shed light on how divergence angle and beam width influence channel capacity, especially in large-scale underwater network deployments [24]. From an application perspective, multi-hop communication schemes in the Internet of Underwater Things (IoUT) have been explored using decode-and-forward relays. System-level analysis under realistic underwater channel constraints demonstrates that energy-efficient relaying protocols can enhance data delivery reliability while ensuring power-aware operation, thereby supporting robust connectivity in distributed underwater networks [25].

13

Table 2.2 Comparative summary of UOWC studies with various relaying technique

Channel Model	Relaying Type	Pointing Error Modelled	Performance Metrics	Remarks
Gamma–Gamma [26]	DF	✗	OP, BER	Did not consider misalignment; focused on basic dual-hop modelling
Log-normal [27]	AF	✓	BER, EC	Covered relay optimization under moderate turbulence
Málaga [28]	DF	✗	OP (closed-form)	Introduced Málaga fading model into dual-hop UOWC
Exponential Generalised Gamma [29]	DF	✓	OP, EC	Jointly model pointing error and EGG.
Proposed Málaga and Pointing [30]	DF	✓	OP, BER, EC (closed-form)	Extends prior models by deriving compact closed-form expressions and showing system-level design insights

2.4 Robust coding techniques for optical underwater links

The impact of atmospheric turbulence on Free-Space Optical (FSO) communication has been addressed through the use of RS-coded coherent Orthogonal Frequency Division Multiplexing (OFDM) system. This approach has shown that RS coding significantly reduces BER under turbulent conditions, thereby improving link quality and reliability in FSO applications [31]. In the context of high-speed UOWC, On–Off

Keying (OOK) modulation combined with RS coding has been used to enhance system reliability. Simulation results indicate that RS codes can effectively correct burst errors caused by underwater fading and misalignment, thereby improving signal integrity [32]. Robustness of RS-coded OFDM-based FSO system over log-normal turbulent channels has also been evaluated. Performance analyses including BER, eye diagrams, and received power highlight the capability of RS coding to counteract turbulence-induced degradation, leading to improved system resilience [33].

For underwater optical channels subject to log-normal turbulence, the integration of Multi-Pulse Pulse Position Modulation (MPPM) with Low-Density Parity-Check (LDPC) coding has been shown to enhance energy efficiency and BER performance. This coding strategy proves especially beneficial under typical fading conditions found in underwater environments [34]. An adaptive method combining channel coding and power control has been proposed for UOWC system operating under turbulent conditions. This strategy dynamically adjusts RS codes and transmission power in response to channel fluctuations, resulting in better BER and power efficiency [35]. LDPC codes have also been analysed for their effectiveness in FSO system affected by turbulence. Simulation outcomes demonstrate that LDPC offers substantial coding gain and resilience, making it a valuable solution for reducing BER in optical wireless links [36]. A comparative study of Bose–Chaudhuri–Hocquenghem (BCH) and LDPC codes has revealed that LDPC provides superior performance in terms of channel capacity and BER, particularly in severe turbulence scenarios. These findings reinforce the suitability of LDPC coding for high-reliability optical communication system [37]. A novel phase-modulated UOWC system employing Mach–Zehnder interferometers has also been developed. Incorporating Forward Error Correction (FEC), this system design demonstrates reliable transmission under turbulent underwater conditions, making it a promising solution for real-time optical links [38]. Table 2.3 shows the summary of various FEC techniques used for UOWC system.

15

Table 2.3 Comparative summary of various forward error correction techniques used for UOWC system

FEC Technique	Channel Model	Modulation Scheme	Performance Metrics	Remarks
Reed–Solomon (RS) [39]	Absorption and Scattering	OOK	BER	RS codes improved BER in turbid underwater environments.
Convolutional Codes [40]	Gamma-Gamma	BPSK, OOK	BER, OP	Convolutional and interleaving provided robustness in moderate turbulence.
LDPC Codes [41]	Experimental Seawater Channel	OOK	BER	LDPC outperformed RS at high SNRs; decoding complexity is higher.
Turbo Codes [42]	Málaga and Pointing Error	BPSK	BER, Capacity	Turbo codes perform well under severe fading and misalignment.
Polar Codes [43]	Log-normal	QAM	BER, Throughput	Polar codes showed strong throughput and performance at low latency.

2.5   Deep learning-based approaches in UOWC

The error performance of UOWC system has been evaluated by analysing the effects of turbulence under various coding and modulation schemes. Results indicate that the careful selection of modulation formats and channel coding is essential for mitigating bit errors in underwater environments [44]. A rapid signal quality monitoring technique for coherent communication system has been developed using deep learning. The CNN-based method processes eye diagrams to efficiently assess signal integrity and is suitable for adaptation in dynamic optical channels [45]. An adaptive channel estimation method leveraging the Sherman–Morrison formula has been introduced to reduce matrix inversion complexity. This approach improves estimation accuracy and presents a practical solution for real-time adaptive channel tracking [46].

To enhance wireless network channel estimation, deep residual networks have been applied for handling the nonlinear characteristics of dynamic environments. The use of deep learning significantly improves estimation accuracy and robustness [47]. For underwater visible light communication system, a novel channel estimation technique has been designed to address challenges related to scattering and absorption. The proposed method offers reliable performance in complex aquatic propagation conditions [48]. Recognition of man-made objects in underwater optical images has been made possible through a specialized Deep Learning (DL) framework. The model demonstrates strong accuracy even in turbid and optically distorted conditions, enabling its use in underwater inspection and monitoring tasks [49]. A DL-based channel estimation scheme has also been proposed for MIMO visible light communication system. The use of neural networks enhances estimation precision, particularly in challenging multipath propagation scenarios [50]. For underwater acoustic channels, a DL-based OFDM system has been implemented. The system employs autoencoders and neural demodulators to increase decoding accuracy under turbulent acoustic conditions [51]. A MIMO-based optical camera communication system tailored for underwater environments has been introduced. The system combines spatial multiplexing with improved channel modelling to enhance the transmission of image data in aquatic settings [52]. Machine Learning (ML) has also

17

been employed to design a dynamic channel selection algorithm for multi-channel underwater wireless system. This approach improves communication performance by selecting the most efficient channels based on real-time metrics [53]. To support AUV applications, an image classification approach using ML has been developed. The classifier delivers high recognition accuracy and supports effective underwater perception and monitoring [54]. Table 2.4 shows the summary of modulation classification approaches in UOWC system.

Table 2.4 Comparative summary of modulation classification approaches in UOWC system

Model Type	Input Features	Modulation Formats	Channel Conditions	Key Findings
Classical ML (SVM, KNN) [55]	Manually extracted (amplitude, phase)	BPSK, QPSK	AWGN, Rayleigh	Requires stable environments, poor underwater generalization
Decision Trees [56]	Time-domain statistics	BPSK, QAM	Fading + mild noise	Limited performance under severe turbulence
CNN [57]	I/Q samples (1D)	BPSK, QPSK, QAM	AWGN, Rayleigh	DL outperforms ML under general fading
CNN [58]	2D Constellation	BPSK, QPSK	Gamma–Gamma fading	CNN captures spatial distortion from fading
SqueezeNet [59]	2D Constellation + Augmentation	BPSK, 8PSK, 16QAM	Strong turbulence	Achieved lightweight high-accuracy recognition

18

Proposed SqueezeNet model [60]	2D Constellation Diagrams	BPSK, QPSK, 8PSK, 16QAM	Gamma–Gamma fading + noise	Accurate, efficient classification for real-time adaptive UOWC system

2.6 Conclusion

This chapter presented a comprehensive review of existing research efforts in the domain of UOWC system. It began with an overview of channel modelling techniques, emphasizing how underwater turbulence, absorption, and scattering significantly affect signal propagation and reliability. Various statistical models, such as GG and Málaga distributions, have been explored to represent these impairments accurately and support realistic system design. The review then focused on relaying techniques, where cooperative and dual-hop strategies were found effective in extending communication range and mitigating high path loss in challenging underwater environments. FEC methods were also discussed, with particular emphasis on RS codes, which play a crucial role in correcting burst errors and preserving data integrity under turbulent conditions. Recent developments in DL-based approaches were examined, highlighting the use of CNNs for modulation classification and adaptive signal processing. These techniques demonstrate strong potential for making UOWC system more intelligent and responsive to dynamic environmental changes.

The literature suggests that addressing UOWC challenges requires a hybrid approach that combines physical-layer design, relaying, robust coding, and intelligent algorithms. The findings of this review provide a strong foundation for the integrated solution proposed in the subsequent chapters of this thesis.

19

CHAPTER 3

DESIGN AND PERFORMANCE EVALUATION OF A NOVEL

MIMO UNDERWATER OPTICAL WIRELESS

COMMUNICATION LINK OVER GAMMA–GAMMA FADING

CHANNEL

3.1   Introduction

The reliable operation of UOWC system is fundamentally challenged by the severe fading effects arising from underwater turbulence, scattering and beam wander. In order to meet the performance demands of modern UOWC applications, the development of accurate channel models, coupled with the adoption of advanced physical layer techniques, has become imperative. Spatial diversity techniques, particularly through the deployment of MIMO architectures, offer a promising approach to mitigating the limitations imposed by LoS constraints and to enhancing the overall flexibility of UOWC links against turbulence-induced impairments.

        The characterization of turbulence effects in UOWC environments is often conducted using the Rytov variance, which serves as a key indicator of turbulence strength. Among statistical fading models, the GG distribution has emerged as a widely accepted model capable of accurately capturing irradiance fluctuations over moderate to strong turbulence conditions. Furthermore, spatial diversity schemes such as Equal Gain Combining (EGC) at the receiver end have demonstrated significant potential in improving the reliability of optical communication system. Building upon these foundations, this chapter presents the design of a MIMO-enabled UOWC system operating over GG-fading channels. Nevertheless, the design and performance analysis of such system are complicated by several challenges. Among these the difficulty in deriving closed-form expressions for key performance metrics such as OP, average BER, and EC under the GG fading model is main. In addition, while OOK modulation has been predominantly explored in earlier works, there remains a pressing

20

need to examine the applicability of more advanced modulation schemes, including QAM and PSK, within practical UOWC scenarios.

In this chapter, a novel UOWC system model employing the GG distribution is proposed to accurately characterize the fading behaviour under turbulent underwater conditions. A spatial diversity-based MIMO configuration is utilized, wherein the total transmitted power is proportionally scaled with the number of transmitters, thereby extending the operational range and improving the robustness of the system. Furthermore, the system performance is comprehensively analysed under the Intensity Modulation/Direct Detection (IM/DD) scheme, using QAM and PSK modulation formats. Closed-form analytical expressions for the OP, average BER, and EC are derived to facilitate a thorough evaluation of the proposed system. The principal contributions of this chapter are summarized as follows:

- A UOWC system model employing the GG distribution is proposed to accurately capture the effects of turbulence-induced fading.
- A spatial diversity MIMO framework is integrated, wherein the transmitted power is increased in proportion to the number of transmitters, enhancing the link range and reliability.
- Performance analysis is extended beyond traditional OOK modulation, incorporating QAM and PSK schemes.
- Analytical expressions for OP, average BER, and EC are derived to provide comprehensive insights into the system performance under GG fading conditions.

3.2 Scintillation characterization in underwater optical channel

In UOWC, the channel is highly affected by environmental conditions such as temperature gradients, salinity fluctuations, and turbulence. To characterize these fluctuations, two key statistical measures are used, the Rytov variance and the Scintillation Index (SI). The Rytov variance quantifies the strength of optical turbulence and is particularly useful in identifying weak-to-strong fluctuation regimes. A low Rytov variance ($\ll 1$) indicates weak turbulence, whereas values approaching or exceeding 1 represent moderate to strong turbulence. As the author [61] presented the

power spectrum (ϕ_n^{ocean}) of RI using the classical Kolmogorov model and various parameters used to calculate the power spectrum are shown in table 3.1.

$$\phi_n^{ocean}(k) = k^{-11/3}\chi_T\frac{\varepsilon^{-1/3}}{2.577\times10^8}\times\left(e^{-A_T\delta}-2\tau^{-1}e^{-A_{TS}\delta}+\tau^{-2}e^{-A_S\delta}\right)\times\left[1+2.35(k\eta)^{2/3}\right] \quad (3.1)$$

Where $\delta = 8.284(k\xi)^{4/3}+12.978(k\xi)^2$, $A_T = 1.863\times10^{-2}, K = 2\pi/\lambda$, $A_{TS} = 1.9\times10^{-4}$, $A_S = 9.41\times10^{-3}$.

Table 3.1 Parameters associated with the calculate the power spectrum of RI.

Symbol	Parameter	Values
K	Spatial frequency	$15MHz$ at $\lambda = 0.417\,\mu m$
η	Kolmogorov scale	$10^{-3}m$
χ_T	Dissipation rate (temperature)	10^{-10} to $10^{-2}K^2/s$
τ	Range of temperature and salinity induced RI	[-5 and 0]
ε	Dissipation rate of the turbulent kinetic energy	$10^{-10}m^2/s^3$ to $10^{-1}m^2/s^3$

Now the power spectrum of RI is used to compute Rytov variance and it is given by

$$\sigma_R^2(z,\lambda) = 78.87zK^2\int_0^1\int_0^\infty k\phi_n^{ocean}(k)\left[1-\cos\left(\frac{zk^2}{K}\xi\right)\right]dkd\xi \quad (3.2)$$

where σ_R^2 is known as Rytov's variance, also α and β are parameters associated with the effective underwater conditions in [62] as

$$\alpha = \frac{1}{\exp\left[\frac{0.49\sigma_R^2}{\left(1+1.11\sigma_R^{12/5}\right)^{7/6}}\right]-1} \quad (3.3)$$

$$\beta = \frac{1}{\exp\left[\frac{0.51\sigma_R^2}{\left(1+0.69\sigma_R^{12/5}\right)^{5/6}}\right]-1} \quad (3.4)$$

Table 3.2 shows the fading parameters (α,β) computed with the help of σ_R^2 [63].

22

Table 3.2 Fading parameters based on the level of turbulence.

Turbulence level	Fading Parameters	
	α	β
Strong	2.296	2
Moderate	4.2	3
Weak	8	4

Fig. 3.1 shows the variation of Rytov variance versus propagating distance, where σ_R^2 increases on increasing the propagating distance.
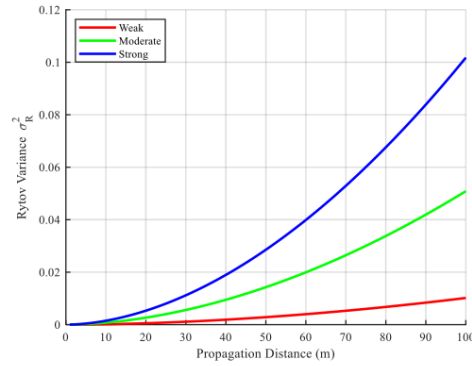
Figure 3.1 Variation of Rytov variance versus propagating distance

Also, due to the random variations in the RI of water, leading to intensity fluctuations known as scintillation in the received signal. Based on the Rytov variance, the SI is defined as the normalized variance of intensity fluctuations and it is calculated to provide a direct measure of signal degradation. Using eqn. (3.3) and eqn. (3.4) the SI is given as

$$\sigma_I^2 = \frac{1}{\alpha} + \frac{1}{\beta} + \frac{1}{\alpha\beta} \tag{3.5}$$

Now eqn. (3.5) has been plotted for various values of α and β. Fig. 3.2 shows the variation of SI and the fading parameters α and β.

23
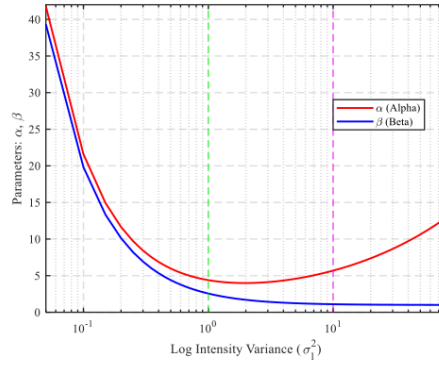
Figure 3.2 Variation of α and β versus scintillation index

Next section deals with the statistical modelling of Underwater Optical Turbulence (UOT) using GG distribution.

3.3 Statistical modelling of underwater optical turbulence using Gamma–Gamma distribution

Channel modelling plays a crucial role in evaluating the performance of any communication system. The incident light is affected due to three major phenomena scattering, absorption and UOT in the underwater channel. A log-normal distribution model has been used for weak UOT whereas GG distribution has been used for large scale and small-scale underwater turbulence. If I being the optical intensity and is a random variable, then the PDF of GG distribution can be expressed as

$$f_I(I) = 2(\alpha\beta)^{(\alpha+\beta)/2} K_{\alpha-\beta}\left(2\sqrt{\alpha\beta I}\right)\frac{I^{(\alpha+\beta)/2-1}}{\Gamma(\alpha)\Gamma(\beta)}, \qquad (3.6)$$

where K is the modified Bessel function.

Using eqn. (3.6) the intensity variation due to strong, moderate and weak turbulence can be computed and fig. 3.3 shows the intensity variation due to GG distribution versus irradiance.

24
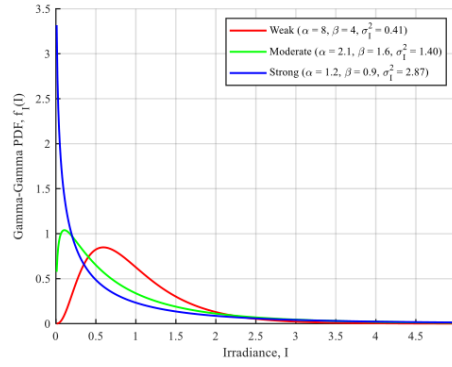
Figure 3.3 Intensity variation due to GG distribution versus irradiance

3.4 Design and analysis of spatial diversity MIMO architecture

Now the information is transmitted through the turbulence channel with the help of a laser. But due to turbulence underwater medium the signal strength gets deteriorated. To overcome this the use of physical layer techniques like spatial diversity has been used. Application of MIMO schemes has in particular been considered as a promising method for turbulence compensation in underwater communication links. With the use of multiple transmitters and/or receivers, MIMO provides multiple independent fading paths to improve signal reception. At the receiver end, multiple incoming signals are combined using methods such as EGC to improve the SNR and ensure more reliable communication. In the UOWC system, M lasers are placed at the transmitter side and N photodiodes are used at the receiver side. The photodiodes capture various optical signals, which are then merged using the EGC approach. A major benefit of using EGC is its ease of implementation, as it does not require adaptive amplifiers on the receiver side. [64]. Fig. 3.4 shows the block diagram of the proposed MIMO scheme for UOWC system using EGC.

25

In EGC technique the amplifiers at the receiving end have equal gains as $A_1 = A_2 = A_N$.
Since intensity variation is collected due to various photodiodes as a result there exist a joint distribution for the signal intensities received for MIMO scheme.
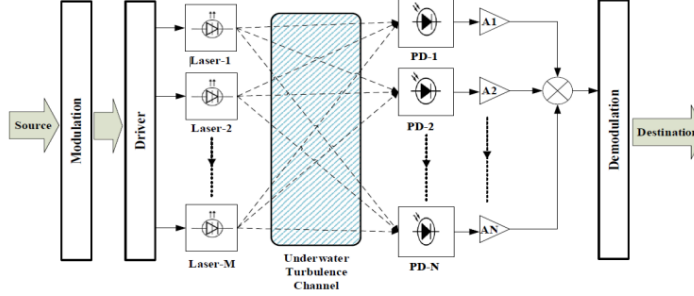
Figure 3.4 Block diagram of the proposed MIMO scheme for UOWC system

In [65] the distribution of intensity has been evaluated by using the generalized power series method and the received signal is given as

$$R = \frac{x\psi}{MN} \sum_{m=1}^{M} \sum_{n=1}^{N} I_{mn} + Y \qquad (3.7)$$

where R is the received signal, ψ is the power conversion factor, Y is the Additive White Gaussian Noise (AWGN) with zero mean and variance $N_o / 2$. Now using eqn. (3.7) in eqn. (3.6) along with $\alpha_1 = MN\alpha$ and $\beta_1 = MN\beta$ the intensity I can be viewed as

$$f_I(I) = \frac{2\left(\frac{\alpha_1\beta_1}{MN}\right)^{(\alpha_1+\beta_1)/2}}{\Gamma(\alpha_1)\Gamma(\beta_1)} I^{(\alpha_1+\beta_1)/2-1} K_{\alpha_1-\beta_1}\left(2\sqrt{\frac{\alpha_1\beta_1}{MN}I}\right) \qquad (3.8)$$

eqn. (3.8) can help in determining the various performance metrics, moreover, it simplifies the analytical calculation also. Two detection mechanisms known as Optical Heterodyne Detection (OHD) and IM/DD with a variety of modulation schemes have been proposed. In the analysis, the fading characteristics have dominated the effect of absorption/scattering and their effects like Inter Symbol Interference (ISI) are also

26

insignificant. General expressions to compute instantaneous SNR is given by eqn. (3.9), average electrical SNR by eqn. (3.10) and average SNR by eqn. (3.11) respectively.

$$\gamma = \frac{(\eta I)^r}{N_o} \tag{3.9}$$

$$\mu_r = \frac{(\eta E[I])^r}{N_o} \tag{3.10}$$

$$\overline{\gamma} = \mu_r \frac{E[I^r]}{E[I]^r} \tag{3.11}$$

Now utilising the above equation, along with $E[I] = MN$, the average electrical SNR is given as $\mu_1 = \overline{\gamma}$. On substituting in eqn. (3.8) and utilizing eqn. (3.12) and (3.13) the PDF of the UOWC system when operated in OHD can be given as eqn. (3.11)

$$G_{0,2}^{2,0}(z \mid b, c) = 2z^{\frac{1}{2}(b+c)} K_{b-c}(2\sqrt{z}) \tag{3.12}$$

$$G_{p,q}^{m,n}\left(z \left| \begin{array}{c} \alpha + a_1, ..., \alpha + a_n, \alpha + a_{n+1}, ..., \alpha + a_p, \\ \alpha + b_1, ..., \alpha + b_m, \alpha + b_{m+1}, ..., \alpha + b_p \end{array}\right.\right) = z^{\alpha} G_{p,q}^{m,n}\left(z \left| \begin{array}{c} a_1, ..., a_n, a_{n+1}, ..., a_p, \\ b_1, ..., b_m, b_{m+1}, ..., b_p \end{array}\right.\right) \tag{3.13}$$

$$f_{\gamma}(\gamma) = \frac{1}{\Gamma(\alpha_1)\Gamma(\beta_1)\gamma} G_{0,2}^{2,0}\left[\frac{\alpha_1\beta_1}{MN}\frac{\gamma}{\mu_1} \left| \begin{array}{c} - \\ \alpha_1, \beta_1 \end{array}\right.\right], \tag{3.14}$$

where $G_{p,q}^{m,n}[.]$ is the Meiger-G function defined in [66]. IM/DD shows lower complexity and it is cost-effective too. While OHD has a high capacity as compared to the previous mechanism. Also, at a low SNR the gap between these two detection mechanisms is constant in terms of capacity, however it increases at high SNR. By utilising eqn. (3.9), (3.10) and (3.11) along with eqn. (3.15), average electrical SNR μ_2 is given as eqn. (3.16).

$$E[I^2] = M^2 N^2 \left(1 + \frac{1}{\alpha_1}\right)\left(1 + \frac{1}{\beta_1}\right) \tag{3.15}$$

$$\mu_2 = \overline{\gamma} \frac{\alpha\beta}{1 + \alpha + \beta + \alpha\beta} \tag{3.16}$$

27

On substituting eqn. (3.16) in eqn. (3.8) and utilizing eqn. (3.12) and (3.13), the PDF of the UOWC system operated under IM/DD can be expressed as

$$f_\gamma(\gamma) = \frac{1}{2.\Gamma(\alpha_1)\Gamma(\beta_1)\gamma} \times G_{0,2}^{2,0}\left[\frac{\alpha_1\beta_1}{MN}\left(\frac{\gamma}{\mu_2}\right)^{1/2}\middle| \begin{array}{c} - \\ \alpha_1,\beta_1 \end{array}\right]. \tag{3.17}$$

Using eqn. (3.14) and (3.17), by utilizing eqn. (8.4.3/1) and (8.2.2/15) from [67], the unified expression for PDF which expressed both OHD and IM/DD schemes has been obtained as

$$f_\gamma(\gamma) = \frac{1}{r\Gamma(\alpha_1)\Gamma(\beta_1)\gamma} G_{0,2}^{2,0}\left[\frac{\alpha_1\beta_1}{MN}\left(\frac{\gamma}{\mu_r}\right)^{1/r}\middle| \begin{array}{c} - \\ \alpha_1,\beta_1 \end{array}\right]. \tag{3.18}$$

Simulation model of the proposed UOWC system implemented in Opti System is shown in fig. 3.5. The system comprises (a) a transmitter section employing QAM modulation and Mach–Zehnder modulation of a 532 nm CW laser and (b) a receiver section incorporating an NLOS underwater channel model with intensity scintillation enabled. Signal visualization tools are used at various stages for performance analysis. Appendix-I contains the respective eye diagrams, constellation diagrams and specifications for the proposed system.

(a)

28

(b)

Figure 3.5 Simulation model of the proposed MIMO UOWC system implemented in Opti System (a) transmitter (b) receiver section
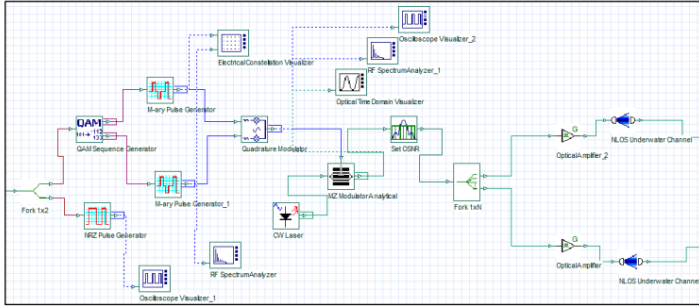
The performance of any UOWC system can be best analysed using its performance parameters like EC, average BER, and OP. In the next section analytical the closed-form expression for performance metrics have been achieved.

3.5   Analytical evaluation of system performance

To better understand how the UOWC system performs under real-world turbulent conditions, the analytical evaluation focusing on three important performance metrics: EC, OP, and average BER. These metrics help capture different aspects of system behaviour, how much data can be reliably transmitted on average (EC, how often the signal quality falls below a certain threshold (OP), and how frequently errors occur during transmission (average BER). Each of these parameters has been calculated using analytical expressions derived from the GG fading model, which accurately reflects underwater turbulence. The results for each metric are presented separately in the following sections, offering a clear picture of how channel conditions impact system efficiency, reliability, and error performance.

29

3.5.1 Ergodic Capacity

EC is an important feature that illustrates the performance of UOWC system. Because instantaneous SNR is a random variable, EC is also a random value, and its average value for UOWC system is determined in [68] as

$$\bar{C} = \int_0^\infty B \log_2(1+\gamma) f_\gamma(\gamma) d\gamma. \tag{3.19}$$

On substituting eqn. (3.18) in eqn. (3.19), the closed-form expression for EC has been derived as

$$\bar{C} = \frac{B}{4\pi \ln 2} \frac{(\alpha_1 \beta_1)^{\frac{(\alpha_1+\beta_1)}{2}}}{\Gamma(\alpha_1)\Gamma(\beta_1)} \left(\frac{1}{\mu_r}\right)^{\frac{(\alpha_1+\beta_1)}{4}}$$

$$\times G_{2,6}^{6,1}\left[\frac{\alpha_1^2 \beta_1^2}{16\mu_r} \middle| \begin{array}{c} -\frac{\alpha_1+\beta_1}{4}, -\frac{\alpha_1+\beta_1}{4}+1 \\ \frac{\alpha_1-\beta_1}{4}, \frac{\alpha_1-\beta_1+2}{4}, \frac{\beta_1-\alpha_1}{4}, \frac{\beta_1-\alpha_1+2}{4}, -\frac{\alpha_1+\beta_1}{4}, -\frac{\alpha_1+\beta_1}{4} \end{array}\right] \tag{3.20}$$

It has been seen from eqn. (3.20) that as SNR increases, channel capacity also increases.

3.5.2 Average Bit Error Rate

A generalized expression has been derived to calculate the average BER for different modulation schemes under both IM/DD and OHD techniques. The general expression of average BER can be expressed as

$$P_e = \frac{\delta}{2\Gamma(p)} \sum_{k=1}^n \int_0^\infty \Gamma(p, q_k \gamma) f_\gamma(\gamma) d\gamma, \tag{3.21}$$

where $\Gamma(p, q_k \gamma)$ is incomplete gamma function and δ, p, q_k, n are the parameter that describes the specific modulation scheme. Table 3.3 shows different values of the parameter associated with various modulation schemes corresponding to detection mechanism i.e. IM/DD or OHD.

30

Table 3.3 Parameters associated with different modulation schemes

Modulation	δ	p	q_k	n
On-Off keying (OOK)	1	1/2	1/4	1
M-ary Phase Shift Keying (M-PSK)	$\dfrac{2}{\max(\log_2 M, 2)}$	1/2	$\sin^2\left(\dfrac{(2k-1)\pi}{M}\right)$	$\max\left(\dfrac{M}{4}, 1\right)$
M-ary Quadrature Amplitude Modulation (M-QAM)	$\dfrac{4}{\log_2 M}\left(1 - \dfrac{1}{\sqrt{M}}\right)$	1/2	$\dfrac{3(2k-1)^2}{2(M-1)}$	$\dfrac{\sqrt{M}}{2}$

Since OOK is the most commonly used modulation technique in practical UOWC system, the average BER for the IM/DD method has been examined. Additionally, the average BER performance of M-PSK and M-QAM, both widely used in coherent communication system has also been analysed. By substituting eqn. (3.18) into eqn. (3.21), utilizing eqn. (1) and eqn. (2) from appendix A-1, an expression for average BER has been derived for OOK, BPSK, M-PSK, and M-QAM, and it is given by

$$P_e = \frac{\delta}{2\Gamma(p)}\left(\frac{r^{\alpha_1+\beta_1}}{(2\pi)^{r-1}}\right)\sum_{k=1}^{n} G_{2,2r+1}^{2r,r}\left[\left(\frac{\alpha_1\beta_1}{MNr^2}\right)^r \frac{1}{\mu_r q_k}\middle| \begin{matrix} 1,(1-p) \\ \Delta(r,\alpha_1),\Delta(r,\beta_1),0 \end{matrix}\right]. \qquad (3.22)$$

3.5.3 Outage Probability

In underwater fading channels, OP serves as an important metric for assessing the performance of UOWC system. It represents the likelihood that the instantaneous SNR drops below a specified threshold. The general expression for OP is given as

$$P_{out} = P_r(\gamma \le \gamma_{th}) = F_\gamma(\gamma_{th}). \qquad (3.23)$$

The CDF can be obtained by evaluating $F_\gamma(\gamma) = \int_0^\gamma f_\gamma(\gamma)d\gamma$. On substituting eqn. (3.18) in the expression of CDF, and utilizing eqn. (3) from appendix A-1. The CDF can be obtained as

31

$$F_I(I) = \frac{(\alpha_1\beta_1)^{(\alpha_1+\beta_1)/2}}{\Gamma(\alpha_1)\Gamma(\beta_1)MN} I^{(\alpha_1+\beta_1)/2} G_{1,3}^{2,1} \left[\alpha_1\beta_1 I \left| \begin{matrix} 1-\frac{\alpha_1+\beta_1}{2} \\ \frac{\alpha_1-\beta_1}{2}, \frac{\beta_1-\alpha_1}{2}, -\frac{\alpha_1+\beta_1}{2} \end{matrix} \right. \right]. \quad (3.24)$$

Substituting eqn. (3.24) into eqn. (3.23), the expression for OP can be obtained as

$$P_{out} = \left(\frac{\gamma_{th}}{\bar{\gamma}}\right)^{(\alpha_1+\beta_1)/2r} \times \frac{(\alpha_1\beta_1)^{(\alpha_1+\beta_1)/2}}{\Gamma(\alpha_1)\Gamma(\beta_1)} \times G_{1,3}^{2,1}\left[\alpha_1\beta_1\left(\frac{\gamma_{th}}{\bar{\gamma}}\right)^{1/r} \left| \begin{matrix} 1-\frac{\alpha_1+\beta_1}{2} \\ \frac{\alpha_1-\beta_1}{2}, \frac{\beta_1-\alpha_1}{2}, -\frac{\alpha_1+\beta_1}{2} \end{matrix} \right. \right]. \quad (3.25)$$

In [10] the EGG model is used to predict the performance of the UOWC system both analytically and experimentally. Table 3.4, shows the effect of the temperature gradient on the strength of turbulence. As temperature gradient increases the SI values increases which signifies strong attenuation.

Table 3.4 Estimated parameters of the EGG model, along with the parameters of the proposed system for temperature gradient UOWC system

Temp. Grad. $^{\circ}Ccm^{-1}$	σ_I^2	σ_r^2	α	β
0.22	3.1952	0.23903	0.9815	0.9276
0.22	1.9328	0.1795	1.4388	1.3661
0.1	0.4769	0.065	4.7488	4.5442
0.05	0.4201	0.0585	5.3286	5.1012
0.15	0.1915	0.0292	11.1556	10.699
0.05	0.1486	0.0231	14.2302	13.653

Table 3.5 Estimated parameters of the EGG model, along with the parameters of the proposed system for uniform temperature UOWC system.

Water Type	σ_I^2	σ_r^2	α	β
	0.1006	0.01596	20.8024	19.9673
Salty water	0.3111	0.04515	7.0445	6.7495
	1.1273	0.1258	2.2346	2.1298
	0.1088	0.0172	19.2796	18.5042
Fresh water	0.315	0.0457	6.954	6.6626
	1.0409	0.1189	2.3898	2.2788

The effect of water under uniform temperature is also analysed experimentally in [10]. Table 3.5 shows the estimated parameters of the EGG and the proposed model in both type of water.

In the next section, the numerical results along with the comparison of the GG model and EGG model with the proposed model are presented.

3.6 Results and discussion

The detailed discussion on the parameters which are responsible for affecting the UOWC system performance has been presented in this section. Analytical results obtained in the previous section are verified using plots and are used to demonstrate the EC, average BER, and OP of the UOWC link using the proposed model for turbulence fading channel. Moreover, various transmitter-receiver diversity MIMO schemes based on the EGC technique have also been incorporated in the proposed model to improve system performance. From table 3.4 it can be verified that higher the level of temperature gradient, higher is the value of SI leading to stronger turbulence resulting in the deterioration of system performance. Table 3.6 shows a comparison of the OP of the proposed system with GG [14] and EGG [10].

Table 3.6 Outage probability comparison of the proposed system with GG and EGG for OHD and IM/DD schemes

SNR (dB)	Outage Probability for OHD scheme			
	GG [14]	EGG [10]	Proposed 1×2 SIMO	Proposed 2×2 MIMO
0	0.99	1.00	1.00	1.00
5	0.92	0.99	0.95	0.98
10	0.72	0.60	0.66	0.62
15	0.46	0.47	0.28	0.13
20	0.25	0.26	0.079	9.9×10^{-3}
25	0.12	0.10	0.016	3.9×10^{-4}
30	0.052	0.035	2.8×10^{-3}	1.0×10^{-5}
35	0.022	0.011	4.4×10^{-4}	2.2×10^{-7}
40	8.6×10^{-3}	3.6×10^{-3}	6.3×10^{-5}	3.9×10^{-9}
45	3.4×10^{-3}	1.1×10^{-3}	8.7×10^{-6}	6.6×10^{-11}
50	1.3×10^{-3}	3.6×10^{-4}	1.2×10^{-6}	1.0×10^{-12}

33

SNR (dB)	Outage Probability for IM/DD scheme			
	GG [14]	EGG [10]	Proposed 1×2 SIMO	Proposed 2×2 MIMO
0	0.98	1.00	0.98	0.99
5	0.94	0.87	0.93	0.93
10	0.86	0.67	0.80	0.73
15	0.76	0.58	0.61	0.44
20	0.63	0.52	0.41	0.19
25	0.49	0.44	0.24	6.6×10^{-2}
30	0.37	0.33	0.13	1.8×10^{-2}
35	0.27	0.22	6.5×10^{-2}	4.0×10^{-3}
40	0.19	0.14	3.0×10^{-2}	7.8×10^{-4}
45	0.13	8.5×10^{-2}	1.3×10^{-2}	1.4×10^{-4}
50	8.7×10^{-2}	5.0×10^{-2}	5.5×10^{-3}	2.2×10^{-5}

Fig. 3.6 shows the OP versus normalized average SNR for strong turbulence condition $(\sigma_I^2 = 3.5918)$ operated under optical heterodyne detection. It is observed that introducing transmitter-receiver diversity leads to a reduction in outage probability, indicating a weakening of the fading effect. However, at low SNR levels (below 15 dB), the impact of the proposed diversity scheme on system performance is minimal. In contrast, at higher SNR values (above 15 dB), the use of diversity schemes results in a noticeable drop in OP, thereby enhancing the overall performance of the UOWC system.

From table 3.4, SI value has been chosen for salty and fresh water condition $(\sigma_I^2 = 1.12735)$ for thermally uniform UOWC channel and using eqn. (3.25) OP have been computed and a comparison with other existing models have been presented in table 3.7. The proposed 2×2 MIMO system achieves the lowest outage probability across all SNR levels, significantly outperforming both classical GG and EGG models. Notably, at 20 dB SNR, it reduces the outage probability to 9.9×10^{-3}, compared to 0.25 for GG and 0.26 for EGG, demonstrating superior reliability under GG-fading.

Table 3.7 Outage probability comparison of proposed model with existing model operated under salty and fresh water for thermally uniform UOWC channel

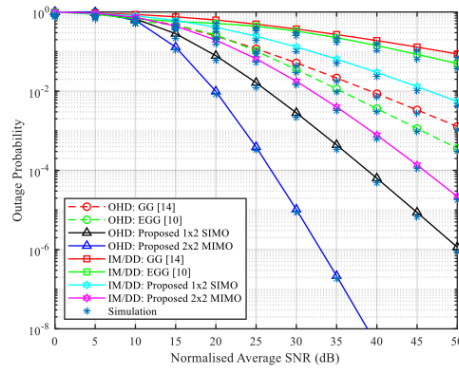| SNR (dB)	Outage Probability				
	GG [14]	EGG [10]	Proposed 1×2 SIMO	Proposed 1×3 SIMO	Proposed 2×2 MIMO
0	0.99	1.00	1.00	1.00	1.00
5	0.92	0.99	0.95	0.97	0.98
10	0.72	0.60	0.66	0.64	0.62
15	0.46	0.47	0.28	0.19	0.13
20	**0.25**	**0.26**	**0.079**	**0.027**	$\mathbf{9.9\times10^{-3}}$
25	0.12	0.10	0.016	2.5×10^{-3}	3.9×10^{-4}
30	0.052	0.035	2.8×10^{-3}	1.7×10^{-4}	1.0×10^{-5}
35	0.022	0.011	4.4×10^{-4}	9.6×10^{-6}	2.2×10^{-7}
40	8.6×10^{-3}	3.6×10^{-3}	6.3×10^{-5}	4.9×10^{-7}	3.9×10^{-9}
45	3.4×10^{-3}	1.1×10^{-3}	8.7×10^{-6}	2.4×10^{-8}	6.6×10^{-11}
50	1.3×10^{-3}	3.6×10^{-4}	1.2×10^{-6}	1.1×10^{-9}	1.0×10^{-12}

Figure 3.6 Outage probability versus normalized average SNR for strong turbulence condition operated under optical heterodyne detection

OP is plotted and a comparison of the existing turbulence models with the proposed model has been presented in fig. 3.7 for fresh and salty water under uniform

temperature conditions. OP as a function of normalized average SNR is presented for the moderate turbulence $(\sigma_I^2 = 1.12735)$ for thermally uniform salty water. Moreover, it can be seen from fig. 3.7 that salinity which creates rapid fluctuations in intensity affects the UOWC system performance but to a smaller extent. In this case, where the effect of turbulence decreases, OP keeps on decreasing. The proposed model outperforms the EGG model. Also, on introducing transmitter-receiver diversity, performance has been improved drastically.
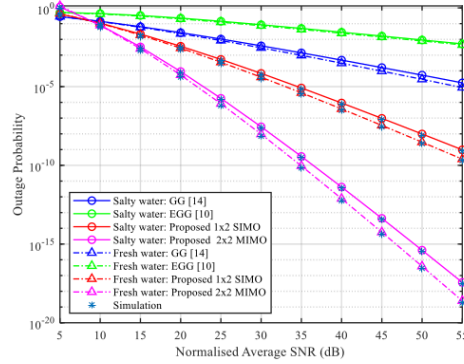
Figure 3.7 Outage probability comparison of proposed model with existing model operated under salty and fresh water for thermally uniform UOWC channel

Average BER comparison of the proposed system with the existing models operated under either OHD and IM/DD schemes under strong fading condition is shown in table 3.8 and 3.9 respectively. The proposed 2×2 MIMO system consistently achieves the lowest Average BER across all SNR values under the IM/DD scheme, indicating superior error performance. At 30 dB SNR, it reduces BER to 1.20×10^{-3}, significantly outperforming GG (2.00×10^{-1}) and EGG (3.90×10^{-2}).

36

Table 3.8 Average BER comparison of the proposed system with the existing models operated under OHD scheme

SNR (dB)	Average Bit Error Rate				
	GG [14]	EGG [10]	Proposed 1×2 SIMO	Proposed 1×3 SIMO	Proposed 2×2 MIMO
5	1.30×10^{-1}	1.30×10^{-1}	2.90×10^{-2}	2.80×10^{-2}	6.00×10^{-2}
10	6.70×10^{-2}	6.70×10^{-2}	7.40×10^{-3}	3.40×10^{-3}	3.50×10^{-3}
15	3.10×10^{-2}	2.90×10^{-2}	1.50×10^{-3}	2.90×10^{-4}	1.30×10^{-4}
20	1.40×10^{-2}	1.10×10^{-2}	2.50×10^{-4}	1.90×10^{-5}	3.20×10^{-6}
25	5.70×10^{-3}	3.60×10^{-3}	3.90×10^{-5}	1.10×10^{-6}	6.60×10^{-8}
30	2.30×10^{-3}	1.20×10^{-3}	5.60×10^{-6}	5.40×10^{-8}	1.20×10^{-9}
35	8.90×10^{-4}	3.80×10^{-4}	7.70×10^{-7}	2.60×10^{-9}	2.00×10^{-11}
40	3.40×10^{-4}	1.20×10^{-4}	1.00×10^{-7}	1.20×10^{-10}	3.10×10^{-13}
45	1.30×10^{-4}	3.90×10^{-5}	1.30×10^{-8}	5.30×10^{-12}	4.70×10^{-15}
50	4.70×10^{-5}	1.20×10^{-5}	1.70×10^{-9}	2.30×10^{-13}	7.10×10^{-17}

Table 3.9 Average BER comparison of the proposed system with the existing models operated under IM/DD scheme

SNR (dB)	Average Bit Error Rate				
	GG [14]	EGG [10]	Proposed 1×2 SIMO	Proposed 1×3 SIMO	Proposed 2×2 MIMO
5	7.30×10^{-1}	9.00×10^{-1}	3.40×10^{-1}	5.30×10^{-1}	1.70×10^{0}
10	6.10×10^{-1}	1.70×10^{-1}	2.10×10^{-1}	2.40×10^{-1}	5.60×10^{-1}
15	4.90×10^{-1}	1.50×10^{-1}	1.20×10^{-1}	9.60×10^{-2}	1.50×10^{-1}
20	3.70×10^{-1}	1.20×10^{-1}	6.30×10^{-2}	3.40×10^{-2}	3.50×10^{-2}
25	2.80×10^{-1}	7.40×10^{-2}	3.10×10^{-2}	1.10×10^{-2}	6.90×10^{-3}
30	$\mathbf{2.00 \times 10^{-1}}$	$\mathbf{3.90 \times 10^{-2}}$	$\mathbf{1.40 \times 10^{-2}}$	$\mathbf{3.00 \times 10^{-3}}$	$\mathbf{1.20 \times 10^{-3}}$
35	1.40×10^{-1}	1.70×10^{-2}	6.10×10^{-3}	8.20×10^{-4}	2.00×10^{-4}
40	9.30×10^{-2}	6.20×10^{-3}	2.60×10^{-3}	2.10×10^{-4}	3.10×10^{-5}
45	6.20×10^{-2}	2.10×10^{-3}	1.00×10^{-3}	5.10×10^{-5}	4.60×10^{-6}
50	4.10×10^{-2}	7.00×10^{-4}	4.10×10^{-4}	1.20×10^{-5}	6.40×10^{-7}

Because direct detection only reaches the shot-noise limit for relatively high signal powers, whereas OHD can reach the standard quantum limit for much lower signal powers, so OHD offers advantage in terms of sensitivity. As a result, this detection method is particularly well suited to very weak signals. Average BER as a function of average SNR for both IM/DD and OHD techniques is shown in fig. 3.8. Under strong fading $(\sigma_I^2 = 3.1952)$, it has been shown that OHD outperforms IM/DD technique. At $P_e = 7.3 \times 10^{-6}$ utilizing 2x2 MIMO almost 10dB SNR has been achieved in comparison with 1x2 SIMO. However, below 15 dB 1x3 SIMO scheme performs better than 2x2 MIMO scheme. Also, it has been observed that the UOWC system based on the SISO scheme using OHD performs nearly the same as 1x2 SIMO IM/DD technique
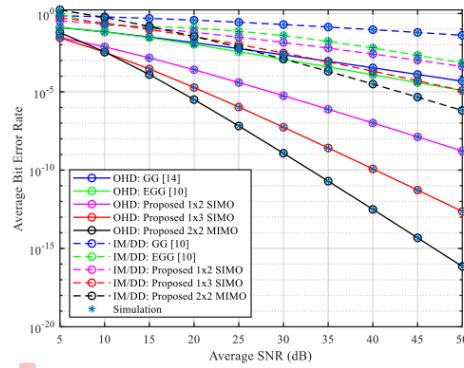

Figure 3.8 Average BER comparison of the proposed system with the existing models operated under either OHD or IM/DD schemes under strong fading condition

The temperature gradient $0.22^o C cm^{-1}$ has been selected from table 3.3, resulting in strong turbulence of SI $(\sigma_I^2 = 3.1952)$. Average BER comparison of the proposed model with existing models for various modulation schemes BPSK, 16PSK, 16QAM and 64QAM has been presented in table 3.10 and 3.11.

Table 3.10 Average BER comparison of the proposed model with existing models for various modulation schemes BPSK, 16-PSK

SNR (dB)	Average Bit Error Rate					
	BPSK			16-PSK		
	GG [14]	EGG [10]	Proposed 1x2 SIMO	GG [14]	EGG [10]	Proposed 1x2 SIMO
0	2.10×10^{-1}	2.00×10^{-1}	8.60×10^{-2}	5.40×10^{-1}	2.50×10^{-1}	3.60×10^{-1}
5	1.30×10^{-1}	1.30×10^{-1}	2.90×10^{-2}	4.10×10^{-1}	1.90×10^{-1}	2.10×10^{-1}
10	6.70×10^{-2}	6.70×10^{-2}	7.40×10^{-3}	2.70×10^{-1}	1.30×10^{-1}	9.40×10^{-2}
15	3.10×10^{-2}	2.90×10^{-2}	1.50×10^{-3}	1.50×10^{-1}	6.90×10^{-2}	3.00×10^{-2}
20	1.40×10^{-2}	1.10×10^{-2}	2.50×10^{-4}	7.90×10^{-2}	3.20×10^{-2}	7.30×10^{-3}
25	5.70×10^{-3}	3.60×10^{-3}	3.90×10^{-5}	3.60×10^{-2}	1.30×10^{-2}	1.40×10^{-3}
30	2.30×10^{-3}	1.20×10^{-3}	5.60×10^{-6}	1.60×10^{-2}	4.40×10^{-3}	2.40×10^{-4}
35	8.90×10^{-4}	3.80×10^{-4}	7.70×10^{-7}	6.40×10^{-3}	1.50×10^{-3}	3.60×10^{-5}
40	3.40×10^{-4}	1.20×10^{-4}	1.00×10^{-7}	2.60×10^{-3}	4.80×10^{-4}	5.10×10^{-6}
45	1.30×10^{-4}	3.90×10^{-5}	1.30×10^{-8}	9.90×10^{-4}	1.50×10^{-4}	6.90×10^{-7}
50	4.70×10^{-5}	1.20×10^{-5}	1.70×10^{-9}	3.80×10^{-4}	4.90×10^{-5}	9.10×10^{-8}

Table 3.11 Average BER comparison of the proposed model with existing models for various modulation schemes 16QAM and 64QAM

SNR (dB)	Average Bit Error Rate					
	16-QAM			64-QAM		
	GG [14]	EGG [10]	Proposed 1x2 SIMO	GG [14]	EGG [10]	Proposed 1x2
0	4.60×10^{-1}	3.80×10^{-1}	2.80×10^{-1}	7.30×10^{-1}	4.10×10^{-1}	-3.80×10^{17}
5	3.30×10^{-1}	3.00×10^{-1}	1.60×10^{-1}	5.50×10^{-1}	4.80×10^{-1}	2.80×10^{-1}
10	2.10×10^{-1}	2.10×10^{-1}	7.10×10^{-2}	3.70×10^{-1}	3.40×10^{-1}	1.60×10^{-1}
15	1.20×10^{-1}	1.20×10^{-1}	2.30×10^{-2}	2.30×10^{-1}	2.20×10^{-1}	7.10×10^{-2}
20	6.10×10^{-2}	5.90×10^{-2}	5.80×10^{-3}	1.30×10^{-1}	1.20×10^{-1}	2.50×10^{-2}
25	2.80×10^{-2}	2.40×10^{-2}	1.10×10^{-3}	6.50×10^{-2}	6.10×10^{-2}	6.50×10^{-3}
30	1.20×10^{-2}	9.00×10^{-3}	2.00×10^{-4}	3.00×10^{-2}	2.60×10^{-2}	1.40×10^{-3}
35	5.00×10^{-3}	3.00×10^{-3}	3.00×10^{-5}	1.30×10^{-2}	9.60×10^{-3}	2.40×10^{-4}
40	2.00×10^{-3}	1.00×10^{-3}	4.30×10^{-6}	5.30×10^{-3}	3.30×10^{-3}	3.70×10^{-5}
45	7.70×10^{-4}	3.20×10^{-4}	5.90×10^{-7}	2.10×10^{-3}	1.10×10^{-3}	5.40×10^{-6}
50	2.90×10^{-4}	1.00×10^{-4}	7.80×10^{-8}	8.30×10^{-4}	3.50×10^{-4}	7.50×10^{-7}

A comparison of the proposed model with the existing models is shown in fig. 3.9. Analytical results obtained in eqn. (3.22) have been verified for the UOWC system operated under a strong turbulence region with OHD scheme using various modulation techniques. BPSK modulation outperforms 16-QAM,16-PSK, and 64-QAM modulation. By utilizing 1x2 SIMO scheme, system performance improves over the conventional SISO scheme. At $P_e = 12.9 \times 10^{-4}$, utilizing 1x2 SIMO almost 15 dB has been achieved. Because power conservation is an important aspect in UOWC, this scheme does not require a carrier signal at the receiver during demodulation, resulting in reduction in complex receivers as compared to QAM. Moreover, the BW requirements are less as compared to BPSK and QAM schemes. Therefore, this scheme is preferred for wireless communication in underwater medium.
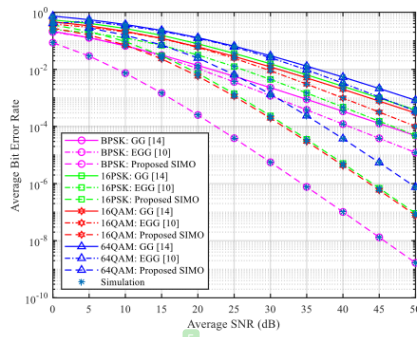
Figure 3.9 Average BER comparison of the proposed model with existing models for various modulation schemes

Under the strong turbulence the EC for the proposed model has been compared with the existing GG and EGG models for UOWC system operated under OHD and IM/DD schemes as shown in table 3.12 and 3.13 respectively. The proposed 2×2 MIMO system consistently outperforms GG and EGG models in terms of EC under both OHD and IM/DD schemes across all SNR levels. It achieves significantly higher spectral efficiency, reaching 16 Nats/s/Hz (OHD) and 15 Nats/s/Hz (IM/DD) at 50 dB SNR. Compared to EGG, which lags behind especially at lower SNRs, the proposed system

ensures robust and efficient data transmission. This highlights its effectiveness in combating turbulence and enhancing link reliability in UOWC.

Table 3.12 Ergodic capacity comparison of the proposed model with GG and EGG model operated under OHD scheme

SNR (dB)	Ergodic Capacity (Nats/Sec/Hz)				
	GG [14]	EGG [10]	Proposed 1×2 SIMO	Proposed 1×3 SIMO	Proposed 2×2 MIMO
0	0.90	0.043	0.96	0.98	0.99
5	1.50	0.12	1.70	1.80	1.80
10	2.30	0.29	2.70	2.90	3.00
15	3.20	0.62	3.90	4.20	4.40
20	4.40	1.20	5.30×10^0	5.70×10^0	5.90×10^0
25	5.60	2.00	6.80×10^0	7.30×10^0	7.50×10^0
30	7.00	3.00	8.40×10^0	8.90×10^0	9.20×10^0
35	8.50	4.20	1.00×10^1	1.10×10^1	1.10×10^1
40	10.00	5.50	1.20×10^1	1.20×10^1	1.20×10^1
45	12.00	6.80	1.30×10^1	1.40×10^1	1.40×10^1
50	13.00	8.30	15.00×10^0	16.00×10^0	16.00×10^0

Table 3.13 Ergodic capacity comparison of the proposed model with GG and EGG model operated under IM/DD scheme

| SNR (dB)	Ergodic Capacity (Nats/Sec/Hz)				
	GG [14]	EGG [10]	Proposed 1×2 SIMO	Proposed 1×3 SIMO	Proposed 2×2 MIMO
0	0.42	0.16	0.59	0.68	0.74
5	0.78	0.37	1.10	1.30	1.50
10	1.30	0.77	1.90	2.30	2.50
15	2.00	1.40	3.00	3.50	3.80
20	3.00	2.30	4.30	4.90	5.30
25	4.10	3.30	5.70	6.50	6.90
30	5.30	4.50	7.20	8.10	8.50
35	6.70	5.90	8.80×10^0	9.70×10^0	10.00
40	8.10	7.30	1.00×10^1	1.10×10^1	1.20×10^1
45	9.60	8.70	1.20×10^1	1.30×10^1	1.30×10^1
50	11.00	10.00	1.40×10^1	1.50×10^1	1.50×10^1

Fig. 3.10 shows EC comparison of the proposed system with other existing models operated under IM/DD or OHD scheme under strong fading condition. As average SNR increases, EC increases which is consistent with the previous work. At low SNR values, it is clear that there is a very small change in the EC on introducing the spatial diversity. But at high SNR above 25 dB, the performance drastically improves. On introducing receiver diversity SIMO, the performance of the UOWC system significantly improves in comparison with GG and EGG models.
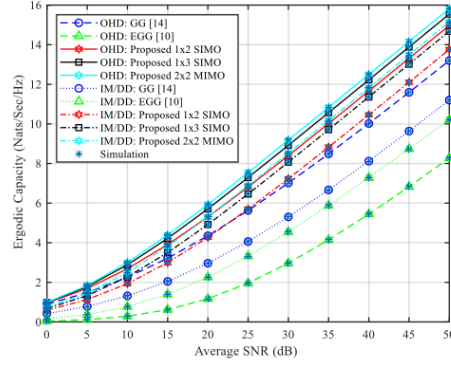
Figure 3.10 Ergodic capacity comparison of the proposed system with other existing models operated under IM/DD or OHD scheme under strong fading condition

Table 3.14 shows the comparison of EC for the proposed model with EGG and GG models operated under strong and weak turbulence regime for IM/DD scheme. It has been shown that capacity decreases by increasing the turbulence-induced fading in the UOWC system. For strong fading $(\sigma_I^2 = 3.1952)$, if 1x3 and above MIMO scheme is employed, then the EC improves and the UOWC system performs as it is working in the weak turbulence regime. The proposed 1×2 SIMO and 2×2 MIMO models consistently achieve higher ECs than both GG and EGG models across all SNR values and turbulence regimes. Under strong turbulence, the proposed 2×2 MIMO model reaches up to 16 Nats/sec/Hz at 50 dB, while GG and EGG models lag at 13 and 5.4 respectively. Similarly, in weak turbulence, the proposed models exhibit near-ideal

42

capacity performance, reaching 16 Nats/sec/Hz even at moderate SNR. These results highlight the robustness and efficiency of the proposed systems, especially in challenging underwater optical communication environments.

Table 3.14 Ergodic capacity comparison of proposed model with EGG and GG models operated under different turbulence regime for IM/DD scheme

SNR (dB)	Ergodic Capacity (Nats/Sec/Hz)							
	Strong Turbulence				Weak Turbulence			
	GG [14]	EGG [10]	Proposed 1×2 SIMO	Proposed 2×2 MIMO	GG [14]	EGG [10]	Proposed 1×2 SIMO	Proposed 2×2 MIMO
0	0.90	0.070	0.96	0.99	0.99	0.17	1.00	1.00
5	1.50	0.16	1.70	1.80	1.90	0.35	2.00	2.00
10	2.30	0.34	2.70	3.00	3.10	0.63	3.30	3.40
15	3.20	0.63	3.90	4.40	4.50	1.00	4.80	4.90
20	4.40	1.10	5.30	5.90	6.10	1.60	6.40	6.50
25	5.60	1.60	6.80	7.60	7.70	2.30	8.00	8.20
30	7.00	2.30	8.40	9.20	9.30	3.10	9.70	9.80
35	8.50	3.00	10.00	11.00	11.00	3.90	11.00	11.00
40	10.00	3.80	12.00	12.00	13.00	4.80	13.00	13.00
45	12.00	4.60	13.00	14.00	14.00	5.80	15.00	15.00
50	**13.00**	**5.40**	**15.00**	**16.00**	**16.00**	**6.80**	**16.00**	**16.00**

Fig. 3.11 shows the performance comparison of the proposed model with EGG and GG model in terms of EC for various levels of turbulence-induced fading operated under IM/DD scheme. The figure illustrates that the proposed 1×2 SIMO and 2×2 MIMO models consistently achieve higher EC compared to GG and EGG models across all SNR values. Under both strong and weak turbulence conditions, the proposed 2×2 MIMO system shows the best performance, closely matching the simulation results. The existing EGG model performs the worst, especially in strong turbulence, highlighting its limitations. Overall, the proposed systems offer robust and scalable capacity improvements, making them more suitable for UOWC.
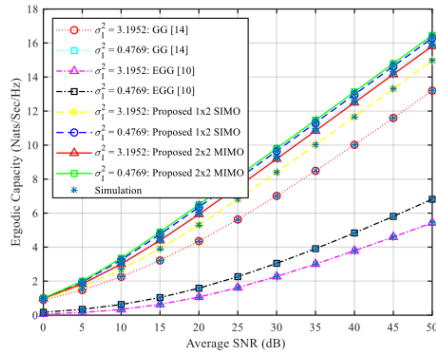
43

Figure 3.11 Ergodic capacity comparison of proposed model with EGG and GG
models operated under IM/DD scheme

Fig. 3.12 shows how received optical power for 16-QAM system at Optical Signal-to-Noise Ratio (OSNR) of 50 dB. Received optical power decreases with distance in UOWC system. Larger receiver apertures (20 cm) consistently capture more power than smaller ones (10 cm), and 2x2 MIMO system outperform SISO setups due to spatial diversity. Thus, both increased aperture size and MIMO configuration enhance signal strength over longer ranges.
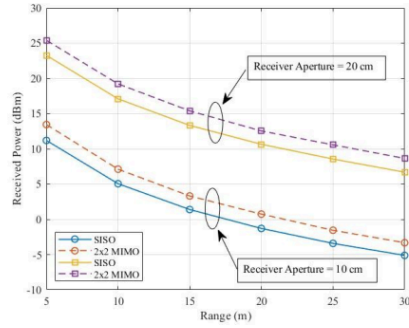
Figure 3.12 Received power vs. range for UOWC system using various receiver
apertures

Fig. 3.13 shows how received optical power at fixed received aperture of 10 cm. Received optical power decreases with distance for SISO and 2x2 MIMO UOWC system under different OSNR values. Higher OSNR (50 dB) results in greater received power than lower OSNR (30 dB), highlighting that improved signal quality leads to better reception. MIMO consistently outperforms SISO at both OSNR levels.
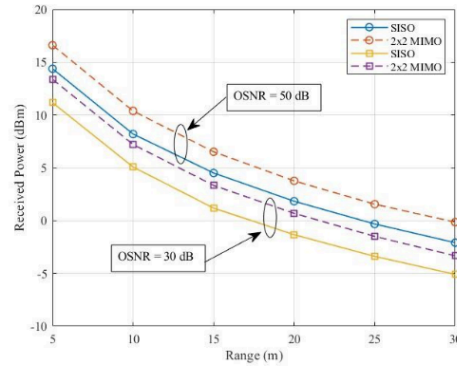
Figure 3.13 Received power vs. range for UOWC system under various OSNR levels

The proposed MIMO UOWC system performed well under GG fading conditions. The system effectively reduced the impact of underwater turbulence, especially in moderate to strong fading cases. Theoretical calculations matched closely with simulation results, confirming the system's effectiveness and reliability.

3.7   Conclusion

In UOWC systems, turbulence-induced fading severely limits performance in terms of reliability, data rate, and error probability. Conventional models such as GG and EGG fail to provide reliable performance across different turbulence conditions and detection schemes. To address these limitations, a novel 2×2 MIMO system along with a 1×2 SIMO configuration was proposed, designed to operate under both IM/DD and OHD schemes.

The proposed models were rigorously evaluated in terms of OP, average BER and EC under both strong and weak turbulence conditions. Results demonstrate that the 2×2 MIMO system significantly outperforms the GG and EGG models in all metrics. At 20 dB SNR, it reduces outage probability to 9.9×10^{-3} far lower than GG (0.25) and EGG (0.26) indicating improved reliability. Similarly, at 30 dB, it achieves an Average BER of just 1.20×10^{-3}, compared to 2.00×10^{-1} and 3.90×10^{-2} for GG and EGG respectively, showcasing superior error resilience.

In terms of spectral efficiency, the proposed system excels across all SNR levels and turbulence regimes. Under both IM/DD and OHD schemes, the 2×2 MIMO model reaches up to 15–16 Nats/sec/Hz at 50 dB SNR, significantly higher than competing models. Particularly in strong turbulence, it demonstrates robust capacity gains up to 16 Nats/sec/Hz compared to 13 for GG and just 5.4 for EGG. Even the 1×2 SIMO model delivers near-optimal performance under weak turbulence.

These findings confirm that the proposed MIMO and SIMO architectures offer substantial improvements in reliability, error performance, and spectral efficiency over classical fading models. Their ability to maintain robust communication under harsh underwater conditions makes them promising solutions for next-generation high-speed UOWC systems.

CHAPTER 4

PERFORMANCE ANALYSIS OF DUAL-HOP RELAYING IN

MÁLAGA -DISTRIBUTED UNDERWATER OPTICAL

WIRELESS COMMUNICATION SYSTEM WITH POINTING

ERROR

4.1   Introduction

The deployment of UOWC system has gained significant attention in recent years due to their potential for enabling high-speed data transmission in aquatic environments. However, despite their advantages over traditional acoustic communication system, UOWC links remain highly vulnerable to several channel impairments, including absorption, scattering, turbulence, and geometric misalignments. These challenges are further exacerbated in practical deployments where establishing a robust direct link between the source and destination nodes becomes infeasible over long distances. Consequently, the adoption of dual-hop relaying architectures has emerged as a compelling solution to extend the communication range and to enhance the overall reliability of UOWC system operating in complex underwater environments.

In modelling underwater optical channel characteristics, it has been recognized that traditional fading models, such as log-normal, exponential-gamma and GG, may not adequately capture the intricate variations of turbulence under strong scattering and heterogeneous water conditions. The Málaga (*M*) distribution has recently been introduced as a highly versatile and generalized statistical model capable of accurately representing the irradiance fluctuations observed in UOWC channels across weak to strong turbulence regimes. By encompassing various classical distributions as special cases, the *M*-distribution provides a more flexible framework for characterizing underwater optical fading, thus offering deeper insights into system performance under diverse environmental conditions.

Alongside turbulence-induced fading, practical UOWC system must also contend with misalignment errors, commonly referred to as pointing errors. These

arise due to the dynamic nature of underwater platforms, such as the movement of AUVs, surface waves, and other environmental disturbances, leading to deviations in beam direction and resulting in substantial power losses at the receiver. Pointing errors introduce additional randomness into the channel, necessitating their incorporation into realistic UOWC system models to ensure accurate performance assessment.

Motivated by these considerations, this chapter presents a dual-hop UOWC system employing Decode-and-Forward (DF) relaying under the M-distributed fading model while accounting for the effects of pointing errors. By introducing an intermediate relay node, the system can overcome the severe limitations associated with direct transmission, thereby improving coverage and reliability. The analysis focuses on deriving closed-form expressions for key performance metrics, including OP, average BER, and EC, under the combined impact of turbulence-induced fading and geometric misalignment.

The major contributions of this chapter are summarized as follows:

- A dual-hop DF relaying model is proposed for UOWC system, with each hop subject to M-distributed fading and pointing errors.
- Analytical expressions for performance metrics have been derived under the combined influence of turbulence and misalignment impairments.
- The impact of key system parameters, such as turbulence strength, pointing error displacement, and relay positioning, on the performance metrics is thoroughly investigated.
- Comparative performance analyses are conducted to highlight the benefits of dual-hop relaying in overcoming the challenges of direct transmission in M-distributed UOWC channels with practical impairments.

4.2 Statistical modelling of dual-hop underwater optical turbulence using Málaga distribution

For a typical optical wireless system, the laser sources and photodiodes are located at the transmitter and receiver sides, respectively. The optical wave is first emitted and then transmitted over a transmission distance (L) through the underwater medium from sensor-1. Due to sun rays the temperature of water varies which results in a variation

of RI. One other factor which indirectly varies the RI of water is the salinity fluctuations in an underwater environment. Both the factors will result in the optical intensity to fluctuate significantly. The photodiode on the relay node will then receive and collect the scattered signal before transmitting it to sensor-2. Fig. 4.1 shows a schematic representation of UOWC system in which two sensors are communicated using a relay node to improve the communication range and data rate.
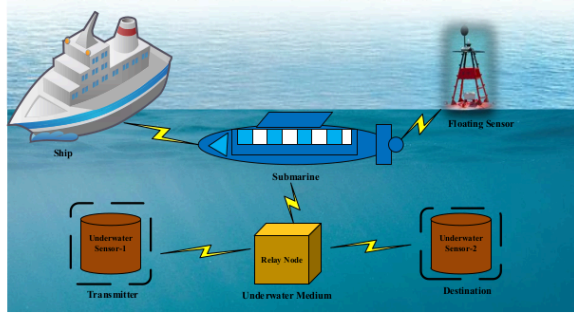

Figure 4.1 Proposed dual-hop relaying scheme for UOWC system

The SI of the optical waves has been investigated in chapter 3 for various turbulence conditions using the Rytov variance model. Further, α, β has been calculate with the help of Rytov variance [69]. Table 3.2 shows the value of α, β for strong, moderate, and weak turbulence conditions. M-distribution function has been used to quantify turbulent channel fading conditions under the scenario of weak-to-strong underwater turbulence. The PDF of generalized M-distribution model for underwater optical turbulence (UOT) is expressed in [23] as

$$f_a(I_a) = \sum_{i=1}^{2} A_i \sum_{k=1}^{\beta_i} a_{i,k} I_a K_{\alpha_i - k} \left(2\sqrt{\frac{\alpha_i \beta_i I_a}{g_i \beta_i + \Omega_i}} \right), \qquad (4.1)$$

and,

$$A_i = \frac{2\alpha_i^{\alpha_i/2}}{g_i^{1+\alpha_i/2} \Gamma(\alpha_i)} \left(\frac{g_i \beta_i}{g_i \beta_i + \Omega_i} \right)^{\beta_i + \alpha_i/2}, \qquad (4.2)$$

49

$$a_{i,k} = \binom{\beta_i - 1}{k - 1} \frac{(g_i \beta_i + \Omega_i')^{1-k/2}}{(k-1)!} \left(\frac{\Omega_i'}{g_i}\right)^{k-1} \left(\frac{\alpha_i}{\beta_i}\right)^{k/2} \quad\quad (4.3)$$

where K_x is the modified Bessel function of 2nd kind, x is the order, α_i, β_i, g_i and Ω_i are the fading parameters, $\Omega_i' = \Omega_i + 2b_o\rho_i + 2\sqrt{2b_o\rho_i\Omega_i}\cos(\phi_A + \phi_B)$, ϕ_A, ϕ_B are the deterministic phases of the LOS and the coupled-to-LOS scatter terms respectively, $g_i = 2b_0(1 - \rho_i)$ and A_i is a variable.
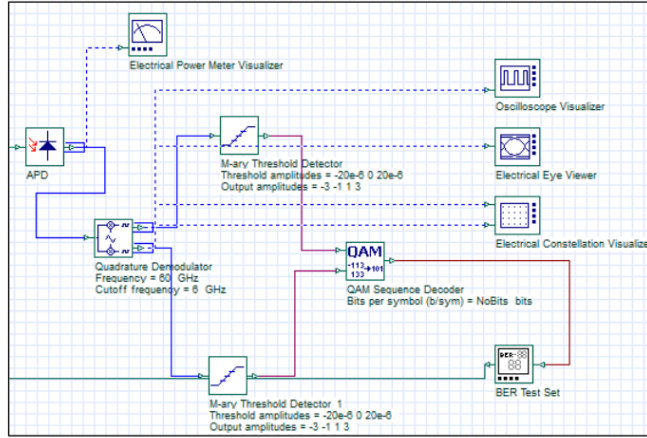
Simulation model of the proposed UOWC system implemented in Opti System is shown in fig. 4.2. The system comprises (a) a transmitter section employing QAM modulation and Mach–Zehnder modulation of a 532 nm CW laser, (b) an intermediate relay node with OSNR control and optical amplification, and (c) a receiver section incorporating an NLOS underwater channel model with intensity scintillation enabled. Signal visualization tools are used at various stages for performance analysis. Appendix I contains the respective eye diagrams and constellation diagrams for the proposed system.

(a)

(b)

50
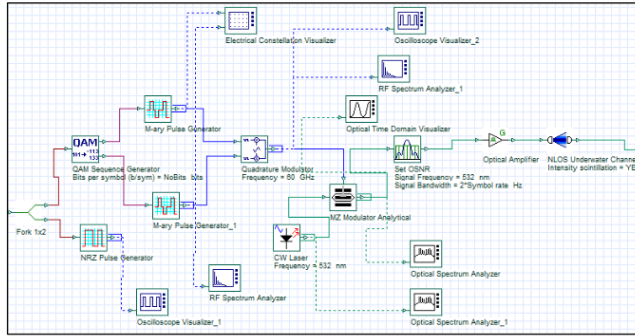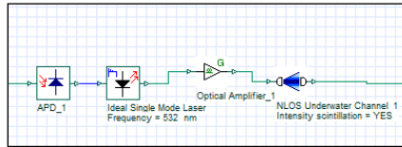
(c)

Figure 4.2 Simulation model of the proposed dual hop UOWC system implemented in Opti System (a) transmitter (b) intermediate relay node (c) receiver section

The next section addresses the modelling and impact of pointing errors within the proposed system.

4.3 Modelling and impact of pointing error

Alongside turbulence-induced fading, practical UOWC system must also contend with misalignment errors, commonly referred to as pointing errors. These arise due to the dynamic nature of underwater platforms, such as the movement of AUVs, surface waves, and other environmental disturbances, leading to deviations in beam direction and resulting in substantial power losses at the receiver. Pointing errors introduce additional randomness into the channel, necessitating their incorporation into realistic UOWC system models to ensure accurate performance assessment. Now the intensity fluctuations due to pointing error impairments can be considered and the PDF is given by [70] as

$$f_p(I_p) = \frac{\xi^2}{A_o^{\xi^2}} I_p^{\xi^2-1}, 0 \leq I_p \leq A_o \tag{4.4}$$

51

where ξ is the ratio between the equivalent beam radius at the receiver and the pointing error displacement standard deviation at the receiver, A_o is a constant term that characterises the pointing loss.

Now the joint probability distribution of $I = I_a I_p$ can be calculated by $f_{I_a, I_p}(I_a, I_p) = f_a(I_a) . f_I(I / I_a)$. Now using eqn. (4.5) in eqn. (4.1) along with random variable transformation in eqn. (4.4) the PDF of the intensity variation due to both turbulence and pointing error impairments is given as eqn. (4.6)

$$K_{\alpha_i - k}\left(2\sqrt{\frac{\alpha_i \beta_i I_a}{g_i \beta_i + \Omega_i}}\right) = \frac{1}{2} G_{0,2}^{2,0}\left(\frac{\alpha_i \beta_i I_a}{g_i \beta_i + \Omega'} \middle| \begin{array}{c} - \\ \frac{\alpha_i - k}{2}, \frac{\alpha_i - k}{2} \end{array}\right) \tag{4.5}$$

$$f_I(I) = \sum_{i=1}^{2} \frac{\xi_i^2 A_i}{2I} \sum_{k=1}^{\beta_i} b_{i,k} G_{1,3}^{3,0}\left[\frac{\alpha_i \beta_i}{g_i \beta_i + \Omega'} \frac{I}{A_o} \middle| \begin{array}{c} \xi_i^2 + 1 \\ \xi_i^2, \alpha_i, k \end{array}\right] \tag{4.6}$$

where $b_{i,k} = a_{i,k}[\alpha_i \beta_i / (g_i \beta_i + \Omega')]^{-(\alpha_i + k)/2}$, $G_{p,q}^{m,n}[.]$ is the Meijer-G function defined in [71]. Fig. 4.3 shows the irradiance fluctuation under various turbulence conditions where the channel is characterised by M-distribution.
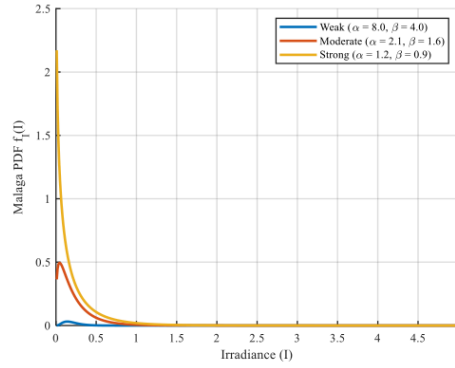

Figure 4.3 PDF of Málaga distribution under different turbulence conditions

Fig. 4.4 show the comparison of irradiance fluctuation due to GG and M-distribution.

52

Since GG is a special case of M- distribution when $\rho = 0$ (NLoS), it was not suitable to deal with alignment issues. So, the proposed system using M- distribution effectively mitigates path loss and accurately models the impact of pointing errors arising from underwater misalignment and mobility.
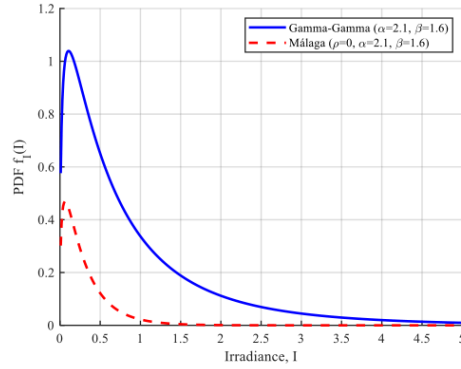

Figure 4.4 Irradiance fluctuation comparison of Málaga PDF with GG-PDF

For the proposed UOWC system, both types of detection schemes IM/DD and OHD taking into account. Since IM/DD techniques is cost-effective and has low complexity in comparison to the OHD technique, but OHD has a higher capacity. Furthermore, at low SNR the gap between capacities of both detection techniques is constant, but it increases at high SNR.

Instantaneous SNR can be given as $\gamma = \frac{(\eta I)^r}{N_0}$ where r is the parameter associated with the type of detection, i^{th} UOWC link where $i = 1$ corresponds to link established between sensor-1 and relay node and $i = 2$ is the link between the relay node and sensor-2 and N_0 is the AWGN sample. A general expression for average electrical SNR is $\mu_{r_i} = \frac{(\eta E[I])^r}{N_0}$. So, the general expression relating to average electrical SNR under OHD ($r = 1$) scheme is given by $\mu_{1_i} = \bar{\gamma}$. The μ_{1_i} is the average electrical SNR for OHD technique for i^{th} hop. On substituting μ_{1_i} in eqn. (4.6), the

53

PDF of the proposed system under OHD scheme for both turbulence and pointing errors is given as

$$f_\gamma(\gamma) = \sum_{i=1}^{2} \frac{\xi_i^2 A_i}{2\gamma} \sum_{k=1}^{\beta_i} b_{i,k} G_{1,3}^{3,0}\left[B_i\left(\frac{\gamma}{\mu_{1_i}}\right) \Bigg| \begin{matrix} \xi_i^2+1 \\ \xi_i^2, \alpha_i, k \end{matrix} \right], \qquad (4.7)$$

where $B_i = \xi_i^2 \alpha_i \beta_i (g_i + \Omega') / [(\xi_i^2+1)(g_i\beta_i + \Omega')]$.

Similarly, under IM/DD ($r=2$) scheme average electrical SNR is given by $\mu_{2_i} = \frac{(\eta E[I])^2}{N_0}$ and can be calculated as

$$\mu_{2_i} = \frac{\alpha_i \xi_i^2 (\xi_i^2+1)^{-2}(\xi_i^2+2)(g_i+\Omega'_i)}{(\alpha_i+1)[2g_i(g_i+2\Omega'_i) + \Omega'^2_i(1+1/\beta_i)]} \mu_{1_i}, \qquad (4.8)$$

Now substituting eqn. (4.8) in eqn. (4.6), the PDF under IM/DD scheme is given as

$$f_\gamma(\gamma) = \sum_{i=1}^{2} \frac{\xi_i^2 A_i}{2^2 \gamma} \sum_{k=1}^{\beta_i} b_{i,k} G_{1,3}^{3,0}\left[B_i\left(\frac{\gamma}{\mu_{2_i}}\right)^{1/2} \Bigg| \begin{matrix} \xi_i^2+1 \\ \xi_i^2, \alpha_i, k \end{matrix} \right], \qquad (4.9)$$

Using (4.7) and (4.9), the unified PDF expression for the proposed system reduces to

$$f_\gamma(\gamma) = \sum_{i=1}^{2} \frac{\xi_i^2 A_i}{2^{r_i} \gamma} \sum_{k=1}^{\beta_i} b_{i,k} G_{1,3}^{3,0}\left[B_i\left(\frac{\gamma}{\mu_{r_i}}\right)^{1/r_i} \Bigg| \begin{matrix} \xi_i^2+1 \\ \xi_i^2, \alpha_i, k \end{matrix} \right], \qquad (4.10)$$

Further this unified PDF expression helps in obtaining the analytical expressions for the performance evaluation under both types of detection schemes.

4.4 Derivation of performance metrics under Málaga and pointing error channel

Any UOWC system's performance can be mainly evaluated using performance metrics such as EC, average BER and OP.

4.4.1 Ergodic Capacity

EC plays a vital role in understanding how well a communication system performs. It refers to the maximum rate at which information can be sent over a UOWC channel while keeping the chances of error extremely low. In this context, the channel is assumed to be memoryless and stable over time, with the added assumption that both

54

the transmitter and receiver have complete knowledge of the channel conditions. Now, the EC with an average value is given as

$$\bar{C} \triangleq E[\log_2(1+\tau\gamma)] \tag{4.11}$$

where τ is constant. For ($\tau = 1$) OHD and ($\tau = e/2\pi$) for IM/DD. On substituting eqn. (4.10) in eqn. (4.11), and utilizing $\ln(1+\gamma) = G_{2,2}^{1,2}\left[\gamma \middle| \begin{matrix} 1,1 \\ 1,0 \end{matrix}\right]$, along with eqn. (1.1.3) of [71], a generalized expression for EC has been obtained as eqn. (4.12). As it can be observed that, as average SNR increases, channel EC increases as well.

$$\bar{C} = \sum_{i=1}^{2} \frac{D_i}{\ln(2)} \sum_{k=1}^{\beta_i} c_{i,k} G_{r_i+2,3r_i+2}^{3r_i+2,1}\left[\left(\frac{E_i}{\mu_{r_i}}\right) \middle| \begin{matrix} 0,1,x_{i1} \\ x_{i2},0,0 \end{matrix}\right], \tag{4.12}$$

4.4.2 Average Bit Error Rate

Average BER is also an important performance parameter that reflects the effectiveness of a UOWC system. To learn more about the performance of dual-hop UOWC system the average BER for various modulation techniques is expressed as

$$P_e = \frac{\delta}{2\Gamma(p)} \sum_{j=1}^{n} \int_0^\infty \Gamma(p, q_k\gamma) f_\gamma(\gamma) d\gamma, \tag{4.13}$$

where p, q_k are the parameters that specify the type of modulation and $\Gamma(p, q_k\gamma)$ is the incomplete gamma function. Table 3.2 presents the various parameter values associated with the modulation techniques.

On substituting eqn. (4.10) in eqn. (4.13), the average BER for Channel State Information (CSI) assisted fixed gain relaying UOWC system employing M-distribution is given as

$$P_e = \sum_{i=1}^{2} \frac{\delta D_i}{2\Gamma(p)} \sum_{j=1}^{n} \sum_{k=1}^{\beta_i} c_{i,k} G_{r_i+2,3r_i+1}^{3r_i,2}\left[\left(\frac{E_i}{\mu_{r_i}q_k}\right) \middle| \begin{matrix} 1-p,1,x_{i1} \\ x_{i2},0 \end{matrix}\right], \tag{4.14}$$

where $G_{p,q}^{m,n}[.]$ is Meiger-G function, $D_i = \xi_i^2 A_i/[2^{r_i}(2\pi)^{r_i-1}]$, $c_{i,k} = b_k r_i^{\alpha_i+k-1}$, $E_i = B^{r_i}/r^{2r_i}$. Both x_{i1} and x_{i2} are the intermediate variables depending upon the

55

detection schemes, pointing errors, fading conditions and $x_{i1} = \frac{\xi_i^2+1}{r_i},....,\frac{\xi_i^2+r_i}{r_i}$ consists of

r_i terms and $X_{i2} = \frac{\xi_i^2}{r_i},...,\frac{\xi_i^2+r_i-1}{r_i},\frac{\alpha_i}{r_i},...,\frac{\alpha_i+r_i-1}{r_i},\frac{k}{r_i},...,\frac{k+r_i-1}{r_i}$ consists of $3r_i$ terms.

4.4.3 Outage Probability

Under various turbulence conditions the OP is an important performance indicator for evaluating the performance of the UOWC system. And it is defined as the probability of the instantaneous SNR falling below a specified threshold value γ_{th}, mathematically OP is expressed as

$$P_{out} = P_r(\gamma \le \gamma_{th}) = F_\gamma(\gamma_{th}), \tag{4.15}$$

where $F_\gamma(\gamma)$ is the CDF under M-fading channel. On substituting eqn. (4.10) in $F_\gamma(\gamma) = \int_0^\gamma f_\gamma(\gamma)d\gamma$, the unified CDF can be evaluated as

$$F_\gamma(\gamma) = \sum_{i=1}^{2} D_i \sum_{k=1}^{\beta_i} c_{i,k} G_{r_i+1,3r_i+1}^{3r_i+1,1} \left[E_i\left(\frac{\gamma}{\mu_{r_i}}\right) \Big|_{x_{i2},0}^{1,x_{i1}} \right], \tag{4.16}$$

Substituting eqn. (4.16) in eqn. (4.15), the closed-form expression for OP is given as

$$P_{out} = F_\gamma(\gamma_{th}) = \sum_{i=1}^{2} D_i \sum_{k=1}^{\beta_i} c_{i,k} G_{r_i+1,3r_i+1}^{3r_i+1,1} \left[E_i\left(\frac{\gamma_{th}}{\mu_{r_i}}\right) \Big|_{x_{i2},0}^{1,x_{i1}} \right], \tag{4.17}$$

In the next section, the performance metrics of the proposed system with varying pointing errors under various turbulent conditions have been analysed.

4.5 Results and discussion

The impact of channel and system characteristics on the EC, average BER and OP of the UOWC system is explored in this section. Every figure is labelled with the type of detection technique along with the values of turbulence and pointing errors.

Under fixed pointing error, the average BER performance of the proposed system under both types of detection techniques operated under various turbulence conditions is shown table 4.1. The results show that the OHD detection scheme consistently achieves lower average BER than IM/DD across all turbulence levels and

56

SNR values. Notably, under strong turbulence at 40 dB SNR, OHD achieves a BER of 1.99×10^{-3}, compared to 4.38×10^{-2} for IM/DD, highlighting its superior error resilience.

Table 4.1 Average BER vs average SNR operated under both OHD and IMDD detection schemes for various turbulence conditions

| SNR (dB)	Average Bit Error Rate					
	OHD			IM/DD		
	Strong	Moderate	Weak	Strong	Moderate	Weak
0	4.53×10^{-1}	4.34×10^{-1}	4.23×10^{-1}	3.90×10^{-1}	3.71×10^{-1}	3.58×10^{-1}
5	2.86×10^{-1}	2.62×10^{-1}	2.47×10^{-1}	3.27×10^{-1}	3.02×10^{-1}	2.85×10^{-1}
10	1.58×10^{-1}	1.38×10^{-1}	1.27×10^{-1}	2.63×10^{-1}	2.35×10^{-1}	2.18×10^{-1}
15	8.03×10^{-2}	6.76×10^{-2}	6.14×10^{-2}	2.04×10^{-1}	1.78×10^{-1}	1.63×10^{-1}
20	3.91×10^{-2}	3.23×10^{-2}	2.91×10^{-2}	1.55×10^{-1}	1.32×10^{-1}	1.19×10^{-1}
25	1.86×10^{-2}	1.53×10^{-2}	1.38×10^{-2}	1.15×10^{-1}	9.61×10^{-2}	8.62×10^{-2}
30	8.83×10^{-3}	7.22×10^{-3}	6.51×10^{-3}	8.45×10^{-2}	6.93×10^{-2}	6.17×10^{-2}
35	4.18×10^{-3}	3.42×10^{-3}	3.08×10^{-3}	6.11×10^{-2}	4.95×10^{-2}	4.39×10^{-2}
40	1.99×10^{-3}	1.62×10^{-3}	1.46×10^{-3}	4.38×10^{-2}	3.51×10^{-2}	3.10×10^{-2}
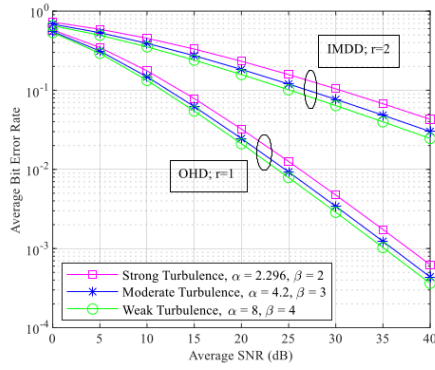
Figure 4.5 Average BER vs average SNR operated under both detection schemes for various turbulence conditions

The fig. 4.5 illustrates the variation of average BER with respect to average SNR for different turbulence regimes under OHD and IM/DD detection schemes. It is evident that the OHD scheme consistently outperforms IM/DD across all SNR levels and turbulence conditions, achieving lower BER values. As expected, performance improves as turbulence weakens (from strong to weak), with the lowest BER observed under weak turbulence ($\alpha = 8, \beta = 4$). This confirms the robustness of the OHD scheme, especially in challenging underwater conditions.

Table 4.2 and 4.3 shows the average BER performance under strong and weak turbulence conditions for various modulation techniques operated under OHD scheme. Under the OHD scheme, BPSK consistently achieves the lowest BER among all modulation schemes across both strong and weak turbulence conditions. In strong turbulence at 40 dB SNR, BPSK achieves a BER of 3.42×10^{-2}, while 64-QAM remains the worst with 5.64×10^{-2}. In weak turbulence, BPSK further outperforms others with a BER as low as 3.25×10^{-4}, demonstrating excellent error resilience. These results highlight that BPSK is the most robust modulation choice for underwater optical wireless links, especially in turbulence-prone environments.

Table 4.2 Average BER vs average SNR under strong turbulence conditions for various modulation techniques operated under OHD scheme

SNR (dB)	Average Bit Error Rate			
	64-QAM	16-PSK	16-QAM	BPSK
0	7.96×10^{-1}	7.24×10^{-1}	5.75×10^{-1}	6.19×10^{-1}
5	6.72×10^{-1}	5.89×10^{-1}	4.50×10^{-1}	4.94×10^{-1}
10	5.34×10^{-1}	4.53×10^{-1}	3.35×10^{-1}	3.74×10^{-1}
15	4.02×10^{-1}	3.31×10^{-1}	2.39×10^{-1}	2.70×10^{-1}
20	2.89×10^{-1}	2.32×10^{-1}	1.64×10^{-1}	1.88×10^{-1}
25	2.00×10^{-1}	1.58×10^{-1}	1.10×10^{-1}	1.27×10^{-1}
30	1.34×10^{-1}	1.04×10^{-1}	7.17×10^{-2}	8.35×10^{-2}
35	8.78×10^{-2}	6.74×10^{-2}	4.59×10^{-2}	5.38×10^{-2}
40	5.64×10^{-2}	4.29×10^{-2}	2.90×10^{-2}	3.42×10^{-2}

58

Under fixed pointing effect the average BER of a CSI-assisted relaying UOWC M-fading system under weak and strong turbulence scenarios operated under various modulation schemes are shown in fig. 4.6. In 16-PSK modulation, different signals are represented solely by changing the phase of the carrier signal, while in 16-QAM modulation, both the amplitude and phase are varied to convey distinct signals. So, under weak turbulence conditions, the effect on optical signal distortion is minimal and hence both 16-PSK and 16-QAM show similar performance. Whereas under high underwater turbulence conditions, there is a significant variance in their performance because in 16-PSK, the phase of the transmitted signal undergoes rapid and unpredictable changes, which result in phase errors. On the other side, the 16-QAM depends both on phase and amplitude variations but mainly relies on amplitude variations to convey symbol information, so it is more robust to phase distortions leading to a better performance under strong turbulence conditions.

Table 4.3 Average BER vs average SNR under weak turbulence conditions for various modulation techniques operated under OHD scheme

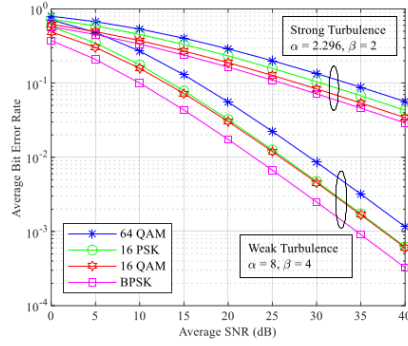| SNR (dB)	Average Bit Error Rate			
	64-QAM	16-PSK	16-QAM	BPSK
0	7.10×10^{-1}	5.76×10^{-1}	4.89×10^{-1}	3.74×10^{-1}
5	4.82×10^{-1}	3.47×10^{-1}	3.02×10^{-1}	2.08×10^{-1}
10	2.70×10^{-1}	1.76×10^{-1}	1.58×10^{-1}	1.00×10^{-1}
15	1.29×10^{-1}	7.85×10^{-2}	7.24×10^{-2}	4.32×10^{-2}
20	5.56×10^{-2}	3.23×10^{-2}	3.03×10^{-2}	1.74×10^{-2}
25	2.23×10^{-2}	1.26×10^{-2}	1.20×10^{-2}	6.70×10^{-3}
30	8.57×10^{-3}	4.74×10^{-3}	4.54×10^{-3}	2.50×10^{-3}
35	3.19×10^{-3}	1.74×10^{-3}	1.67×10^{-3}	9.09×10^{-4}
40	1.16×10^{-3}	6.25×10^{-4}	6.05×10^{-4}	3.25×10^{-4}

Figure 4.6 Average BER vs average SNR under strong and weak turbulence conditions for various modulation techniques operated under OHD scheme

Fig. 4.7 shows the average BER performance for various turbulence conditions under the varying effect of pointing errors (i.e., $(\xi_1 = 1.1, \xi_2 = 0.8)$ for strong and $(\xi_1 = 6, \xi_2 = 6.7)$ for weak) using 16-PSK modulation. It can be observed that at low SNR up to 5 dB the effect of noise is high which overshadowed the effect of turbulence and hence shows similar performance. Whereas at high SNR, and system operated under strong pointing errors are due to the misalignment of the transmitted signal and receiver's aperture, causing signal loss which degrade the UOWC system performance.

Under strong pointing errors $(\xi_1 = 1.1, \xi_2 = 0.8)$, the average BER performance of the proposed system operated under various turbulence conditions is shown in fig. 4.8. Here mixed detection scheme is employed, and it shows that OHD/OHD scheme outperforms OHD/IMDD scheme. In OHD, the incoming signal is mixed with a local oscillator frequency, resulting in a beat frequency that is much easier to detect even in the presence of noise. This enhanced SNR helps maintain signal integrity over longer transmission distances and through multiple hops the performance of OHD/OHD is better than OHD/IMDD.
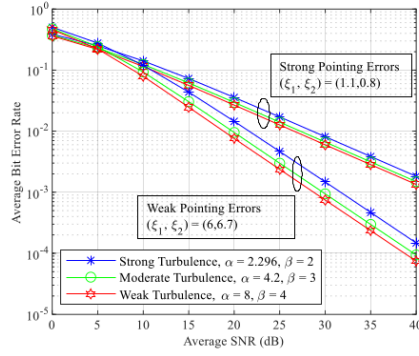
60

Figure 4.7 Average BER vs average SNR for various turbulence conditions under weak and strong pointing errors using 16-PSK modulation
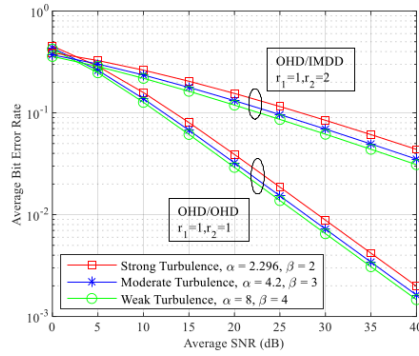

Figure 4.8 Average BER vs average SNR for various turbulence conditions operated under mixed detection schemes

Table 4.4 shows that EC increases with SNR for both OHD and IM/DD schemes under all turbulence levels. OHD consistently outperforms IM/DD, especially in strong turbulence, achieving up to 24.3 Nats/sec/Hz at 40 dB. The performance gap widens with increasing SNR, highlighting OHD's robustness. This signifies the suitability of OHD for high-capacity UOWC in severe underwater conditions.

Table 4.4 Ergodic capacity vs average SNR for various turbulence conditions
operated under both detection schemes

SNR (dB)	Ergodic Capacity					
	OHD			IM/DD		
	Strong	Moderate	Weak	Strong	Moderate	Weak
0	1.533	1.598	1.638	1.123	1.274	1.380
5	3.010	3.153	3.238	1.915	2.173	2.351
10	5.115	5.348	5.484	2.972	3.351	3.603
15	7.725	8.037	8.215	4.265	4.759	5.076
20	10.672	11.038	11.243	5.749	6.338	6.705
25	13.811	14.209	14.429	7.371	8.033	8.434
30	17.050	17.464	17.692	9.090	9.801	10.225
35	20.336	20.758	20.989	10.870	11.614	12.051
40	23.643	24.068	24.301	12.688	13.453	13.899

Fig. 4.9 shows the EC of the proposed system under the various level of turbulence. As the effect of turbulence and/or severe pointing condition, the EC deteriorates. For fixed pointing error $(\xi = 1)$ under both detection schemes, the OHD technique outperforms IM/DD technique. It can be seen that at higher SNR the transmitted signal becomes more robust against noise so the capacity improves drastically.
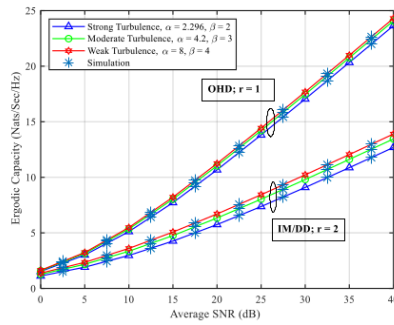

Figure 4.9 Ergodic capacity vs average SNR for various turbulence conditions
operated under both detection schemes

62

Table 4.5 shows that the proposed dual-hop relaying significantly outperforms single-hop relaying across all turbulence levels under strong pointing conditions. At 50 dB SNR, dual-hop achieves up to 23.26 Nats/sec/Hz, compared to only 14.74 for single-hop under weak turbulence. The performance gain is more pronounced at higher SNRs, emphasizing dual-hop's efficiency. This demonstrates the effectiveness of dual-hop relaying in enhancing UOWC capacity in adverse environments. Fig. 4.10 presents the EC under the strong-pointing error condition $(\xi_1 = 1.1, \xi_2 = 0.8)$. As underwater turbulence (α, β) increases, the proposed system's EC decreases. Also, with a higher SNR, the signal power is much greater than the noise power in the channel. Consequently, the impact of noise on the received signal is reduced, leading to an increase in EC. Proposed system employed dual-hop relaying, whereas [23] used single relaying. In dual-hop data transmission, data transmission takes place with the help of a relay node. By splitting the total path into two hops, scattering and signal degradation can be mitigated, thereby improving the signal quality and enhancing EC.

Table 4.5 Comparison of ergodic capacity of single-hop and proposed dual-hop relaying for various turbulence conditions operated under strong pointing conditions.

| SNR (dB)	Ergodic Capacity (Nats/Sec/Hz)					
	Single-hop relaying			Proposed dual-hop relaying		
	Strong	Moderate	Weak	Strong	Moderate	Weak
0	0.043	0.070	0.075	1.141	1.189	1.219
5	0.216	0.358	0.395	2.226	2.331	2.393
10	0.677	1.098	1.230	3.772	3.943	4.042
15	1.454	2.282	2.557	5.700	5.929	6.059
20	2.441	3.722	4.162	7.891	8.163	8.314
25	3.528	5.270	5.879	10.245	10.542	10.707
30	4.652	6.855	7.637	12.689	13.001	13.172
35	5.789	8.454	9.408	15.181	15.501	15.676
40	6.930	10.056	11.184	17.697	18.021	18.198
45	8.072	11.659	12.960	20.225	20.551	20.729
50	**9.215**	**13.263**	**14.737**	**22.759**	**23.086**	**23.264**
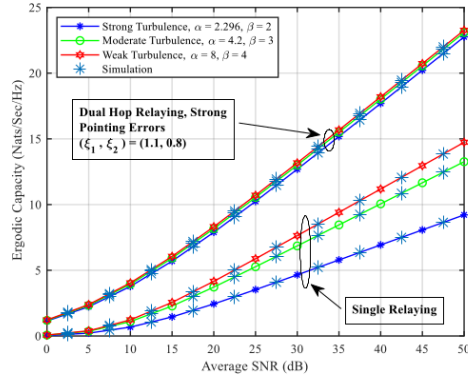
Figure 4.10 Comparison of ergodic capacity vs average SNR for single-hop and proposed dual-hop relaying for strong pointing conditions

Table 4.6 shows that under weak pointing conditions, the proposed dual-hop relaying offers a substantial capacity advantage over single-hop relaying across all turbulence levels. At 50 dB SNR, dual-hop achieves up to 35.75 Nats/sec/Hz whereas only 14.74 Nats/sec/Hz for single-hop. The capacity gap widens with increasing SNR, especially under weak turbulence. This highlights dual-hop relaying's superior resilience and efficiency in alignment-challenged underwater environments.

Fig. 4.11 shows the EC under the weak pointing error conditions $(\xi_1 = 6, \xi_2 = 6.7)$. The signal loss due to underwater turbulence is minimal, so there is an increase in EC. At low SNR, the noise is dominant in the signal, so the EC of proposed dual-hop relaying and single relaying becomes comparable. Noise overshadows the advantages of dual-hop relaying at low SNR values. When the SNR is high, the difference in EC between dual-hop and single-relaying increases due to the variations in SNR distributions and diversity gains. In DF dual-hop relaying, the relay node first decodes the incoming signal to remove any noise or errors. It then re-encodes and forwards a clean version of the signal to the destination. This process helps in improving the overall performance of the system compared to sending the signal in a single-hop.

64

Table 4.6 Comparison of ergodic capacity vs average SNR for single-hop and
proposed dual-hop relaying for weak pointing conditions

| SNR (dB) | Ergodic Capacity (Nats/Sec/Hz) | | | | | |
| | Single-hop relaying | | | Proposed dual-hop relaying | | |
	Strong	Moderate	Weak	Strong	Moderate	Weak
0	0.043	0.070	0.075	1.847	1.925	1.972
5	0.216	0.358	0.395	3.671	3.848	3.954
10	0.677	1.098	1.230	6.243	6.533	6.703
15	1.454	2.282	2.557	9.367	9.746	9.962
20	2.441	3.722	4.162	12.815	13.249	13.490
25	3.528	5.270	5.879	16.426	16.887	17.141
30	4.652	6.855	7.637	20.110	20.583	20.842
35	5.789	8.454	9.408	23.823	24.301	24.562
40	6.930	10.056	11.184	27.548	28.028	28.290
45	8.072	11.659	12.960	31.278	31.759	32.021
50	**9.215**	**13.263**	**14.737**	**35.009**	**35.490**	**35.752**
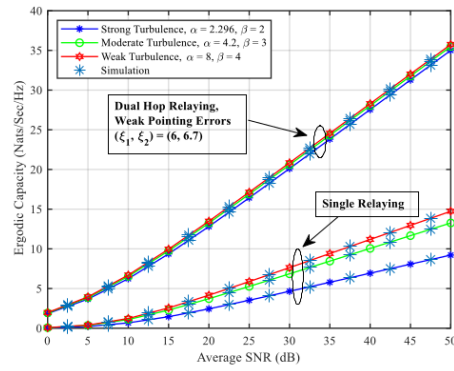
Figure 4.11 Comparison of ergodic capacity vs average SNR for single-hop and
proposed dual-hop relaying for weak pointing conditions

Table 4.7 shows that OP decreases with increasing SNR for both OHD and IM/DD detection schemes under all turbulence conditions. OHD consistently exhibits lower OP than IM/DD, especially under strong turbulence. For instance, at 40 dB SNR, OHD achieves as low as 2.28×10^{-3} compared to IM/DD's 1.57×10^{-4} under weak turbulence. This demonstrates OHD's superior reliability and robustness for UOWC systems in challenging environments.

Table 4.7 Outage probability vs average SNR for various turbulence conditions operated under both detection schemes

| SNR | Outage Probability | | | | | |
| | OHD | | | IM/DD | | |
(dB)	Strong	Moderate	Weak	Strong	Moderate	Weak
0	4.72×10^{-1}	4.74×10^{-1}	4.76×10^{-1}	7.06×10^{-1}	7.16×10^{-1}	7.23×10^{-1}
5	3.63×10^{-1}	3.51×10^{-1}	3.43×10^{-1}	5.03×10^{-1}	4.83×10^{-1}	4.67×10^{-1}
10	2.25×10^{-1}	2.04×10^{-1}	1.92×10^{-1}	2.44×10^{-1}	1.99×10^{-1}	1.72×10^{-1}
15	1.21×10^{-1}	1.04×10^{-1}	9.55×10^{-2}	9.14×10^{-2}	6.47×10^{-2}	5.24×10^{-2}
20	6.04×10^{-2}	5.04×10^{-2}	4.57×10^{-2}	3.05×10^{-2}	2.01×10^{-2}	1.60×10^{-2}
25	2.91×10^{-2}	2.39×10^{-2}	2.16×10^{-2}	9.80×10^{-3}	6.29×10^{-3}	4.99×10^{-3}
30	1.38×10^{-2}	1.13×10^{-2}	1.02×10^{-2}	3.11×10^{-3}	1.98×10^{-3}	1.57×10^{-3}
35	6.54×10^{-3}	5.35×10^{-3}	4.81×10^{-3}	9.84×10^{-4}	6.26×10^{-4}	4.96×10^{-4}
40	**3.10×10^{-3}**	**2.53×10^{-3}**	**2.28×10^{-3}**	**3.11×10^{-4}**	**1.98×10^{-4}**	**1.57×10^{-4}**

Using fixed-gain relaying and strong pointing conditions the OP for various UOWC detection schemes has been shown in fig. 4.12. Using IM/DD detection in a single UOWC link, regardless of pointing defects, results in a significant performance reduction when compared to all OHD-based UOWC transmissions since OHD uses complex coherent receivers.
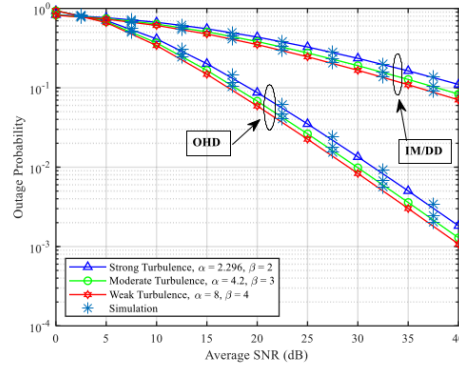
Figure 4.12 Outage probability vs average SNR for various turbulence conditions
under fixed pointing condition operated under both detection schemes

Table 4.8 shows that OP decreases with increasing SNR under both strong and weak
pointing conditions for all turbulence levels. Systems under strong pointing conditions
consistently outperform those under weak pointing, especially at higher SNRs. At 40
dB SNR, OP drops to as low as 1.07×10^{-3} under strong pointing and weak turbulence.
This highlights the critical role of accurate alignment in minimizing signal degradation
in UOWC systems. In fig. 4.13, the OP of the UOWC system is plotted as a function
of average SNR for three different values set of values of α and β. It is self-evident
that the OP is substantially influenced by underwater turbulence conditions. As a
result, the OP in weak turbulence is substantially lower than in moderate and heavy
turbulence. It's worth noting that similar conclusions have been reached for optical
waves in FSO. The OP degrades as expected for smaller ξ, or for smaller α and β.
Results show that the performance degradation caused by strong turbulence is more
severe under weak pointing error conditions rather than strong pointing error levels.

Table 4.8 Outage probability vs average SNR for various turbulence conditions operated under variable pointing errors.

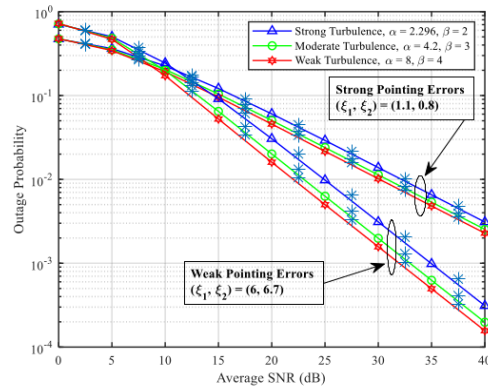| SNR	Outage Probability					
	Strong pointing conditions $(\xi_1 = 1.1, \xi_2 = 0.8)$			Weak turbulence conditions $(\xi_1 = 6, \xi_2 = 6.7)$		
(dB)	Strong	Moderate	Weak	Strong	Moderate	Weak
0	9.29×10^{-1}	9.36×10^{-1}	9.41×10^{-1}	8.31×10^{-1}	8.25×10^{-1}	8.20×10^{-1}
5	7.03×10^{-1}	6.80×10^{-1}	6.63×10^{-1}	7.65×10^{-1}	7.46×10^{-1}	7.32×10^{-1}
10	4.13×10^{-1}	3.68×10^{-1}	3.41×10^{-1}	6.69×10^{-1}	6.35×10^{-1}	6.10×10^{-1}
15	2.01×10^{-1}	1.66×10^{-1}	1.48×10^{-1}	5.55×10^{-1}	5.07×10^{-1}	4.76×10^{-1}
20	8.71×10^{-2}	6.79×10^{-2}	5.91×10^{-2}	4.36×10^{-1}	3.83×10^{-1}	3.50×10^{-1}
25	3.51×10^{-2}	2.63×10^{-2}	2.25×10^{-2}	3.27×10^{-1}	2.75×10^{-1}	2.46×10^{-1}
30	1.35×10^{-2}	9.84×10^{-3}	8.32×10^{-3}	2.35×10^{-1}	1.90×10^{-1}	1.66×10^{-1}
35	5.02×10^{-3}	3.59×10^{-3}	3.01×10^{-3}	1.63×10^{-1}	1.27×10^{-1}	1.09×10^{-1}
40	1.83×10^{-3}	1.29×10^{-3}	1.07×10^{-3}	1.10×10^{-1}	8.32×10^{-2}	7.04×10^{-2}

Figure 4.13 Outage probability vs average SNR for various turbulence conditions operated under variable pointing errors

The fig. 4.14 illustrates the variation in received power with transmission range for UOWC system under different configurations. It compares single-hop and dual-hop

communication setups, each evaluated using two different receiver aperture sizes of 10 cm and 15 cm. As expected, the received power decreases with increasing range due to fading in the underwater channel. However, system employing dual-hop communication show a noticeable improvement in received power across all distances compared to their single-hop counterparts. This is because dual-hop setups use an intermediate relay, which helps reduce the total transmission loss over long distances. Additionally, increasing the receiver aperture from 10 cm to 15 cm significantly enhances the received power, as a larger aperture allows more optical signal to be collected, thereby improving detection efficiency. Overall, the combination of dual-hop communication and a larger receiver aperture yields the best performance, making it a favourable choice for extending the range and reliability of UOWC system.
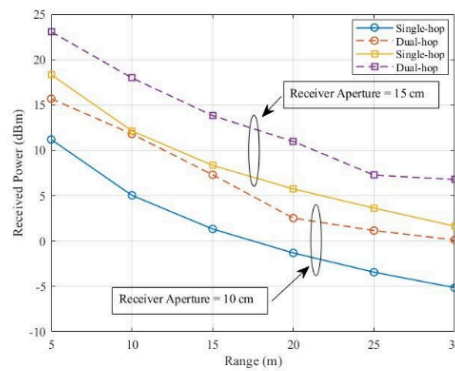
Figure 4.14 Received power vs. transmission range for UOWC system with various receiver apertures

The fig. 4.15 presents the received power as a function of transmission range for UOWC system under varying OSNR levels. It compares both single-hop and dual-hop configurations at OSNR values of 30 dB and 50 dB. Across all scenarios, received power decreases with increasing range due to signal attenuation in the underwater environment. However, system operating at higher OSNR (50 dB) consistently exhibit better performance, with stronger received signals maintained over longer distances.

69

Additionally, the dual-hop configuration clearly outperforms the single-hop system at both OSNR levels, as the presence of an intermediate relay helps mitigate propagation loss. Notably, the improvement offered by dual-hop communication becomes more pronounced at larger distances. This highlights the combined benefits of higher OSNR and dual-hop architecture in enhancing the transmission range and reliability of UOWC system.
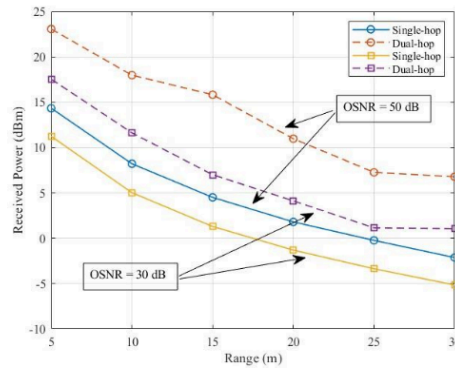

Figure 4.15 Received power versus transmission range for UOWC system under different OSNR levels

The dual-hop relaying system using the *M*- distribution was analysed for UOWC with pointing errors. The results showed that using a relay significantly improved signal strength and reduced bit error rates, especially in severe fading and misalignment conditions. The impact of pointing errors and water turbulence was thoroughly studied, and the system showed better performance with optimal relay placement. Theoretical expressions closely matched simulation outcomes, confirming the accuracy of the analysis and the advantages of dual-hop relaying in challenging underwater environments.

4.6   Conclusion

This chapter addressed the critical challenge of performance degradation in UOWC systems caused by turbulence-induced fading and misalignment errors. To overcome these limitations, a novel dual-hop UOWC architecture was proposed, modelled using the M-distribution to accurately characterize underwater turbulence. The system employed fixed-gain relaying to extend communication range and reduce individual node power requirements, with analysis conducted under various turbulence and pointing error conditions.

Comprehensive results demonstrate that the proposed dual-hop relaying model significantly enhances system performance over traditional single-hop configurations. Across all turbulence regimes, the dual-hop system achieved higher EC, lower OP and better received power, particularly under strong and weak pointing conditions. For example, under strong turbulence and high SNR, dual-hop achieved up to 23.26 Nats/sec/Hz compared to 14.74 23.26 Nats/sec/Hz in single-hop, and under weak pointing conditions, capacity reached as high as 35.75 Nats/sec/Hz. Additionally, dual-hop links maintained stronger received power and exhibited better tolerance to signal attenuation across longer distances.

The results further show that the OHD detection scheme consistently outperformed IM/DD in terms of average BER and OP, particularly under strong turbulence. OHD achieved lower BER values (e.g., 1.99×10^{-3} at 40 dB under strong turbulence) and more reliable communication with lower OP's, reinforcing its robustness and suitability for underwater scenarios. The impact of pointing errors was also examined, revealing that system performance deteriorates significantly under weak pointing conditions, emphasizing the need for precise beam alignment in practical deployments.

In summary, the proposed dual-hop UOWC system with OHD detection presents a robust, high-capacity, and power-efficient solution for long-range UOWC. The integration of relaying and optimal detection strategies ensures enhanced reliability and performance, making it a promising approach for future underwater monitoring, surveillance and data transfer applications.

71

CHAPTER 5

PERFORMANCE EVALUATION OF REED–SOLOMON CODED UNDERWATER OPTICAL WIRELESS COMMUNICATION SYSTEM OVER GAMMA-GAMMA FADING CHANNEL

5.1   Introduction

In modern underwater monitoring and defence systems, establishing a reliable communication bridge between submerged assets and terrestrial control centres is crucial. This hybrid communication framework often involves Free Space Optical (FSO) communication above the surface and UOWC below it. As illustrated in Fig. 5.1, the onshore station communicates with a submarine using an FSO link, which serves as the airborne communication path. However, this FSO channel is vulnerable to environmental factors such as rain, fog and haze, which can cause severe attenuation and signal degradation. To overcome such degradation and ensure robust data transmission, coding techniques such as Optical Code Division Multiple Access (OCDMA) can be used. These codes enable secure, simultaneous multi-user communication and offer resilience against atmospheric disruptions due to their low cross-correlation properties.

Once the data reaches the submarine, it is relayed to a network of AUVs and underwater optical sensors through a UOWC link. Unlike acoustic systems, UOWC offers high-speed, low-latency data transfer but suffers from absorption, scattering and turbulence in the aquatic environment. To combat these channel impairments, RS codes are integrated into the system. RS codes are highly effective in correcting burst errors and enhancing data reliability, making them ideal for underwater applications. By deploying RS coding techniques in the UOWC path, the system achieves improved error performance, ensuring that mission-critical data collected by underwater sensors is transmitted accurately back to the surface via the submarine and onward to the onshore command centre. Among various error-control coding techniques, RS codes

are recognized for their strong burst-error correction capabilities and resilience against symbol-level distortions, making them highly suitable for underwater optical applications.
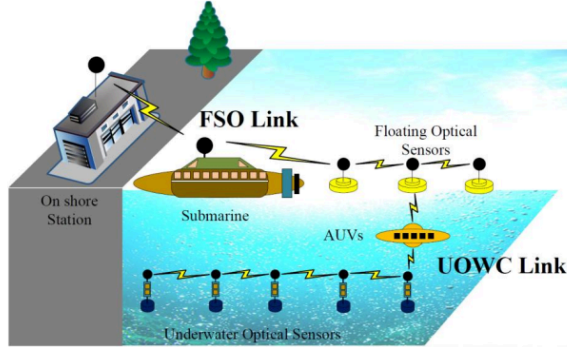

Figure 5.1 FSO and UOWC links in underwater communication

This chapter presents the design of a UOWC system enhanced by the application of RS coding, specifically tailored for channels characterized by GG-distributed fading. This model serves as an established statistical framework to represent irradiance fluctuations under moderate-to-strong turbulence conditions in underwater optical environments. By combining RS coding with this realistic channel model, the study aims to quantify the gains achievable in terms of BER reduction and system reliability.

A modular communication system is developed that encompasses RS encoding, modulation, transmission through the GG-fading channel, optical signal detection, demodulation and RS decoding. Both IM/DD and OHD schemes are considered to evaluate the coded system's adaptability across different receiver configurations. Analytical expressions for the BER are derived for multiple modulation formats, including OOK, PSK and QAM, facilitating a detailed comparative analysis. The influence of RS code parameters, namely the codeword length (n) and the number of message symbols (k), on system performance is thoroughly examined. By varying these parameters, the coding overhead versus performance trade-offs are analysed

under varying turbulence regimes. Simulation results validate the analytical findings, demonstrating that RS-coded UOWC system can achieve significant improvements in BER, particularly in challenging channel conditions where traditional un-coded system experience severe degradation.

The principal contributions of this chapter are summarized as follows:

- A RS coded UOWC system model is proposed and evaluated under GG distributed fading conditions.
- Analytical derivations for BER and decoding error probability performance are presented for multiple modulation schemes, covering both IM/DD and OHD receiver architectures.
- A systematic study of RS code parameter variations is conducted to understand their impact on system reliability and coding efficiency.
- Simulation results highlight the effectiveness of RS coding in improving communication robustness across different turbulence strengths.

5.2 Gamma–Gamma distributed channel modelling for turbulence induced fading

UOWC system models typically include a transmitter, a channel and a receiver. The transmitter encodes the data to be transferred using various modulation and coding techniques, converts it to an optical signal and broadcasts it underwater using a high-power LED or laser. Various processes including absorption, scattering and turbulence can produce signal attenuation, dispersion and distortion in the underwater channel. As a result, the received signal has defects such as fading, noise and ISI. Taking into account the intensity variability caused by underwater turbulence. The GG model is employed at UOWC to characterize the random fluctuations in signal strength generated by water turbulence. The GG distribution is a two-parameter statistical distribution that is frequently used to describe small-scale fading in UOWC system, in which the received signal strength varies rapidly over short distances and time intervals. The received signal is given as

$$R = \eta I x + n,\tag{5.1}$$

74

where η represents the optical-to-electrical conversion coefficient, I is the normalized irradiance, x denotes the transmitted information bit i.e., 1, 0 and n is the AWGN with zero mean and variance $N_0/2$.

Now the GG model for underwater channels described as,

$$f_I(I) = \frac{2(\alpha\beta)^{(\alpha+\beta)/2}}{\Gamma(\alpha)\Gamma(\beta)} I^{(\alpha+\beta)/2-1} K_{\alpha-\beta}\left(2\sqrt{\alpha\beta I}\right), \qquad (5.2)$$

Where $K_{\alpha-\beta}$ is the Bessel function of 2nd kind and α, β are the parameters associated with temperature and salinity variations. Now utilizing eqn. (1) and eqn. (2) from appendix -I in eqn. (5.3), the PDF of the UOWC system can be given as

$$f_I(I) = \frac{1}{\Gamma(\alpha)\Gamma(\beta)I} G_{0,2}^{2,0}\left[\alpha\beta I \Big|\begin{matrix}-\\\alpha,\beta\end{matrix}\right]. \qquad (5.3)$$

Now under the heterodyne detection technique, the PDF corresponding to the GG model is given as

$$f_\gamma(\gamma) = \frac{1}{\Gamma(\alpha)\Gamma(\beta)\gamma} G_{0,2}^{2,0}\left[\alpha\beta\frac{\gamma}{\mu_1} \Big|\begin{matrix}-\\\alpha,\beta\end{matrix}\right]. \qquad (5.4)$$

Under the Intensity-modulated/ Direct detection technique, the average electrical SNR is given as

$$\mu_2 = \frac{\bar{\gamma}\alpha\beta}{1+\alpha+\beta+\alpha\beta} \qquad (5.5)$$

So, the PDF of GG distribution under the IM/DD technique is given as

$$f_\gamma(\gamma) = \frac{1}{2\Gamma(\alpha)\Gamma(\beta)\gamma} G_{0,2}^{2,0}\left[\alpha\beta\left(\frac{\gamma}{\mu_2}\right)^{1/2} \Big|\begin{matrix}-\\\alpha,\beta\end{matrix}\right]. \qquad (5.6)$$

By utilizing eqn. (5.7) and $e^{-x} = G_{0,1}^{1,0}\left(x\Big|\begin{matrix}-\\0\end{matrix}\right)$ along with eqn. (5.4) and eqn. (5.6), combined PDF under both types of detection technique is given as eqn. (5.8).

$$G_{p,q}^{m,n}\left(z\left|\begin{matrix}\alpha+a_1,...,\alpha+a_n,\alpha+a_{n+1},...,\alpha+a_p,\\\alpha+b_1,...,\alpha+b_m,\alpha+b_{m+1},...,\alpha+b_p\end{matrix}\right.\right) = z^\alpha G_{p,q}^{m,n}\left(z\left|\begin{matrix}a_1,...,a_n,a_{n+1},...,a_p,\\b_1,...,b_m,b_{m+1},...,b_p\end{matrix}\right.\right) \qquad (5.7)$$

75

$$f_\gamma(\gamma) = \frac{1}{r\Gamma(\alpha)\Gamma(\beta)\gamma} G_{0,2}^{2,0}\left[\alpha\beta\left(\frac{\gamma}{\mu_r}\right)^{1/r} \middle| \begin{array}{c} - \\ \alpha, \beta \end{array} \right]. \qquad (5.8)$$

eqn. (5.8) is further termed as the unified PDF under GG distributed fading channels.

5.3   Reed–Solomon based forward error correction in UOWC System

In FSO communication systems, achieving reliable transmission is highly challenging due to atmospheric disturbances such as rain, fog, haze and turbulence, which cause severe signal attenuation, scattering, and fading. These effects significantly degrade system performance, especially over long distances and in multi-user scenarios. To overcome these challenges, multi-diagonal Optical Code Division Multiple Access (OCDMA) codes are employed, enabling simultaneous multi-user access with low cross-correlation and improved interference rejection. The fig. 5.2 illustrates such an architecture, where each user's data is modulated, multiplexed using unique codes and decoded using Fiber Bragg Gratings (FBGs) at the receiver end, ensuring high-fidelity reception and reduced multi-access interference.
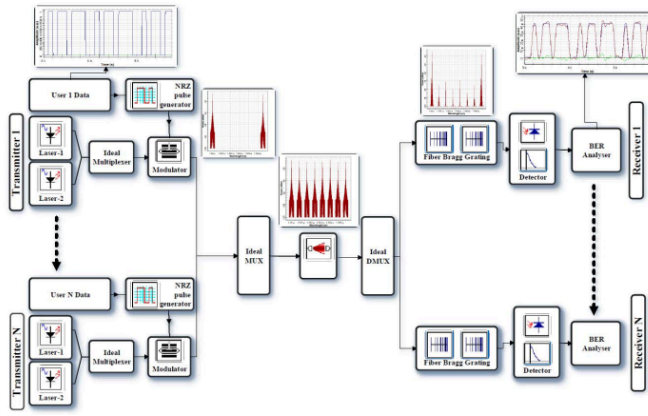

Figure 5.2 Implementation of MD-OCDMA code for FSO link in Opti System

76

However, when transitioning from atmospheric FSO links to UOWC systems, additional challenges arise due to severe absorption, scattering by water particles and random turbulence-induced fading. These underwater effects are more dynamic and unpredictable than those in air, making reliable data recovery even more difficult. To address this, RS error correction codes are integrated into the UOWC system. RS codes are highly effective in correcting burst errors and improving decoding reliability, especially under strong turbulence conditions. RS-coded UOWC systems show substantial reduction in Decoding Error Probability (DEP), making them a robust solution for high-speed, error-resilient underwater communication. Figure 5.3 presents the block diagram of an RS-coded UOWC system, comprising a transmitter, an underwater fading channel and a receiver. At the transmitter end, the source data is first encoded using the RS encoder to introduce redundancy and enable error correction. The encoded symbols are then modulated into optical signals suitable for underwater transmission. These signals propagate through the underwater fading channel, where they are subjected to impairments such as absorption, scattering, turbulence, and varying salinity factors that heavily degrade signal quality. At the receiver, the signal is first demodulated, and the RS decoder is then employed to correct any symbol errors introduced by the channel. Finally, the corrected data is delivered to the destination. This robust framework ensures enhanced communication reliability in underwater environments by leveraging the error correction strength of RS codes. RS-code can be referred to as (n,k), where n is the codeword length and k indicates the number of message symbols in the codeword. The error-correcting capability of the code is $t_{ec} = (n-k)/2$ and the minimum distance of the code is $d_{min} = n-k-1$. The following algorithm outlines the step-by-step implementation of the RS encoding and decoding processes within this UOWC framework.

Algorithm: Reed Solomon coding in UOWC

---
1. Define the message to be transmitted.
2. Choose a RS code with parameters (n,k), where n is the length of the codeword and k is the length of the message.
3. Encode the message using the RS code to generate a codeword.

---

4. Modulate the codeword using a suitable modulation scheme (OOK, PSK & QAM) for UOWC.
5. Transmit the modulated signal through the UOWC fading channel.
6. Receive the signal at the receiver end.
7. Demodulate the received signal to recover the modulated codeword.
8. Decode the codeword using the same RS code used for encoding to recover the original message.
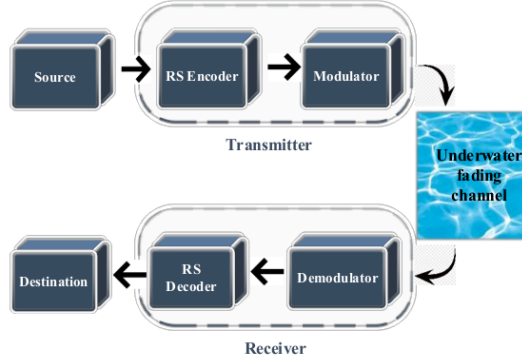

Figure 5.3 Block diagram of RS coded UOWC system

The algorithm to compute the RS coding in UOWC is shown below.

5.4   Performance evaluation across RS code configurations

Building upon the RS-coded UOWC system architecture described earlier, this section presents a comprehensive evaluation of system performance across various RS code configurations. In UOWC system, signal variations due to underwater turbulence have been modelled using the GG-distribution for weak to strong turbulence. Generalized expression for average BER for various modulation schemes is given as

$$P_e = \frac{\delta}{2\Gamma(p)} \sum_{k=1}^{n} \int_{0}^{\infty} \Gamma(p, q_k \gamma) f_\gamma(\gamma) d\gamma, \qquad (5.8)$$

where n, p, q_k, δ are the variables depending on various modulation schemes and r is the type of detection ($r = 1$ for OHD and $r = 2$ for IM/DD). Table 5.1 shows various parameters associated with different modulation schemes.

Table 5.1 Parameters associated with different modulation schemes

Modulation Scheme	δ	p	q_k	n
OOK	1	1/2	1/4	1
BPSK	1	1/2	1	1
16-PSK	1/2	1/2	$\sin^2\left(\dfrac{(2k-1)\pi}{16}\right)$	4
16-QAM	3/4	1/2	$\dfrac{(2k-1)^2}{10}$	2
64-QAM	7/12	1/2	$\dfrac{3(2k-1)^2}{126}$	4

By substituting eqn. (5.7) in eqn. (5.8) and utilizing eqn. (1) and eqn. (2) from appendix-I, the generalized expression for average BER under both detection schemes and under various modulation schemes as

$$P_e = \frac{\delta}{2\Gamma(p)}\left(\frac{r^{\alpha+\beta}}{(2\pi)^{r-1}}G_{2,2r+1}^{2r,2}\left[\left(\frac{\alpha\beta}{r^2}\right)^r \frac{1}{\mu_r q_k}\middle|\begin{array}{l}1,(1-p)\\\Delta(r,\alpha),\Delta(r,\beta),0\end{array}\right]\right). \tag{5.9}$$

RS codes are capable of correcting up to $t = \left\lceil\frac{n-k}{2}\right\rceil$ symbol errors in a codeword of n symbols. If more than t symbols are in error, the decoder fails. Assuming symbol errors are independent and identically distributed with probability P_e, the DEP P_b is the probability of receiving more than t errors and it is given as

$$P_b = \sum_{j=t_{ec}+1}^{n}\binom{n}{j}P_e^j(1-P_e)^{n-j} \tag{5.10}$$

This represents the tail probability of the binomial distribution and quantifies the likelihood of RS decoder failure. The average BER is approximated from the DEP as

79

$$P_b \approx \frac{1}{n} \sum_{j=t_{ec}+1}^{n} j \binom{n}{j} P_e^j (1-P_e)^{n-j} \qquad (5.11)$$

where $\binom{n}{j} = \frac{n!}{j!(n-j)!}$. This formula estimates the average number of erroneous bits per symbol per codeword when the decoder fails. The final expression for DEP is given as

$$P_b \approx \frac{1}{n} \sum_{j=t_{ec}+1}^{t} j \frac{n!}{j!(n-j)!} P_e^j (1-P_e)^{n-j} \qquad (5.12)$$

In the next section, the goal is to assess how different parameter choices such as codeword length n, message length k and error-correcting capability t impact the reliability and efficiency of data transmission under underwater fading conditions.

5.5   Results and discussion

In this section, the proposed RS coded model has been compared with the uncoded UOWC model under various turbulence conditions. RS codes perform better than uncoded data transmission because these codes provide a higher level of error correction through the use of redundant symbols. These redundant symbols are used to detect and correct errors that may occur during transmission. To support the performance analysis, table 5.2 presents the estimated parameters of the proposed UOWC system under different turbulence conditions classified as weak, moderate, and strong based on the SI. These conditions directly influence the attenuation characteristics of the optical channel and hence the reliability of the UOWC link.

Table 5.2 Estimated parameters of the proposed system for various types of attenuation based on SI

Attenuation	σ_I^2	σ_r^2	α	β
Strong	3.1952	0.23903	0.9815	0.9276
Moderate	1.9328	0.1795	1.4388	1.3661
Weak	0.4769	0.065	4.7488	4.5442

Tables 5.3 and 5.4 compare the DEP for uncoded and RS-coded UOWC systems under strong and moderate turbulence, respectively, using both OHD and IM/DD detection schemes. In both cases, RS-coded systems show dramatic error reduction, especially when combined with OHD. Under strong turbulence at 50 dB, RS-OHD achieves a DEP of 1.4×10^{-27}, compared to 1.6×10^{-4} without coding. Under moderate turbulence, DEP further drops. These results highlight the significance of RS coding in enhancing error resilience, with OHD offering superior performance over IM/DD. The findings confirm that combining powerful error correction with optimal detection is crucial for achieving ultra-reliable UOWC communication, even in severe channel conditions.

Table 5.3 Comparison of DEP for uncoded and proposed RS system using both types of detection techniques under strong turbulence condition

E_b/N_o (dB)	Decoding Error Probability			
	Uncoded OHD	Uncoded IM/DD	Proposed RS OHD	Proposed RS IM/DD
0	3.3×10^{-1}	8.3×10^{-1}	3.4×10^{-1}	8.5×10^{-1}
5	2.3×10^{-1}	7.3×10^{-1}	2.5×10^{-1}	7.5×10^{-1}
10	1.4×10^{-1}	6.1×10^{-1}	1.6×10^{-1}	6.3×10^{-1}
15	7.7×10^{-2}	4.9×10^{-1}	5.5×10^{-2}	5.1×10^{-1}
20	3.7×10^{-2}	3.7×10^{-1}	1.6×10^{-3}	3.9×10^{-1}
25	1.6×10^{-2}	2.8×10^{-1}	2.6×10^{-6}	2.9×10^{-1}
30	6.8×10^{-3}	2.0×10^{-1}	6.1×10^{-10}	2.1×10^{-1}
35	2.8×10^{-3}	1.4×10^{-1}	4.8×10^{-14}	1.4×10^{-1}
40	1.1×10^{-3}	9.3×10^{-2}	2.0×10^{-18}	8.0×10^{-2}
45	4.1×10^{-4}	6.2×10^{-2}	5.9×10^{-23}	2.1×10^{-2}
50	$\mathbf{1.6 \times 10^{-4}}$	$\mathbf{4.1 \times 10^{-2}}$	$\mathbf{1.4 \times 10^{-27}}$	$\mathbf{2.1 \times 10^{-3}}$

Fig. 5.4 clearly demonstrates the advantage of incorporating RS coding in UOWC systems under varying turbulence conditions. Under strong turbulence, both uncoded OHD and IM/DD schemes exhibit high DEP across all E_b/N_o values, indicating poor resilience to fading. However, the proposed RS-coded schemes significantly improve error performance, with the RS IM/DD configuration showing the steepest decline in DEP, reaching below 10^{-5} at $E_b/N_o > 35$ dB. Under moderate turbulence, the performance gain is even more pronounced, as the RS-coded systems achieve much

lower error floors at lower SNR levels. This validates the effectiveness of RS codes in enhancing system robustness, particularly when paired with IM/DD detection, making them highly suitable for turbulent underwater environments.

Table 5.4 Comparison of DEP for uncoded and proposed RS system using both types of detection techniques under moderate turbulence condition

| E_b/N_o (dB)	Decoding Error Probability			
	Uncoded OHD	Uncoded IM/DD	Proposed RS OHD	Proposed RS
0	2.3×10^{-1}	5.8×10^{-1}	2.4×10^{-1}	5.9×10^{-1}
5	1.5×10^{-1}	4.8×10^{-1}	1.6×10^{-1}	5.0×10^{-1}
10	7.8×10^{-2}	3.7×10^{-1}	6.0×10^{-2}	3.9×10^{-1}
15	3.2×10^{-2}	2.7×10^{-1}	7.9×10^{-4}	2.8×10^{-1}
20	1.1×10^{-2}	1.8×10^{-1}	1.0×10^{-7}	1.9×10^{-1}
25	3.3×10^{-3}	1.1×10^{-1}	5.5×10^{-13}	1.2×10^{-1}
30	8.9×10^{-4}	6.8×10^{-2}	5.0×10^{-19}	3.3×10^{-2}
35	2.3×10^{-4}	3.9×10^{-2}	1.7×10^{-25}	1.8×10^{-3}
40	5.5×10^{-5}	2.2×10^{-2}	3.3×10^{-32}	2.1×10^{-5}
45	1.3×10^{-5}	1.2×10^{-2}	4.3×10^{-39}	7.5×10^{-8}
50	3.0×10^{-6}	6.1×10^{-3}	4.3×10^{-46}	1.2×10^{-10}
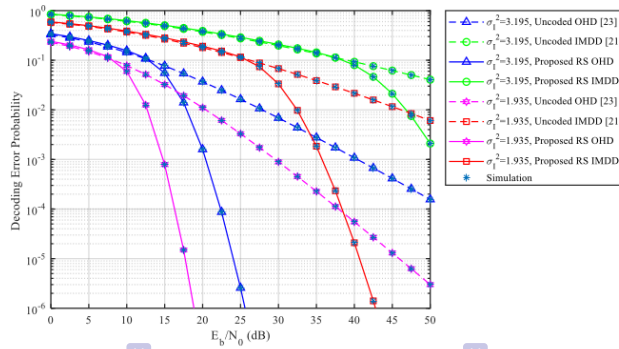
Figure 5.4 DEP using both types of detection techniques under strong and moderate turbulence conditions

82

Tables 5.5 and 5.6 present a detailed comparison of the DEP for uncoded and RS-coded OOK systems under **strong** and **moderate turbulence** conditions, respectively. Under strong turbulence, the proposed RS (127,106) configuration exhibits a dramatic improvement in DEP, achieving values as low as 6.77×10^{-6} at $E_b/N_0 = 50$ dB, compared to 4.06×10^{-2} for the uncoded case. Other RS code variants, such as RS (31,15) and RS (31,21), also provide significant DEP reductions, although the level of improvement varies with code rate and error correction capability.

Table 5.5 DEP comparison of uncoded and RS-coded OOK system in strong turbulence

E_b/N_o (dB)	Decoding Error Probability				
	Uncoded	Proposed RS (127,106)	Proposed RS (31,15)	Proposed RS (31,21)	Proposed RS (31,27)
0	8.33×10^{-1}	8.87×10^{-1}	8.44×10^{-1}	8.63×10^{-1}	8.47×10^{-1}
5	7.28×10^{-1}	7.96×10^{-1}	7.42×10^{-1}	7.66×10^{-1}	7.46×10^{-1}
10	6.09×10^{-1}	6.85×10^{-1}	6.24×10^{-1}	6.50×10^{-1}	6.28×10^{-1}
15	4.87×10^{-1}	5.63×10^{-1}	5.01×10^{-1}	5.28×10^{-1}	5.06×10^{-1}
20	3.73×10^{-1}	4.37×10^{-1}	3.86×10^{-1}	4.10×10^{-1}	3.90×10^{-1}
25	2.75×10^{-1}	2.80×10^{-1}	2.86×10^{-1}	2.99×10^{-1}	2.89×10^{-1}
30	1.97×10^{-1}	1.11×10^{-1}	2.03×10^{-1}	1.82×10^{-1}	2.08×10^{-1}
35	1.37×10^{-1}	2.28×10^{-2}	1.35×10^{-1}	7.85×10^{-2}	1.44×10^{-1}
40	9.28×10^{-2}	2.48×10^{-3}	7.83×10^{-2}	2.20×10^{-2}	7.99×10^{-2}
45	6.19×10^{-2}	1.59×10^{-4}	3.83×10^{-2}	4.15×10^{-3}	2.12×10^{-2}
50	4.06×10^{-2}	6.77×10^{-6}	1.58×10^{-2}	5.67×10^{-4}	2.09×10^{-3}

Fig. 5.5 shows the comparison of DEP performance of uncoded and proposed RS coded system under IM/DD scheme using OOK modulation under strong and moderate turbulence conditions. For both turbulence levels, the uncoded IM/DD scheme performs the worst, showing high decoding error probability even at higher E_b/N_0. Applying RS codes dramatically improves performance, reducing the DEP by several orders of magnitude. RS (127,106) (higher block length and code rate) consistently outperforms shorter codes like RS (31,15), RS (31,21) and RS (31,27).

This is because longer codes can spread the error correction capability over a larger number of symbols, offering better resilience. Under weaker turbulence ($\sigma_I^2 = 1.1935$), all RS-coded curves shift downward and leftward, achieving lower error probabilities at lower SNR values compared to the strong turbulence case ($\sigma_I^2 = 3.195$). This confirms that RS coding is more effective in moderate conditions but still beneficial under strong fading. For some low SNR values (e.g., E_b/N_0 < 10 dB), the differences between codes are small. However, as SNR increases, the advantage of strong RS coding becomes more significant, especially for RS (127,106), which achieves near-zero decoding errors at E_b/N_0 > 40 dB even in strong turbulence.

Table 5.6 DEP comparison of uncoded and RS-coded OOK system in moderate turbulence

E_b/N_o (dB)	**Decoding Error Probability**				
	Uncoded	**Proposed RS (127,106)**	**Proposed RS (31,15)**	**Proposed RS (31,21)**	**Proposed RS (31,27)**
0	5.78×10^{-1}	6.30×10^{-1}	5.89×10^{-1}	6.07×10^{-1}	5.92×10^{-1}
5	4.80×10^{-1}	5.44×10^{-1}	4.92×10^{-1}	5.15×10^{-1}	4.96×10^{-1}
10	3.71×10^{-1}	4.33×10^{-1}	3.84×10^{-1}	4.07×10^{-1}	3.88×10^{-1}
15	2.67×10^{-1}	2.74×10^{-1}	2.78×10^{-1}	2.92×10^{-1}	2.82×10^{-1}
20	1.79×10^{-1}	9.13×10^{-2}	1.86×10^{-1}	1.59×10^{-1}	1.91×10^{-1}
25	1.13×10^{-1}	1.14×10^{-2}	1.07×10^{-1}	4.90×10^{-2}	1.16×10^{-1}
30	6.78×10^{-2}	5.12×10^{-4}	4.69×10^{-2}	7.40×10^{-3}	3.33×10^{-2}
35	3.89×10^{-2}	9.69×10^{-6}	1.49×10^{-2}	5.85×10^{-4}	1.84×10^{-3}
40	2.15×10^{-2}	9.33×10^{-8}	3.54×10^{-3}	2.78×10^{-5}	2.09×10^{-5}
45	1.16×10^{-2}	5.44×10^{-10}	6.73×10^{-4}	9.14×10^{-7}	7.47×10^{-8}
50	6.08×10^{-3}	2.19×10^{-12}	1.09×10^{-4}	2.30×10^{-8}	1.22×10^{-10}
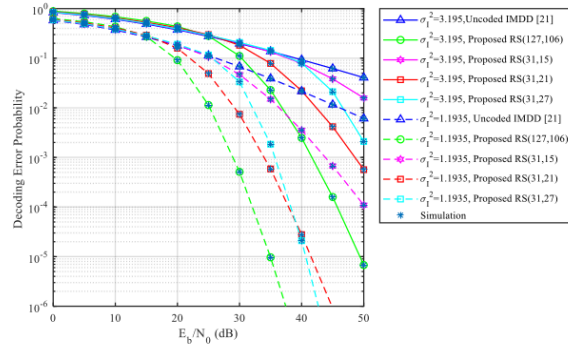
Figure 5.5 DEP for IM/DD using OOK modulation under strong turbulence condition

Fig. 5.6 demonstrates the DEP performance of BPSK-modulated OHD system using different RS codes, tested under strong and moderate turbulence conditions. The modulation used here is BPSK, which is widely favoured in underwater communication system due to its robustness and simplicity. The system performance is further enhanced through RS error correction. The uncoded BPSK-OHD system exhibits a high DEP across all E_b/N_0 values, especially under strong turbulence. Introducing RS coding dramatically reduces the error floor. Even short RS codes like RS (31,15) show more than three orders of magnitude improvement at $E_b/N_0 = 20$ dB compared to the uncoded case. Among the tested codes, RS (127,106) provides the best performance, reaching error probabilities as low as 10^{-6}, particularly under moderate turbulence. As expected, RS (31,15) outperforms RS (31,21) and RS (31,27) due to its stronger error correction capability (i.e., lower code rate). However, this comes at the cost of redundancy and throughput. For all codes, performance improves by ~5–10 dB when moving from $\sigma_I^2 = 3.195$ to $\sigma_I^2 = 1.1935$. The simulation results (marked as stars) closely align with theoretical curves, validating the derived decoding error probability expression based on BPSK symbol error rates under GG-fading.
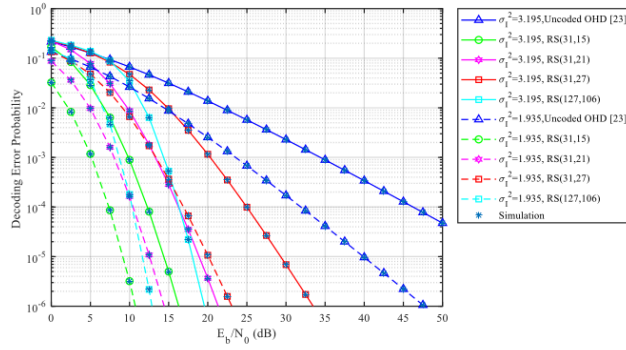
Figure 5.6 DEP for OHD using BPSK modulation under strong and moderate
turbulence conditions

Tables 5.7 and 5.8 present a detailed analysis of the DEP for RS-coded systems using various modulation formats BPSK, 8-PSK, 16-QAM, and 64-QAM under strong turbulence conditions. The analysis includes RS (31,27) and RS (31,15) codes. It is evident that BPSK consistently offers the lowest DEP across all SNR values due to its high resilience to noise and channel distortions. For example, RS (31,27)-coded BPSK achieves a DEP of 6.61×10^{-11} at E_b/N_0 = 50 dB, whereas higher-order schemes like 64-QAM, while more bandwidth-efficient, show comparatively higher error rates at the same SNR. This trend becomes more prominent in RS (31,15), where the enhanced error correction capability further reduces the DEP of all modulation types, with BPSK reaching an impressively low DEP of 1.96×10^{-30} at 50 dB.

Table 5.7 DEP analysis of uncoded and RS-coded (31,27) system with different
modulation formats in strong turbulence

| E_b/N_0 (dB) | Decoding Error Probability | | | | |
| | Uncoded | Proposed RS (31,27) | | | |
		BPSK	8PSK	16QAM	64QAM
0	8.33×10^{-1}	2.25×10^{-1}	4.11×10^{-1}	4.77×10^{-1}	7.01×10^{-2}
5	7.28×10^{-1}	1.28×10^{-1}	2.92×10^{-1}	3.49×10^{-1}	8.14×10^{-2}

10	6.09×10^{-1}	4.72×10^{-2}	1.80×10^{-1}	2.27×10^{-1}	5.60×10^{-2}
15	4.87×10^{-1}	9.60×10^{-3}	8.25×10^{-2}	1.20×10^{-1}	3.50×10^{-2}
20	3.73×10^{-1}	1.16×10^{-3}	2.20×10^{-2}	4.04×10^{-2}	1.85×10^{-2}
25	2.75×10^{-1}	9.92×10^{-5}	3.27×10^{-3}	7.43×10^{-3}	6.42×10^{-3}
30	1.97×10^{-1}	6.89×10^{-6}	3.19×10^{-4}	8.35×10^{-4}	1.23×10^{-3}
35	1.37×10^{-1}	4.22×10^{-7}	2.40×10^{-5}	6.82×10^{-5}	1.41×10^{-4}
40	9.28×10^{-2}	2.39×10^{-8}	1.54×10^{-6}	4.60×10^{-6}	1.18×10^{-5}
45	6.19×10^{-2}	1.28×10^{-9}	9.00×10^{-8}	2.77×10^{-7}	8.02×10^{-7}
50	4.06×10^{-2}	6.61×10^{-11}	4.93×10^{-9}	1.55×10^{-8}	4.86×10^{-8}

Table 5.8 DEP analysis of uncoded and RS-coded (31,15) system with different modulation formats in strong turbulence

E_b/N_o (dB)	Uncoded	Decoding Error Probability			
		Proposed RS (31,15)			
		BPSK	8PSK	16QAM	64QAM
0	5.78×10^{-1}	1.69×10^{-1}	4.64×10^{-1}	5.36×10^{-1}	7.45×10^{-1}
5	4.80×10^{-1}	2.87×10^{-2}	3.12×10^{-1}	4.02×10^{-1}	9.51×10^{-2}
10	3.71×10^{-1}	8.91×10^{-4}	9.84×10^{-2}	1.92×10^{-1}	6.82×10^{-2}
15	2.67×10^{-1}	5.00×10^{-6}	6.57×10^{-3}	2.55×10^{-2}	3.51×10^{-2}
20	1.79×10^{-1}	7.55×10^{-9}	7.28×10^{-5}	5.58×10^{-4}	5.10×10^{-3}
25	1.13×10^{-1}	4.74×10^{-12}	1.81×10^{-7}	2.32×10^{-6}	1.19×10^{-4}
30	6.78×10^{-2}	1.70×10^{-15}	1.58×10^{-10}	2.86×10^{-9}	5.27×10^{-7}
35	3.89×10^{-2}	4.24×10^{-19}	6.97×10^{-14}	1.57×10^{-12}	6.86×10^{-10}
40	2.15×10^{-2}	8.28×10^{-23}	1.99×10^{-17}	5.17×10^{-16}	3.93×10^{-13}
45	1.16×10^{-2}	1.36×10^{-26}	4.28×10^{-21}	1.22×10^{-19}	1.33×10^{-16}
50	6.08×10^{-3}	1.96×10^{-30}	7.53×10^{-25}	2.29×10^{-23}	3.21×10^{-20}

Fig. 5.7 compares the DEP for different modulation formats like BPSK, 8-PSK, 16-QAM and 64-QAM, with RS-coded schemes RS (31,15) and RS (31,27). The results clearly demonstrate how modulation choice and error-correction strength affect system reliability over a wide range of signal-to-noise ratios E_b/N_0. The RS (31,15) code (lower rate, stronger correction) consistently outperforms RS (31,27), reducing DEP by several orders of magnitude. This is most evident at high E_b/N_0, where RS (31,15)

helps push the error floor as low as 10^{-15} for BPSK. BPSK with RS (31,15) achieves the best performance, offering extremely low error rates even at moderate SNRs. 8PSK and 16-QAM offer a good trade-off between spectral efficiency and error performance. 8-PSK performs better than 16-QAM for both RS codes. 64-QAM, though spectrally efficient, suffers the most in turbulent conditions, especially with weaker RS (31,27), due to its higher susceptibility to noise. The gap between RS (31,15) and RS (31,27) widens as modulation order increases, indicating that higher-order modulations benefit more from stronger coding. For applications prioritizing throughput, RS (31,27) with 16QAM or 64QAM might be acceptable at high E_b/N_0, but for reliability-critical system, BPSK with RS (31,15) is preferable.
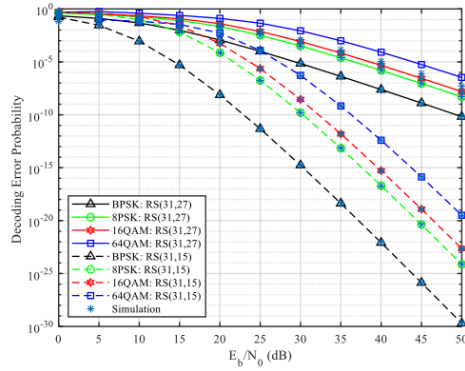
Figure 5.7 DEP for proposed RS codes over OHD with different modulation schemes

Table 5.9 analyses the decoding error probability (DEP) for uncoded and RS-coded systems with varying error correction capabilities (t = 1, 2, 6, 13) across a range of E_b/N_0 values. The results clearly show that as the error correction capability (t) increases, the DEP reduces significantly especially in the mid-to-high SNR regions. For instance, at $E_b/N_0 = 20$ dB, RS (15,23) with t = 1 achieves a DEP of 1.49×10^{-2}, whereas RS (127,101) with t = 13 drops to 1.13×10^{-4}, indicating a two-order magnitude improvement. This trend continues consistently, emphasizing that higher values of t offer more robust error correction, which is crucial for maintaining reliable communication in strongly turbulent underwater optical channels.

88

Table 5.9 Analysis of decoding error performance in uncoded and RS-coded system for different values of error correction capability t.

E_b/N_o (dB)		Decoding Error Probability			
	Uncoded	Proposed RS (15,23), $t=1$	Proposed RS (31,27), $t=2$	Proposed RS (63,51), $t=6$	Proposed RS (127,101), $t=13$
0	3.29×10^{-1}	2.82×10^{-1}	2.83×10^{-1}	2.87×10^{-1}	2.89×10^{-1}
5	2.34×10^{-1}	2.01×10^{-1}	2.04×10^{-1}	2.10×10^{-1}	2.11×10^{-1}
10	1.44×10^{-1}	1.16×10^{-1}	1.22×10^{-1}	1.25×10^{-1}	1.30×10^{-1}
15	7.69×10^{-2}	4.92×10^{-2}	5.05×10^{-2}	3.31×10^{-2}	2.31×10^{-2}
20	3.69×10^{-2}	1.49×10^{-2}	1.16×10^{-2}	1.70×10^{-3}	1.13×10^{-4}
25	1.64×10^{-2}	3.42×10^{-3}	1.54×10^{-3}	1.89×10^{-5}	1.88×10^{-8}
30	6.85×10^{-3}	6.50×10^{-4}	1.39×10^{-4}	7.71×10^{-8}	3.58×10^{-13}
35	2.76×10^{-3}	1.09×10^{-4}	1.00×10^{-5}	1.74×10^{-10}	1.94×10^{-18}
40	1.08×10^{-3}	1.71×10^{-5}	6.27×10^{-7}	2.78×10^{-13}	5.06×10^{-24}
45	4.14×10^{-4}	2.53×10^{-6}	3.60×10^{-8}	3.58×10^{-16}	8.52×10^{-30}
50	1.56×10^{-4}	3.61×10^{-7}	1.95×10^{-9}	4.01×10^{-19}	1.07×10^{-35}

Fig. 5.8 presents the DEP of the proposed OHD system under strong turbulent underwater optical conditions, using RS codes with different error correction capabilities (t). The uncoded OHD system shows the highest DEP, struggling even at $E_b/N_0 > 40$ dB. As soon as RS coding is introduced even with minimal correction (e.g., RS (15,13), $t = 1$) there is a visible improvement in reliability. Each step up in t brings a noticeable gain. RS (31,27), $t = 2$ improves over RS (15,13). RS (63,51), $t = 6$ delivers significantly better performance, reaching error probabilities below 10^{-10} at around 40 dB. RS (127,101), t = 13 achieves exceptional performance, dropping decoding errors to near zero at 45 dB, highlighting the power of deep redundancy. This shows that higher t leads to exponential error reduction, especially in the high SNR regime. Larger codes like RS (127,101) provide the best performance but at the cost of higher latency and computational complexity. Shorter codes (e.g., RS (15,13)) are suitable for real-time or low-latency system where moderate performance is acceptable.
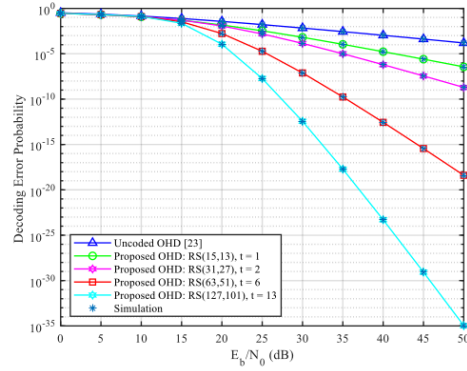
Figure 5.8 DEP for proposed RS codes for various t values

Table 5.10 evaluates the impact of varying RS code rates (R_c) on DEP under identical channel conditions. As expected, lower code rates such as RS (31,9) with $R_c = 0.2903$ offer stronger error correction capability, resulting in significantly lower DEP values, especially in the mid-to-high SNR range. At $E_b/N_0 = 20$ dB, the DEP for RS (31,9) drops to 8.36×10^{-7}, while RS (31,27) with a higher code rate of $R_c = 0.8710$ achieves only 1.16×10^{-2}. This highlights a clear trade-off between redundancy and reliability: as the code rate increases, the amount of redundancy decreases, leading to reduced error correction strength.

Fig. 5.9 evaluates how the code rate ($R_c = k / n$) of RS codes influences the DEP in OHD based UOWC system. This figure clearly shows that the code rate R_c plays a critical role in determining the system's reliability in turbulent underwater optical environments. Lower code rates like RS (31,9) offer exceptional robustness at the cost of bandwidth, making them ideal for deep-sea sensing, defence, or exploration, where error-free communication is a must. On the other hand, RS (31,27) provides faster data transmission but with limited error protection, suitable for real-time, high-throughput applications in calmer conditions. Choosing the right balance between error protection and data rate is key to optimizing performance for different underwater communication scenarios.

90

Table 5.10 Analysis of decoding error performance in uncoded and RS-coded system for various code rate R_c

Eb/No (dB)	Uncoded	Decoding Error Probability			
		RS (31,9) $R_C = 0.2903$	RS (31,15) $R_C = 0.4839$	RS (31,23) $R_C = 0.7419$	RS (31,27) $R_C = 0.8710$
0	3.29×10^{-1}	2.56×10^{-1}	2.96×10^{-1}	2.92×10^{-1}	2.83×10^{-1}
5	2.34×10^{-1}	1.19×10^{-1}	1.72×10^{-1}	2.10×10^{-1}	2.04×10^{-1}
10	1.44×10^{-1}	1.74×10^{-2}	3.90×10^{-2}	1.04×10^{-1}	1.22×10^{-1}
15	7.69×10^{-2}	3.64×10^{-4}	1.75×10^{-3}	2.24×10^{-2}	5.05×10^{-2}
20	3.69×10^{-2}	8.36×10^{-7}	1.36×10^{-5}	1.66×10^{-3}	1.16×10^{-2}
25	1.64×10^{-2}	2.90×10^{-10}	2.58×10^{-8}	5.18×10^{-5}	1.54×10^{-3}
30	6.85×10^{-3}	2.60×10^{-14}	1.88×10^{-11}	9.09×10^{-7}	1.39×10^{-4}
35	2.76×10^{-3}	9.45×10^{-19}	7.40×10^{-15}	1.12×10^{-8}	1.00×10^{-5}
40	1.08×10^{-3}	1.91×10^{-23}	1.97×10^{-18}	1.11×10^{-10}	6.27×10^{-7}
45	4.14×10^{-4}	2.60×10^{-28}	4.01×10^{-22}	9.55×10^{-13}	3.60×10^{-8}
50	1.56×10^{-4}	2.67×10^{-33}	6.79×10^{-26}	7.46×10^{-15}	1.95×10^{-9}
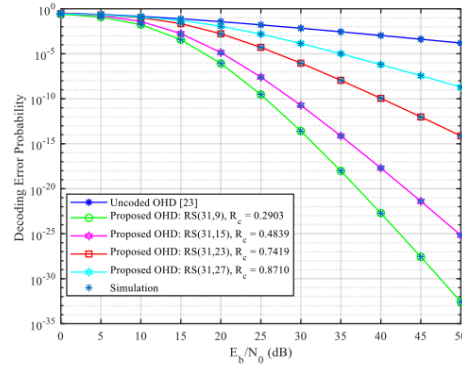
Figure 5.9 DEP for proposed RS codes for various code rate R_c

The performance of RS coded UOWC system was evaluated over GG fading channels. The use of error correction coding significantly reduced BER, especially under moderate to strong turbulence. The system maintained reliable communication even in

harsh underwater conditions. Analytical results closely matched simulation data, confirming that RS coding effectively improves the robustness and accuracy of data transmission in fading environments.

5.6 Conclusion

UOWC systems are critically affected by severe underwater environment, where factors like absorption, scattering, and turbulence cause severe signal degradation. These channel impairments significantly increase the DEP, making it difficult to maintain reliable communication, especially under strong turbulence conditions.

To address this challenge, a robust RS-coded UOWC model was proposed. The model was evaluated under various modulation formats, detection schemes, code lengths, code rates, and turbulence levels. The aim was to enhance the system's resilience to turbulence-induced errors by leveraging the strong error correction capabilities of RS codes.

The results clearly validate the effectiveness of the proposed approach. In one scenario, the DEP dropped from 1.6×10^{-4} in the uncoded system to as low as 1.4×10^{-27} when RS coding was applied under strong turbulence with OHD detection. Similarly, under moderate turbulence, the DEP reduced drastically, demonstrating near error-free performance. RS codes also provided considerable improvements across different modulation schemes. For instance, when BPSK modulation was combined with RS $(127,106)$ coding, the system achieved DEP below 10^{-6} at moderate SNR levels several orders of magnitude better than the uncoded case.

The evaluation further showed that the performance of RS-coded systems is highly dependent on code parameters. Lower code rates and higher error correction capabilities offer better reliability but reduce throughput, while higher code rates support faster data transmission at the cost of reduced protection. This trade-off allows the system to be tuned for specific application needs whether it's low-latency transmission in calm waters or robust sensing in high-turbulence underwater environments.

In conclusion, the integration of RS codes significantly strengthens UOWC system performance by reducing error rates and improving link reliability under challenging underwater conditions. The proposed model offers a flexible and scalable solution that can be adapted to diverse underwater applications, establishing RS coding as a critical component for the development of next-generation, high-reliability UOWC systems.

CHAPTER 6

DEEP LEARNING BASED CONSTELLATION SIGNAL

CLASSIFICATION IN UNDERWATER OPTICAL WIRELESS

COMMUNICATION SYSTEM

6.1 Introduction

As UOWC system evolve toward supporting increasingly complex applications such as underwater sensor networks, real-time video transmission and autonomous vehicle communications, efficient signal processing techniques become critical. One important aspect of ensuring reliable link performance is the accurate classification of modulation schemes at the receiver. Modulation classification plays a vital role in adaptive communications, cognitive networking and electronic warfare, enabling dynamic signal detection and identification under varying channel conditions. Traditional approaches to modulation recognition have typically relied on manual feature extraction followed by ML classifiers such as K-Nearest Neighbors (KNN) or Support Vector Machines (SVM). However, these methods often lack robustness when faced with rapidly changing or highly impaired channel environments, as encountered in underwater optical links. The inherent complexity of optical turbulence, scattering and absorption effects in the underwater medium further exacerbates the difficulty of achieving reliable modulation identification. Recent advances in deep learning (DL), particularly the use of CNNs, offer a promising alternative by enabling automatic feature extraction directly from signal representations without manual intervention. CNNs have demonstrated remarkable success in pattern recognition tasks across various fields, suggesting their potential applicability for modulation classification in UOWC system as well.

In this chapter, a DL-based framework has been proposed for constellation signal classification in UOWC environments. The transmitted optical signals are mapped into two-dimensional constellation diagrams, which are subsequently used as input to a CNN architecture. To achieve efficient and accurate classification, the

lightweight SqueezeNet model is adapted and trained on these constellation patterns corresponding to multiple modulation formats. This approach leverages the ability of CNNs to learn discriminative spatial features, enabling robust modulation identification even under challenging underwater channel conditions.

The primary contributions of this chapter are summarized as follows:

- A DL-based signal classification framework is developed for UOWC system utilizing constellation diagrams as input features.
- The SqueezeNet CNN model is employed to perform efficient modulation recognition across various modulation schemes.
- The influence of underwater channel impairments on constellation characteristics and classification performance is systematically analysed.
- The effectiveness of the proposed approach is validated through simulation studies, highlighting its potential for enhancing adaptive signal processing in future UOWC deployments.

6.2 Constellation diagram as a feature representation

To prepare training data for deep learning-based modulation classification in UOWC system, a simulation process is used to generate constellation signals and fig. 6.1 shows the steps for constellation signal generation for various modulation schemes. The process begins by creating random bitstreams, which are then grouped and converted into complex symbols based on the chosen modulation scheme such as, QPSK, 8-PSK, or M-QAM formats like 16-QAM and 64-QAM. These modulated symbols are passed through a simulated underwater channel modelled using the GG fading distribution. This model accurately captures the effects of underwater turbulence by combining two independent Gamma-distributed random variables, each representing different scales of turbulence in the water. The resulting channel fading introduces realistic distortions in the signal amplitude.

To further mimic real-world conditions, AWGN is added to the faded signals, based on a predefined SNR. The final received signals now affected by both fading and noise are plotted in the complex plane, creating scatter plots known as constellation diagrams. These plots visually depict how signal points cluster or spread

under different channel conditions, offering valuable insights into the reliability and robustness of each modulation scheme. Each of these constellation plots is saved as an image and labelled according to the modulation type. These images form the foundation of a dataset used to train deep learning models particularly CNNs to automatically identify and classify modulation formats even under challenging underwater conditions.

| Step 1: Bitstream Generation and Modulation | Step 2: Gamma–Gamma Fading Coefficient | Step 3: Apply Fading and AWGN | Step 4: Scatter Plot for Constellation Diagram | Step 5: Save Constellation Image |
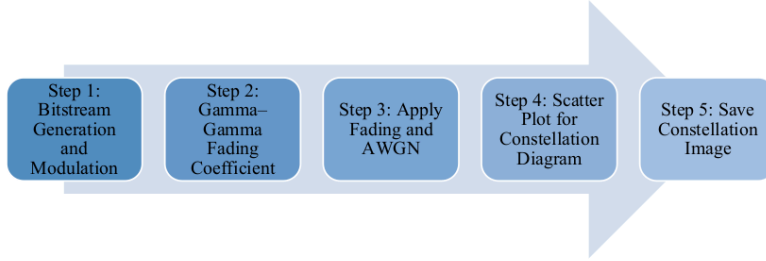
Figure 6.1 Steps for constellation signal generation for various modulation schemes

In the first step, a sequence of random bits is generated and grouped based on the number of bits per symbol required by the modulation scheme. Table 6.1 show the bitstream mapping for QPSK, 8-PSK, 4-QAM, 16-QAM and 64-QAM with respective constellation points. The resulting baseband symbol stream is denoted as: $s = [s_1, s_2, \ldots, s_M], s_k \in C$.

Table 6.1 Bitstream mapping for QPSK, 8-PSK, 4-QAM, 16-QAM and 64-QAM

Modulation Scheme	Bits per Symbol	Constellation Points
QPSK	2 bits	$e^{j0}, e^{j\pi/2}, e^{j\pi}, e^{j3\pi/2}$
8-PSK	3 bits	$e^{j2\pi k/8}, k = 0 \ldots 7$
4-QAM	2 bits	$\pm 1 \pm j1$
16-QAM	4 bits	$\{-3, -1, +1, +3\} + j\{-3, -1, +1, +3\}$
64-QAM	6 bits	$\{-7, -5, \ldots, +7\} + j\{-7, -5, \ldots, +7\}$

The underwater optical wireless channel is simulated using the GG-fading model, which effectively captures turbulence-induced intensity fluctuations. If I being the optical intensity and is a random variable, then the PDF of GG distribution can be expressed as

$$f_I(I) = 2(\alpha\beta)^{(\alpha+\beta)/2} K_{\alpha-\beta}\left(2\sqrt{\alpha\beta I}\right)\frac{I^{(\alpha+\beta)/2-1}}{\Gamma(\alpha)\Gamma(\beta)}, \qquad (6.1)$$

where K is the modified Bessel function, α and β are parameters associated with the σ_R^2. The modulated symbols are transmitted through the simulated fading channel and then corrupted by AWGN to simulate background noise. The received signal is computed as
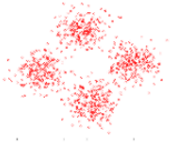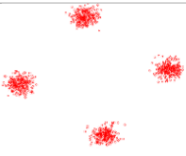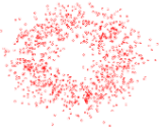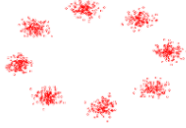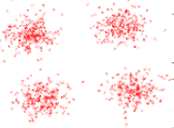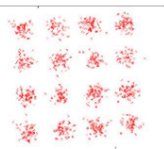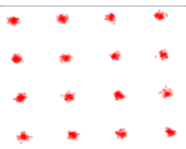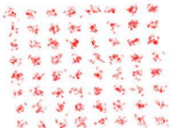
$$R = s_k \times h_k + Y, \qquad (6.2)$$

where R is the received signal, h_k is a fading vector, s_k is the resulting symbol stream and Y is the AWGN with zero mean and variance $N_o/2$. The entire received symbol vector is $R = [R_1, R_2, \ldots, R_M]$.

The received symbol with noise has been calculated and plotted real, imaginary parts on a complex plane. A constellation diagram is commonly employed as a two-dimensional depiction of a modulated signal. It accomplishes this by assigning signal samples to scattering points on a complicated plane. It is important to understand that the complex plane has unlimited extent, whereas the area that an image may represent is finite. In order to create a constellation diagram image, a certain region of the complex plane has to be chosen. In the event that the chosen region is insufficiently large, certain signal samples may be omitted from the image and discarded due to high levels of noise. In contrast, if the area is excessively expansive, signal samples may gather in a confined space and potentially intersect. 351 constellation images were generated by adjusting the number of samples in each modulation category from 300 to 1000, with an increment of two samples. For a single SNR value 1755 constellation images were generated. A total of 15795 constellation images were generated, encompassing 9 different SNR values ranging from -4 to 12 dB. Table 6.3. shows the

constellation diagrams of QPSK, 8PSK, 4QAM, 16QAM & 64QAM at different SNR values of 2 dB & 12 dB.

Table 6.2 Constellation diagrams of QPSK, 8PSK, 4QAM, 16QAM & 64QAM at different SNR values of 2 & 12 dB

SNR	2dB	12dB
QPSK		
8PSK		
4QAM		
16QAM		
64QAM		

Next section provides a comprehensive overview of DL, CNN and the SqueezeNet model.

6.3 CNN-based architecture for modulation classification

After preparing the labeled constellation image dataset, the next critical step involves training a deep learning model to accurately classify the modulation schemes under varying levels of turbulence. In this work, a CNN is employed due to its proven capability in image classification tasks, especially when spatial patterns and local dependencies (as seen in constellation diagrams) are key features. CNNs utilize convolution operations instead of generic matrix multiplication in at least one of their layers. Typical CNN architectures are comprised of three distinct types of layers, namely the convolutional layer, pooling layer and fully connected layer. Many CNN models are available for classification of images like, AlexNet, GoogLeNet, ResNet, SqueezeNet etc. [72]. The SqueezeNet CNN model is a lightweight CNN model specifically intended for efficient image classification. It is particularly well-suited for contexts with limited resources. In UOWC, limited computational resources are available as they are operated on external batteries. So, a SqueezeNet CNN model for image classification in UOWC channel has been selected.

The feature extraction process employs a pre-trained SqueezeNet model. The SqueezeNet system operates as a stochastic feature extractor, which allows the input image to propagate forward until it reaches a predetermined layer, known as the feature extraction layer. The process accomplished at this point, utilizing the outputs of the final layer as the features. This proposed solution utilizes the SqueezeNet model, a pre-trained CNN in DL. The objective of the SqueezeNet model is to develop a compact neural network with reduced parameters, enabling it to be stored in computer memory and communicated efficiently over a computer network. SqueezeNet is a sophisticated CNN architecture that exclusively employs 3×3 and 1×1 convolutional kernels [73]. The fundamental component of SqueezeNet is referred to as the fire module.

The initial step involves feeding the input image of dimension 875×656×3 and the model resize the input image to 227×227×3 into an independent convolutional layer referred to as conv1. A squeeze convolutional layer consists of only one filter. The inputs are passed into an enlarged layer that consists of a combination of 1×1 and 3×3 convolution filters. These filters collect spatial information at different scales.

99

Following this layer, there are eight consecutive fire modules which are labeled as fire2 to fire9. Max-pooling is applied with a stride of 2 after the conv1, fire3, fire5 and conv10 layers for 2D global average pooling. The ReLU activation function links the compression and expansion layers within the fire module. Dropout layers are incorporated subsequent to the fire9 module to mitigate overfitting. The down sampling process is implemented towards the end of the architecture, leading to the inclusion of a complex bypass in SqueezeNet. Fig. 6.2 depicts an overview of the DL based CNN SqueezeNet architecture.
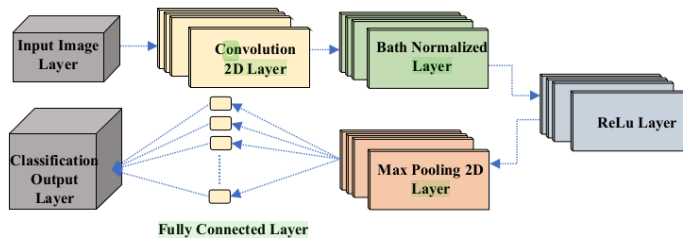
Figure 6.2 Proposed DL based CNN SqueezeNet architecture

Fig. 6.3 shows the SqueezeNet architecture with elaborated fire model. SqueezeNet constitutes a streamlined CNN design strategically crafted to minimize parameters without compromising accuracy. It consists of a fire module with a convolution layer that includes both "squeeze" and "expand" layers. This optimization is accomplished through the utilization of 1x1 convolutional filters, effectively decreasing the parameter count in contrast to conventional architectures.
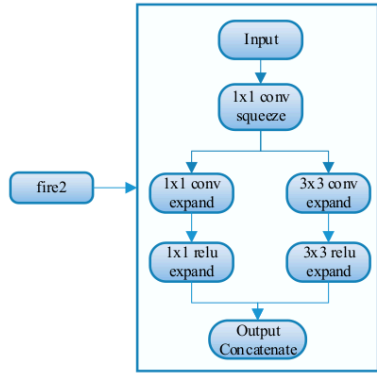
Figure 6.3 SqueezeNet architecture with elaborated fire model

6.4   Simulation setup under turbulent condition for UOWC

The training process utilizes the Stochastic Gradient Descent with Momentum (SGDM) optimizer, where the momentum coefficient is set to 0.9 and the initial learning rate is fixed at 0.001. An early stopping criterion is also implemented to prevent overfitting by halting training when validation accuracy does not improve over several consecutive epochs. To ensure robustness and improved generalization, L2 regularization (also known as weight decay) is applied with a coefficient of 0.0001.

The dataset is randomly divided into three subsets: 70% for training, 15% for validation and 15% for testing. Data shuffling is performed before each epoch to promote diverse batch formation, which enhances convergence behavior during training. The training progress is evaluated based on categorical cross-entropy loss and classification accuracy on the validation set. The trained SqueezeNet model is then tested on unseen constellation images generated under different levels of GG fading to assess its modulation recognition performance across varying turbulence conditions. Table 6.3 shows various parameters of the proposed model in the simulation environment using Matlab tool.

Table 6.3 Parameters associated with the proposed CNN model

Parameter	Specification
Input Image	$227 \times 227 \times 3$
Number of Layers	68
Number of Connections	74
Convolution Layers	26
Depth Concatenation	8
ReLU	26
Softmax Layer	1
Max Pooling Layer	4
Solver	SGDM
Execution Environment	Single GPU
L2Regularization	0.0001

Now the performance of the proposed model can be better understood by generating a confusion matrix. It provides an overview of the classification model by showing the number of true positives (TP), true negative (TN), false positive (FP) and false negative (FN). Fig. 6.4 shows the confusion matrix with predicted and real labels.

Real Label

		Positive	Negative
Predicted Label	Positive	True Positive (TP)	False Positive (FP)
	Negative	False Negative (FN)	True Negative (TN)

Figure 6.4 Representation of a confusion matrix to compute the performance

Based on the above confusion matrix, the classification accuracy of the proposed CNN model can be given as,

$$Accuracy(\%) = \frac{TP + TN}{TP + TN + FP + FN} \times 100 \qquad (6.3)$$

Now using eqn. (6.3) the performance of various modulation schemes can be computed and compared at various SNR levels.

6.5   Results and discussion

The dataset was divided into a training set encompassing 70% of the data and a validation set containing 30% of the data. The proposed model was trained using 1229 constellation images and validated by 526 constellation images for different modulation schemes (QPSK, 8-PSK, 4-QAM, 16-QAM, 64-QAM) at a SNR of -4dB.

Fig. 6.5 displays the training and validation curves with model parameters of initial learning rate 0.001, validation frequency 50, maximum epochs 5 and minimum batch size of 128. However, training is performed under single GPU execution environment with L2Regularization 0.0001. The confusion matrix in fig. 6.6 shows the classification performance of five modulation schemes. At low SNR of -4dB, the constellation images exhibit distortion, resulting in reduced accuracy for higher modulation schemes. The classification performance deteriorates to 49.5%, particularly for higher order modulation such as 64-QAM, but the classification accuracy remains nearly unchanged for QPSK and 8-PSK.
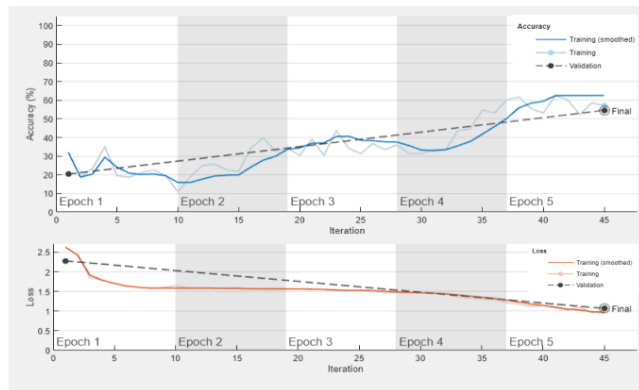
Figure 6.5 Training progress of the proposed CNN model for the constellation images at SNR of -4 dB

103

Figure 6.6 Confusion matrix of different modulation schemes at SNR of -4 dB

Fig. 6.7 shows Receiver Operating Characteristic (ROC) curves for different modulation schemes evaluated based on their classification performance. The Area Under the Curve (AUC) values indicate the ability of each scheme to distinguish between correct and incorrect classifications. QPSK achieves the highest AUC of 0.90, followed by 8-PSK (0.82), while higher-order modulations such as 16-QAM and 64-QAM show comparatively lower performance with AUC values of 0.70, reflecting increased difficulty in accurate modulation identification under similar conditions.
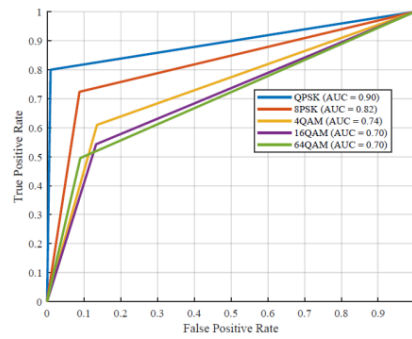
Figure 6.7 ROC curves for different modulation schemes evaluated based on their classification performance at SNR of -4 dB

104

Fig. 6.8 shows Precision–Recall curves for various modulation formats. QPSK consistently achieves the best trade-off between precision and recall, indicating its superior classification reliability. In contrast, higher-order modulation schemes such as 16-QAM and 64-QAM exhibit reduced performance, with lower precision and recall values, reflecting increased classification difficulty due to their complex symbol structures.
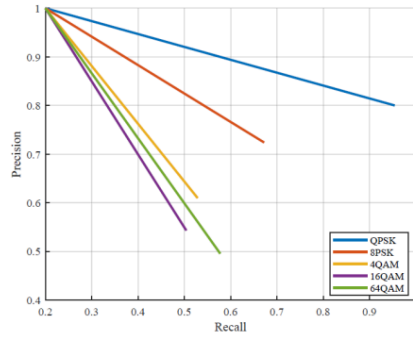
Figure 6.8 Precision vs recall curve for various modulation formats at SNR of -4 dB

Fig. 6.9 displays the training and validation curve at an SNR of 8 dB with model parameters of initial learning rate 0.001, validation frequency 50, maximum epochs 5 and minimum batch size of 128.
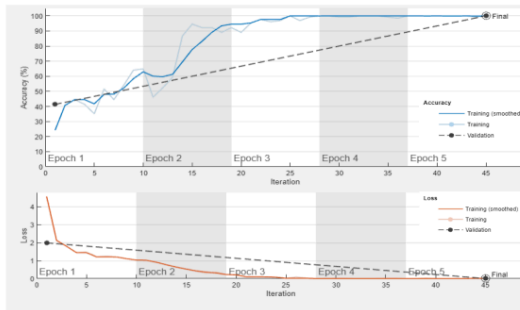
Figure 6.9 Training progress of the proposed SqueezeNet model for the constellation images at SNR of 8 dB

105

The classification accuracy of five modulation schemes at SNR of 8 dB is presented in fig. 6.10 using a confusion matrix. At a SNR of 8 dB, the constellation images exhibit greater precision, leading to improved accuracy. This can be verified by referring the confusion matrix displayed in fig. 6.10. The classification accuracy decreases to 91%, specifically for higher order modulation schemes like 64-QAM, while maintaining a classification accuracy of 100% for QPSK.

Figure 6.10 Confusion matrix of different modulation schemes at SNR of 8 dB
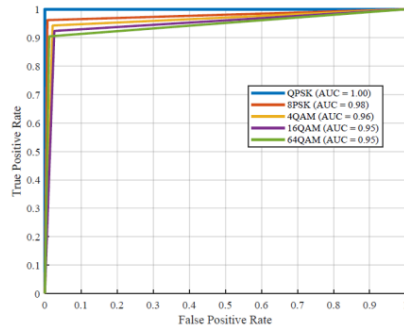
Figure 6.11 ROC curve for different modulation schemes based on their classification performance at SNR of 8 dB

Fig. 6.11 shows the ROC curves for different modulation formats, demonstrating their classification accuracy. The AUC values indicate excellent

106

detection capability across all schemes, with QPSK achieving perfect discrimination (AUC = 1.00), followed by 8-PSK (AUC = 0.98) and 4-QAM (AUC = 0.96). Slightly lower yet still high performance is observed for 16-QAM and 64-QAM (AUC = 0.95), confirming reliable modulation recognition even for higher-order constellations.

Fig. 6.12 shows the Precision vs recall curve for different modulation schemes illustrating their classification performance. QPSK maintains perfect precision across all recall values, reflecting its robust separability under the tested conditions. Other schemes show a gradual decline in precision with increasing recall, with 8-PSK performing better than 4-QAM, 16-QAM and 64-QAM. The reduced performance of higher-order modulations highlights the trade-off between spectral efficiency and classification accuracy.
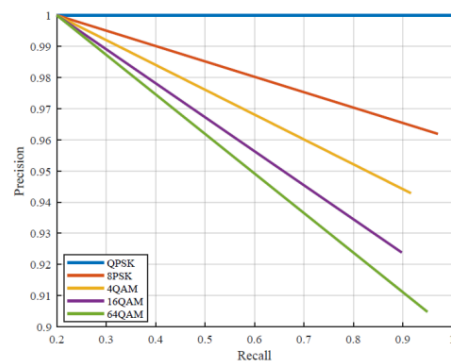
Figure 6.12 Precision vs recall curves for various modulation formats at SNR of 8 dB

Now a detailed comparison of classification accuracy of various modulation schemes at various SNR levels is presented in table 6.4. As the SNR value increases the constellation images shows better precision and the classification accuracy of the proposed model improves gradually.

Table 6.4 presents the classification accuracy of different modulation schemes over a range of SNR values from - 4 dB to 12 dB. QPSK shows superior performance, maintaining over 80% accuracy even at - 4 dB and achieving 100% accuracy from 8

dB onward. 8-PSK and 4-QAM follow closely, with 8PSK reaching 100% accuracy at 12 dB. Higher-order modulations such as 16-QAM and 64-QAM initially lag in low SNR conditions (54% and 50% accuracy at - 4 dB, respectively) but progressively improve, reaching full accuracy at 12 dB. The results demonstrate the increased robustness of lower-order modulation formats in noisy environments and the convergence of all schemes at higher SNRs.

Table 6.4 Percentage classification accuracy of various modulation schemes at different SNR values

SNR	Percentage Classification Accuracy				
(dB)	QPSK	8PSK	4QAM	16QAM	64QAM
- 4	80	72	61	54	50
-2	84	76	65	63	51
0	89	80	72	67	61
2	91	85	77	70	72
4	94	90	81	81	84
6	98	94	89	88	90
8	100	96	94	92	91
10	100	98	98	97	96
12	100	100	100	100	100

Fig. 6.13 shows the classification accuracy versus SNR for various modulation schemes. As expected, classification accuracy improves with increasing SNR for all modulation types. QPSK consistently achieves the highest accuracy across the SNR range, reaching near-perfect performance above 10 dB. In contrast, higher-order modulation schemes such as 16-QAM and 64-QAM start with lower accuracy at low SNRs but gradually converge toward the performance of lower-order schemes at higher SNRs, indicating increased susceptibility to noise but eventual convergence in cleaner channel conditions.
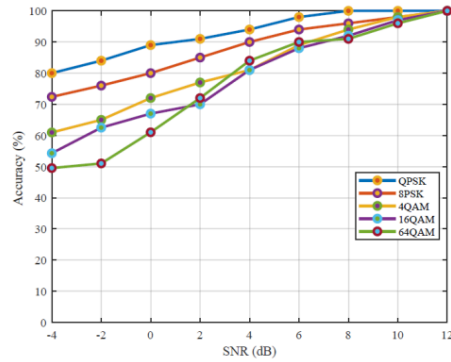
Figure 6.13 Classification accuracy versus SNR for various modulation schemes using proposed CNN model

A DL-based method was developed for classifying constellation signals in UOWC system. The model accurately identified signal patterns even under severe fading and noise conditions. It outperformed traditional classification techniques in terms of accuracy and robustness. The impact of different turbulence levels was studied and the system maintained high classification performance. Simulation results confirmed that the DL approach is reliable and effective for signal detection in challenging underwater environments.

6.6 Conclusion

In this chapter, a comprehensive investigation into the classification performance of various digital modulation schemes in UOWC system was presented. The analysis focused on evaluating constellation signal classification accuracy across multiple modulation formats namely QPSK, 8-PSK, 4-QAM, 16-QAM and 64-QAM under a range of SNR conditions. The results demonstrated that lower-order modulations such as QPSK consistently achieved higher classification accuracy, especially in low SNR regimes, owing to their simpler constellation structure and greater resilience to channel distortions. In contrast, higher-order modulations like 16-QAM and 64-QAM showed reduced performance at low SNR values but gradually improved with increasing SNR,

eventually converging to near-perfect accuracy. Performance metrics such as ROC curves, AUC values and Precision–recall plots further confirmed the superior separability of QPSK and 8-PSK signals, with QPSK achieving perfect classification at higher SNRs. These findings underline the importance of choosing modulation schemes that balance spectral efficiency with classification robustness based on prevailing channel conditions. The outcomes of this chapter provide valuable insights into the modulation classification capabilities of modern communication receivers operating in the challenging and dynamic underwater optical environment.

CHAPTER 7

CONCLUSION, FUTURE SCOPE AND SOCIAL IMPACT

This chapter highlights the important conclusions drawn from these research objectives and gives the details of future scope of work in the field of UOWC.

7.1   Conclusion

UOWC holds tremendous potential for enabling fast, low-latency data transfer through underwater surfaces. However, despite its advantages over traditional acoustic communication, UOWC systems face serious challenges due to the severe underwater environment. Factors like absorption, scattering, turbulence and even minor misalignments can severely degrade signal quality. These challenges not only limit communication range but also lead to high error rates and unreliable links, making UOWC systems difficult to deploy in real-world conditions.

To address these limitations, this thesis explored a series of practical and innovative solutions aimed at improving the reliability, capacity, and overall robustness of UOWC systems. The work was organized around four key research objectives, each targeting a different aspect of system performance.

To begin with, a novel approach using 1×2 SIMO and 2×2 MIMO architectures was proposed to tackle the problem of turbulence-induced fading. These designs leveraged spatial diversity and were tested under both IM/DD and OHD detection schemes. The results were compelling, the 2×2 MIMO system consistently outperformed traditional GG and EGG models. It achieved dramatically lower OP and BERs while delivering higher spectral efficiency even in the presence of strong turbulence. This confirmed that spatial diversity could play a critical role in enhancing the reliability of underwater links.

In the next phase, the research turned to the problem of limited communication range and signal degradation over distance. Here, a dual-hop UOWC system was introduced, modelled using the Málaga distribution to more accurately represent

111

underwater turbulence. The system used fixed-gain relays and was tested under different levels of pointing error and turbulence. Results showed a clear improvement over conventional single-hop systems, with increased capacity and better tolerance to misalignment. The OHD detection scheme, in particular, demonstrated excellent performance in maintaining low error rates even under severe conditions.

The third objective focused on overcoming decoding errors using RS coding. A robust RS-coded UOWC model was developed and evaluated across different modulation formats and coding parameters. The findings showed that RS coding significantly reduced decoding error probability by many orders of magnitude in some cases especially under strong turbulence. Importantly, the model offered flexibility, it could be tuned for high-speed data transmission or high-reliability applications depending on the scenario.

Finally, the thesis explored the modulation classification capabilities of UOWC systems. In dynamic and noisy underwater environments, recognizing the transmitted modulation format accurately is crucial for adaptive and intelligent communication. The research showed that lower-order modulations like QPSK and 8-PSK delivered high classification accuracy at low SNR, while higher-order modulations like 64-QAM required stronger signals but achieved near-perfect classification at high SNRs. These insights are valuable for designing adaptive receivers that can adjust to real-time underwater conditions.

Together, these four contributions form a holistic solution to the core challenges in UOWC, improving link reliability, extending communication range, minimizing error rates and enabling smarter signal interpretation. More than just theoretical paradigms, these models were tested and validated across realistic channel conditions, and they demonstrated strong, practical potential. Reliable underwater communication opens new possibilities in marine science, such as monitoring ocean health, studying climate change, and tracking pollution levels with greater accuracy. It also enhances early warning systems for disasters like tsunamis or underwater earthquakes, enabling faster responses and potentially saving lives. The improvements

112

also benefit underwater robotics, allowing them to operate more autonomously in tasks like deep-sea exploration, pipeline inspections, or search-and-rescue missions.

Looking forward, the models and insights presented in this thesis can support the development of secure, energy-efficient subsea communication networks, with applications ranging from national defence to underwater archaeology and even futuristic concepts like smart underwater cities.

In summary, this work has taken a step closer to making UOWC more reliable, intelligent and applicable. By blending theoretical rigor with practical relevance, the research lays a strong foundation for the next generation of UOWC systems that are not only technically advanced but also profoundly useful to society and the environment.

7.2   Future Scope

- This work lays the foundation for intelligent and more resilient UOWC systems, while also opening avenues for future exploration and development. One promising avenue is hybrid communication system that leverage optical, acoustic and radio signals. Such system could combine the advantages associated with each of these technologies to enable reliable communication in the most challenging underwater environments, so where one single method never would succeed on its own.

- While CNN models continue to evolve, reinforcement learning presents promising opportunities, enabling underwater systems to dynamically adapt and learn from real-time environmental feedback. Additionally, advanced methods like beamforming can enhance the precision of optical signal steering, thereby improving the efficiency and reliability of underwater communication.

7.3   Social Impact

- Despite its technical complexity, this research carries substantial practical significance. Enhancing underwater communication capabilities provides

researchers and environmental scientists with advanced tools for more precise monitoring of marine environments. Such advancements are expected to support improved assessment of climate change, pollution levels and overall ocean health, which serve as critical indicators of the planet's environmental condition.

- These innovations can also reach their full potential in contributing to early warning system for natural disasters like tsunamis or underwater earthquakes. Faster, more reliable communication allows for earlier detection and response to these threats, saving lives and protecting ecosystem.

- Advancements in communication infrastructure also have benefits for the underwater robotics realm. From deep-sea exploration to pipeline inspections and even search-and-rescue missions, a strong, stable communication link means that this robotic system can run more efficiently and with a lot more autonomy.

- On a larger scale, this research lays the groundwork for a more secure and energy-efficient subsea communication network, which can be used for everything from national defence operations to underwater archaeology, to helping power an underwater smart city in the future.

Thesis

Turbulence in Underwater Optical Wireless Communications", Optik, 2024
Publication

10   Long Huang, Siming Liu, Pan Dai, Mi Li, Gee-Kung Chang, Yuechun Shi, Xiangfei Chen. "Unified Performance Analysis of Hybrid FSO/RF System with Diversity Combining", Journal of Lightwave Technology, 2020
Publication   <1%

11   Emna Zedini, Hamza Soury, Mohamed-Slim Alouini. "Dual-Hop FSO Transmission Systems Over Gamma–Gamma Turbulence With Pointing Errors", IEEE Transactions on Wireless Communications, 2017
Publication   <1%

12   Emna Zedini, Hassan Makine Oubei, Abla Kammoun, Mounir Hamdi, Boon S. Ooi, Mohamed-Slim Alouini. "Unified Statistical Channel Model for Turbulence-Induced Fading in Underwater Wireless Optical Communication Systems", IEEE Transactions on Communications, 2019
Publication   <1%

13   Lajos Hanzo, Yosef Jos Akhtman, Li Wang, Ming Jiang. "MIMO-OFDM for LTE, Wi-Fi and WiMAX", Wiley, 2010
Publication   <1%

14   Springer Series in Optical Sciences, 2015.
Publication   <1%

15   arxiv.org
Internet Source   <1%

16   livrepository.liverpool.ac.uk
Internet Source   <1%

17   Submitted to IIT Delhi
Student Paper

<1%

18 v-des-dev-lnx1.nwu.ac.za
Internet Source
<1%

19 www.mdpi.com
Internet Source
<1%

20 Prakriti Saxena, Aashish Mathur, Manav R. Bhatnagar, Zabih Ghassemlooy. "BER of an optically pre-amplified FSO system under Málaga turbulence, pointing errors, and ASE noise", 2017 IEEE 28th Annual International Symposium on Personal, Indoor, and Mobile Radio Communications (PIMRC), 2017
Publication
<1%

21 Submitted to Visvesvaraya National Institute of Technology
Student Paper
<1%

22 Submitted to University of Wollongong
Student Paper
<1%

23 Submitted to Birla Institute of Technology and Science Pilani
Student Paper
<1%

24 preview-futurecitiesenviro.springeropen.com
Internet Source
<1%

25 doc.lagout.org
Internet Source
<1%

26 Jwaifel, Arwa Mahmoud. "Impact of Co-Channel Interference on Performance of Multi-Hopwireless Ad-Hoc Networks with Cooperative Diversity", Princess Sumaya University for Technology (Jordan), 2021
Publication
<1%

27 Suman Malik, Prasant Kumar Sahu. "M-ary phase-shift keying-based single-input-multiple-output free space optical communication system with pointing errors over a gamma–gamma fading channel", Applied Optics, 2019
Publication
<1%

28 deepai.org
Internet Source
<1%

29 dokumen.pub
Internet Source
<1%

30 "Computer Vision and Graphics", Springer Science and Business Media LLC, 2018
Publication
<1%

31 Submitted to University of Edinburgh
Student Paper
<1%

32 Imran Shafique Ansari, Mohamed-Slim Alouini, Julian Cheng. "Ergodic Capacity Analysis of Free-Space Optical Links With Nonzero Boresight Pointing Errors", IEEE Transactions on Wireless Communications, 2015
Publication
<1%

33 text.123docz.net
Internet Source
<1%

34 d-nb.info
Internet Source
<1%

35 ebin.pub
Internet Source
<1%

36 fastercapital.com
Internet Source
<1%

37 Submitted to University of Michigan Flint
Student Paper
<1%

38 citycollege.ac.in
Internet Source
<1%

39 hal.univ-nantes.fr
Internet Source
<1%

40 lirias.kuleuven.be
Internet Source
<1%

41 opg.optica.org
Internet Source
<1%

42 theses.lib.polyu.edu.hk
Internet Source
<1%

43 www.hindawi.com
Internet Source
<1%

44 www.scribd.com
Internet Source
<1%

45 Xin Li, Yongjun Li, Shanghong Zhao, Xinkang Song, Jianjia Li. "Performance Analysis of Parallel Free-Space Optical/Radio Frequency Transmissions in Satellite–Aerial–Ground Integrated Network with Power Allocation", Photonics, 2024
Publication
<1%

46 Zixuan Xu, Guanjun Xu, Zhengqi Zheng. "BER and Channel Capacity Performance of an FSO Communication System over Atmospheric Turbulence with Different Types of Noise", Sensors, 2021
Publication
<1%

47 eprints.soton.ac.uk
Internet Source
<1%

48 Abdulgani Ibrahim, Eylem Erdogan, Tansal Gucluoglu. "Performance of subcarrier intensity modulation over an imprecise
<1%

gamma-gamma channel", 2018 26th Signal Processing and Communications Applications Conference (SIU), 2018
Publication

49   Abu Jahid, Mohammed H. Alsharif, Trevor J. Hall. "A contemporary survey on free space optical communication: Potentials, technical challenges, recent advances and research direction", Journal of Network and Computer Applications, 2022   <1%
Publication

50   Wang, Xinao. "Vehicle-To-Vehicle Communication: Design, Performance, and Disruption Mitigation in Real-World Environment", University of Nottingham (United Kingdom)   <1%
Publication

51   academic-accelerator.com   <1%
Internet Source

52   Chatzidiamantis, Nestor D., Athanasios S. Lioumpas, George K. Karagiannidis, and Shlomi Arnon. "Adaptive Subcarrier PSK Intensity Modulation in Free Space Optical Systems", IEEE Transactions on Communications, 2011.   <1%
Publication

53   Submitted to King Fahd University for Petroleum and Minerals   <1%
Student Paper

54   Submitted to UT, Dallas   <1%
Student Paper

55   Submitted to University of Northumbria at Newcastle   <1%
Student Paper

56 mediatum.ub.tum.de
Internet Source
<1%

57 www.frontiersin.org
Internet Source
<1%

58 www.science.org
Internet Source
<1%

59 Chengwei Fang, Shuo Li, Yinong Wang, Ke Wang. "High-Speed Underwater Optical Wireless Communication with Advanced Signal Processing Methods Survey", Photonics, 2023
Publication
<1%

60 Francis Ring. "Learning Approaches in Signal Processing", Pan Stanford, 2019
Publication
<1%

61 Jolly Parikh. "Study on statistical models of atmospheric channel for FSO communication link", 2011 Nirma University International Conference on Engineering, 12/2011
Publication
<1%

62 Xiang Yi, Zengji Liu, Peng Yue, Tao Shang. "BER Performance Analysis for M-ary PPM over Gamma-Gamma Atmospheric Turbulence Channels", 2010 International Conference on Computational Intelligence and Software Engineering, 2010
Publication
<1%

63 odr.chalmers.se
Internet Source
<1%

64 www.x-mol.com
Internet Source
<1%

65 Mohammed Ahmed Magzoub Albashier, Azlan Abdaziz, Hadhrami Abd. Ghani.
<1%

"Performance analysis of physical layer security over different error correcting codes in wireless sensor networks", 2017 20th International Symposium on Wireless Personal Multimedia Communications (WPMC), 2017
Publication

66   Souad Labghough, Fouad Ayoub, Mostafa Belkasmi. "Error Probability Analysis for Dual-Hop Mixed RF-FSO System using CSOC Codes with MLGD Decoding", 2019 15th International Wireless Communications & Mobile Computing Conference (IWCMC), 2019   <1%
Publication

67   Submitted to University of Bristol   <1%
Student Paper

68   c.coek.info   <1%
Internet Source

69   digitalcommons.lsu.edu   <1%
Internet Source

70   dspace.mist.ac.bd:8080   <1%
Internet Source

71   pure.tue.nl   <1%
Internet Source

72   "Artificial Intelligence in China", Springer Science and Business Media LLC, 2020   <1%
Publication

73   Ahmed Hassan Abd El-Malek, Mohamed Abdelkarim Aboulhassan, Anas M. Salhab, Salam A. Zummo. "Performance Analysis and Power Optimization for Spectrum-Sharing Mixed RF/FSO Relay Networks with Energy Harvesting", IEEE Photonics Journal, 2019   <1%
Publication

74   Guanjun Xu, Jiahui Lai. "Average capacity analysis of the underwater optical plane wave over anisotropic moderate-to-strong oceanic turbulence channels with the Málaga fading model", Optics Express, 2020
Publication

<1%

75   Imran Shafique Ansari, Mohamed M. Abdallah, Mohamed-Slim Alouini, Khalid A. Qaraqe. "Outage Analysis of Asymmetric RF-FSO Systems", 2016 IEEE 84th Vehicular Technology Conference (VTC-Fall), 2016
Publication

<1%

76   Submitted to Universiti Tenaga Nasional
Student Paper

<1%

77   Wei Yang, Haoran Liu, Guangpeng Cheng, Zike Su, Yuanyuan Fan. "RIS-Aided V2I–VLC for the Next-Generation Intelligent Transportation Systems in Mountain Areas", Photonics, 2025
Publication

<1%

78   Zhang, Y.. "Capacity for non-Kolmogorov turbulent optical links with beam wander and pointing errors", Optics and Laser Technology, 201110
Publication

<1%

79   ena.lp.edu.ua:8080
Internet Source

<1%

80   ghcmarijuana.com
Internet Source

<1%

81   research.library.mun.ca
Internet Source

<1%

82   www.arxiv-vanity.com
Internet Source

<1%

83   www.diplomarbeiten24.de
Internet Source

<1 %

84 www.researching.cn
    Internet Source
<1 %

85 www.scilit.net
    Internet Source
<1 %

86 Amr G. AbdElKader, Ahmed Allam, Kazutoshi
    Kato, Hossam M.H. Shalaby. " Performance
    enhancement of RIS-assisted MRR-UOWC
    systems using the spectral-power-efficient
    QAM-MPPM ", Optics Communications, 2024
    Publication
<1 %

87 George K. Karagiannidis. "<formula
    formulatype=(quote)inline(quote)>
    <tex>$N{\ast}$</tex></formula>Nakagami: A
    Novel Stochastic Model for Cascaded Fading
    Channels", IEEE Transactions on
    Communications, 8/2007
    Publication
<1 %

88 Jeongchan Kim, Youngnam Han, Seung-Hwan
    Lee. "Time-Domain Repetition Coding for
    MISO Transmission over Free-Space Optical
    Channel", 2013 IEEE 78th Vehicular
    Technology Conference (VTC Fall), 2013
    Publication
<1 %

89 Kwang Eui Yoo, Norman Ashford. "An
    application of a comparative analysis of
    revealed preference and stated preference
    methods to the air transport choice problem",
    Transportation Planning and Technology,
    1998
    Publication
<1 %

90 Qing-Song Hu, , Jun-Bo Wang, Jin-Yuan Wang,
    Ming Chen, and Xiaoyu Song. "Outage
<1 %

probability analysis of multi-hop free space optical communications over strong turbulence channels", 2013 International Conference on Wireless Communications and Signal Processing, 2013.
Publication

91	core.ac.uk Internet Source	<1%
92	digital.library.unt.edu Internet Source	<1%
93	etd.lib.metu.edu.tr Internet Source	<1%
94	export.arxiv.org Internet Source	<1%
95	geokarag.webpages.auth.gr Internet Source	<1%
96	idr.nitk.ac.in Internet Source	<1%
97	www.degruyter.com Internet Source	<1%
98	www.isteonline.in Internet Source	<1%
99	www.slideshare.net Internet Source	<1%
100	Daqi Shen, Langyi Tao, Jinghao Yu, Pengfei Ye et al. "Disruptive Technology of Building Internet of Underwater Things: Laser-based Underwater Solid-State Lighting", 2021 5th IEEE Electron Devices Technology & Manufacturing Conference (EDTM), 2021 Publication	<1%

101 K. ARAKI. "Capacity Analysis of MIMO Rayleigh Channel with Spatial Fading Correlation", IEICE Transactions on Fundamentals of Electronics Communications and Computer Sciences, 10/01/2008
Publication

<1%

102 Kenji Natori, Takashi Kurusu. "Novel aspects of nanoscale transistors", 2006 International Workshop on Nano CMOS, 2006
Publication

<1%

103 Pehlivanoglu, Yücel. "Formulation of a Beam Finite Element for Micro Beams.", Middle East Technical University (Turkey), 2024
Publication

<1%

104 Wang, Yingge. "Synchrotron X-Ray Studies of Metal-Ion Partitioning at Biofilm (Organic Film)/Metal-Oxide/Water Interfaces.", Stanford University, 2020
Publication

<1%

105 Hamidreza Hosseinzadeh, Zahra Einalou Writing-original draft, Farbod Razzazi. "A Weakly Supervised Representation Learning for Modulation Recognition of Short Duration Signals", Measurement, 2021
Publication

<1%

106 Wenxiao Shi, Pengxia Wu, Wei Liu. "Hybrid polarization-division-multiplexed quadrature phase-shift keying and multi-pulse pulse position modulation for free space optical communication", Optics Communications, 2015
Publication

<1%

Thesis

FINAL GRADE

/100

GENERAL COMMENTS

PAGE 1

PAGE 2

PAGE 3

PAGE 4

PAGE 5

PAGE 6

PAGE 7

PAGE 8

PAGE 9

PAGE 10

PAGE 11

PAGE 12

PAGE 13

PAGE 14

PAGE 15

PAGE 16

PAGE 17

PAGE 18

PAGE 19

PAGE 20

PAGE 21

PAGE 22

PAGE 23

PAGE 24

PAGE 25

PAGE 26

PAGE 27

PAGE 28

PAGE 29

PAGE 30

PAGE 31

PAGE 32

PAGE 33

PAGE 34

PAGE 35

PAGE 36

PAGE 37

PAGE 38

PAGE 39

PAGE 40

PAGE 41

PAGE 42

PAGE 43

PAGE 44

PAGE 45

PAGE 46

PAGE 47

PAGE 48

PAGE 49

PAGE 50

PAGE 51

PAGE 52

PAGE 53

PAGE 54

PAGE 55

PAGE 56

PAGE 57

PAGE 58

PAGE 59

PAGE 60

PAGE 61

PAGE 62

PAGE 63

PAGE 64

PAGE 65

PAGE 66

PAGE 67

PAGE 68

PAGE 69

PAGE 70

PAGE 71

PAGE 72

PAGE 73

PAGE 74

PAGE 75

PAGE 76

PAGE 77

PAGE 78

PAGE 79

PAGE 80

PAGE 81

PAGE 82

PAGE 83

PAGE 84

PAGE 85

PAGE 86

PAGE 87

PAGE 88

PAGE 89

PAGE 90

PAGE 91

PAGE 92

PAGE 93

PAGE 94

PAGE 95

PAGE 96

PAGE 97

PAGE 98

PAGE 99

PAGE 100

PAGE 101

PAGE 102

PAGE 103

PAGE 104

PAGE 105

PAGE 106

PAGE 107

PAGE 108

PAGE 109

PAGE 110

PAGE 111

PAGE 112

PAGE 113

PAGE 114